



Metka Majerič, BSc

Quality and Reliability Analysis of Point Measurements Derived from Structure from Motion and Bundle Adjustment Techniques

MASTER'S THESIS

to achieve the university degree of

Diplom-Ingenieurin

Master's degree program: Geomatics Science

submitted to

Graz University of Technology

Supervisor

Univ.-Prof. Dipl.-Ing. Dr.techn. Werner Lienhart

Institute of Engineering Geodesy and Measurement Systems

Graz, December 2017

AFFIDAVIT

I declare that I have authored this thesis independently, that I have not used other than the declared sources/resources, and that I have explicitly indicated all material which has been quoted either literally or by content from the sources used. The text document uploaded to TUGRAZonline is identical to the present master's thesis dissertation.

.....

Date

.....

Signature

Acknowledgments

This master's thesis is based on the system designed by Leica Geosystems AG. I would like to express my sincere gratitude to all of my colleagues who were always there to support me. I would especially like to thank David Grimm for all the advice and for the way he has inspired me throughout the course of the past year. My appreciation also goes to Bernhard Richter who gave me the opportunity to write my master's thesis in the collaboration with Leica Geosystems AG.

I owe a great sense of gratitude to my supervisor Univ.-Prof.Dr.techn. Werner Lienhart. His advice, scientific approach, and generous guidance helped me complete my thesis. It was a great honour to work with a supervisor who enthusiastically confronted me with all the difficulties.

Most importantly, I want to thank Stefan who was always there to encourage me. His constant willingness to help me understand the functionality of the single components of the system made it possible to find extra inspiration and additional ideas for my thesis.

Finally, I am deeply thankful to my parents Štefka and Janko for allowing me to realize my potential. They were by my side through all my years of study, following my challenges and supporting me in the hardest of times. I would like to express my gratitude to my sister Katjuša for being such a great role model and for paving the way for me.

Abstract

Development within surveying have successively given rise to new possibilities for measuring the coordinates of points in terrestrial coordinate systems. The desire to measure greater and greater amounts of point coordinates is growing. It is of big importance to reduce the time spent in the field and to use the system that can automatically process captured data.

Revolutionary changes have taken place by developing a system that combines a camera, a GNSS sensor and an IMU. When performing measurements with the system the camera captures the images while the position and the orientation of the images are being measured. Using the GNSS and the IMU measurements, the Structure from Motion algorithm at first defines approximate camera poses from which the images were taken. The Bundle Adjustment algorithm then iteratively adjusts the camera poses in space. This way the best approximation of camera poses from which the images were taken is determined in near real-time. The captured images can therefore be used for photogrammetric measurements right away.

In order to investigate the capability and the limitations of the system, the influences on the uncertainty of photogrammetrically measured object points were analysed. It was investigated how the photogrammetric measurements are influenced by the single components of the system and the synchronisation of main components.

Further investigation was made by performing measurements with the system in the test field. The test field was established so that the optimal conditions could be provided for the test measurements. Consequently, it was possible to investigate the accuracy of the system, as well as how the type of trajectory and the camera-to-object distance influence the accuracy of the measurements performed with the system. In addition, the measurements in the test field were also performed under real-use conditions. This enabled the investigation and analysis of the limitations of the system.

Zusammenfassung

Die Entwicklung innerhalb des Vermessungswesens hat kontinuierlich zu neuen Möglichkeiten geführt, die Koordinaten von Punkten in terrestrischen Koordinatensystemen zu messen. Der Wunsch wächst, immer größere Mengen von Punkten zu messen. Den Zeitaufwand für das Erfassen von Messpunkten auf dem Feld zu reduzieren und die Daten im Büro verarbeiten zu können, ist von großer Bedeutung.

Durch die Entwicklung eines Systems, welches eine Kamera, einen GNSS Empfänger und eine IMU kombiniert, hat eine revolutionäre Veränderung stattgefunden. Werden Messungen mit einem solchen System durchgeführt, können die aufgenommen Kamerabilder zusätzlich mit einer Position und einer Orientierung versehen werden. Um die Kameraposen exakt zu bestimmen, ermittelt der sogenannte Structure from Motion Algorithmus zunächst die ungefähre Kamerapose unter Verwendung der GNSS- und IMU-Messungen. Der sogenannte Bundle Adjustment Algorithmus optimiert danach diese ungefähre Kamerapose und korrigiert die Lage der Bilder im Raum. Mit Hilfe dieser beiden Algorithmen wird die beste Annäherung der Kameraposen nahezu in Echtzeit bestimmt. Durch dies können die aufgenommenen Bilder sofort für photogrammetrische Messungen verwendet werden.

Die Auswirkungen auf die Unsicherheit photogrammetrisch gemessener Objektpunkte wurden untersucht um die Möglichkeiten und die Grenzen des Systems ausfindig zu machen. Es wurde untersucht, wie die photogrammetrischen Messungen von den einzelnen Komponenten des Systems und der Synchronisation der Hauptkomponenten beeinflusst werden.

Weitere Untersuchungen wurden durchgeführt, indem Messungen mit dem System im Testfeld durchgeführt wurden. Das Testfeld wurde so eingerichtet, dass die optimalen Bedingungen für die Messungen sichergestellt sind. Die Genauigkeit des Systems konnte somit untersucht werden. Ebenfalls wurde untersucht, wie die Art der Bewegungsbahn sowie deren Entfernung zwischen Kamera und Objekt, die Genauigkeit der Messungen beeinflussen. Außerdem wurden Messungen im Testfeld unter realen Einsatzbedingungen durchgeführt. Die Grenzen des Systems konnten somit untersucht, analysiert und aufgezeigt werden.

Abbreviations

2D	Two Dimensional
3D	Three Dimensional
ARP	Antenna Reference Point
CMOS	Complementary Metal Oxide Semiconductor
CPU	Central Processing Unit
DoF	Degree of Freedom
dps	degrees per second
EDM	Electronic Distance Meter
FoV	Field of View
FuMo	Functional Model
GNSS	Global Navigation Satellite System
ID	Identification Definition
IMU	Inertial Measurement Unit
ITRF2008	International Terrestrial Reference Frame 2008
PPS	Pulse Per Second
RTK	Real Time Kinematics
SfM	Structure from Motion
ToW	Time of Week
UHF	Ultra High Frequency
USB	Universal Serial Bus
WLAN	Wireless Local Area Network

Contents

Acknowledgments	i
Abstract	ii
Zusammenfassung	iii
Abbreviations	iv
Contents	v
1 Introduction	1
1.1 Goals of the thesis	2
1.2 Introduction of the Terms	3
1.2.1 Bearing.....	3
1.2.2 Heading.....	3
1.2.3 Geodetic North Direction	3
1.2.4 Attitude.....	3
1.2.5 Camera Pose	4
1.2.6 Epipolar Lines	4
1.2.7 Camera-to-Object Distance	4
1.2.8 Object Point.....	5
1.2.9 Image Coordinate System	5
1.2.10 Terrestrial Coordinate System.....	6
1.2.11 Global Object Coordinate System	6
1.3 Existing Knowledge.....	7
2 State of the Art in Terrestrial Remote Point Measurements	8
2.1 Remote Point Measurements Using Total Stations	8
2.2 Remote Point Measurements Using Laser Scanners.....	8
2.3 Remote Point Measurements Using Photogrammetry	9
3 Functional Model	10
3.1 Measurement Principle	11
3.2 Application Areas.....	11
3.2.1 Limitations of the System.....	12
3.3 Main Components of the FuMo	13
3.4 Camera specifications.....	14
4 Photogrammetry	15
4.1 Close-Range Terrestrial Photogrammetry.....	15

4.2	Fundamental Principle of Remote Point Capturing Using Images	16
4.2.1	Exterior Orientation.....	17
4.2.2	Interior Orientation	18
4.2.3	Structure from Motion (SfM)	19
4.2.4	Bundle Adjustment.....	20
4.3	Geometry.....	21
4.3.1	Intersection Angle	23
4.3.2	Camera-to-Object Distance	24
4.3.3	Number of Images	24
5	Processing of the Data.....	25
5.1	Communication between Main Components	25
5.2	Determining the Camera Pose from Which the Images Were Captured	28
5.2.1	Feature Generation	28
5.2.2	Structure from Motion (SfM)	31
5.2.3	Bundle Adjustment.....	32
5.2.4	Summary.....	33
5.3	Measuring the Coordinates of the Object Point	34
6	Uncertainty of Photogrammetric Measurements	35
6.1	Influences on the Uncertainty of Perspective Centre	36
6.1.1	Uncertainty of the GNSS Measurements	36
6.1.2	Calibration	36
6.1.3	Synchronization of Main Components	36
6.1.4	Trajectory	36
6.2	Influences on the Uncertainty of the Image Point	37
6.2.1	Lighting Conditions	37
6.2.2	Perspective of an Object	37
6.2.3	Contrast of Measured Object Point.....	37
6.2.4	Pixel Size	38
7	Test Field	39
7.1	Goal of the Measurements in the Test Field	40
7.2	Local Geodetic Network	41
7.3	Targets.....	43
7.4	Objects of Interest.....	44
7.5	Conditions of the Test Field.....	45
7.5.1	GNSS Reception	45
7.5.2	Geometry.....	46

7.5.3	Structure of the Object.....	46
8	Subject of the Research.....	47
8.1	Impact of Trajectory.....	48
8.1.1	“I-Trajectory”.....	48
8.1.2	“U-trajectory”.....	48
8.2	Error Considerations.....	49
8.2.1	Error in the Direction Parallel to the Wall of the Object.....	50
8.2.2	Error in the Direction Perpendicular to the Object.....	50
8.2.3	Error in the Height Direction.....	51
9	Measurements and Data Processing.....	54
9.1	Transformation of the Coordinates.....	55
9.2	Computation.....	59
9.2.1	Mean Coordinate Errors of the Measurement Group.....	59
9.2.2	3D Error of the Measured Target.....	59
9.2.3	Accuracy of the Measurement group.....	60
10	Evaluation.....	61
10.1	3D Error of the Targets.....	61
10.1.1	Influence of the Target Height on the 3D Error.....	62
10.1.2	Influence of the Perspective of the Camera According to the Target on the 3D Error.....	64
10.1.3	Influence of the Target Type on the 3D Error.....	66
10.2	Mean Error of the Measurement Class.....	69
10.2.1	Error of the X Coordinate.....	70
10.2.2	Error of the Y Coordinate.....	71
10.2.3	Error of the Z Coordinate.....	72
10.3	Accuracy.....	73
11	Limitations of the FuMo.....	76
11.1	GNSS Reception.....	76
11.2	Lighting Conditions.....	76
11.3	Camera-to-object Distance.....	78
11.4	Trajectory.....	79
11.5	Structure of an Object.....	79
11.6	Fast Rotations and Bumps.....	79
11.7	Changing Surrounding of Image Point.....	80

- 12 Conclusion and Outlook 81**
- 13 References..... 83**
- Appendix A Calculation of the Area Captured in One Pixel 84**
 - A.1 Horizontal Length..... 84
 - A.2 Vertical Length 85

1 Introduction

Photogrammetry, the science of making measurements from images, has come to the fore together with the development of digital photography. The use of photogrammetry is also becoming more and more common in the field of surveying, where remote point measurements are becoming extremely important. A big advantage of photogrammetric measurements is that a big amount of data can be collected in the field in a very short time period. Total stations with an integrated camera have recently been enabling photogrammetric measurements by capturing images of object points from different stations. With an imaging sensor (e.g. Trimble V10) images can be taken from different locations called standpoints. The position of standpoints can be defined with geodetic measurements and the camera poses can be adjusted manually by the user. After the adjustment, object points can be measured photogrammetrically in captured images.

In order to make photogrammetric measurements even simpler, a camera was combined with a Global Navigation Satellite System (GNSS) sensor and an Inertial Measurement Unit (IMU) by Leica Geosystems AG. The components of the system were designed into a Functional Model (FuMo). The FuMo was designed for close-range terrestrial photogrammetric applications. In comparison to other imaging sensors that are used for such applications, the FuMo allows near real-time measurements that do not require any post-processing by user. There is no need for time-consuming positioning and orienting of the sensor in the place, like it is required while using total stations or other imaging sensors. That makes measurements with the FuMo much easier, faster, and even more accessible for the users without prior surveying or photogrammetric knowledge.

The FuMo is an imaging sensor that allows video capturing^[1] while moving along the object of interest. The GNSS measurements are taken while the camera captures a scene, so that the position of the sensor is defined at each moment when an image is captured. At the same time, the accelerations and the angular changes of the FuMo are measured by the IMU. Right after the measurements are taken, the GNSS and IMU data are processed and used to define the attitude of the sensor. The attitude of the sensor is used to define the initial camera poses from which the images were taken. The initial camera poses have to be adjusted in space, so that the optimal geometry between the images can be computed. The adjustment of the camera poses is processed by the algorithms implemented in the system. The camera poses are adjusted by the Structure from Motion and the Bundle Adjustment algorithms. After the adjustment, the images can be used for measurements of object points of the captured area.

The goal of geodetic measurements is to obtain point coordinates along with the level of uncertainty of the taken measurements. When measuring an object at a distance of 5 meters, the level of uncertainty of photogrammetrically measured points with FuMo should be in a range of up to 5 cm in addition to the GNSS point accuracy. Considering the accuracy requirements, such measurements can be used in numerous surveying applications, where the accuracy of a few centimetres is satisfactory. Measurements with the FuMo can also be used in forensics e.g. for the reconstruction of traffic accidents. Remote measurements with the FuMo can be performed photogrammetrically for object points, where the GNSS signal is not strong enough to perform Real Time Kinematics (RTK) measurements of ground points (e.g. under a bridge). In any case, the following two conditions have

^[1] Capturing images in defined time intervals

to be met. Firstly, the sensor needs access to the open sky to ensure good GNSS reception of the sensor. Secondly, measured object points should not be more than 10 m away from the sensor while capturing the images.

To investigate the capability of the measurements taken with the FuMo, test measurements were carried out under optimal environmental conditions. In order to do so, the characteristics of an appropriate test field were defined and the corresponding test field was established. The accuracy of the system was determined for the measurements taken from different camera-to-object distances.

Furthermore, the limitations of the system were defined. The measurements were therefore performed in the test field under real-use conditions. The images were captured at different light conditions and along different trajectories.

1.1 Goals of the thesis

This master's thesis was written in collaboration with Leica Geosystems AG in order to investigate the capability and limitations of the FuMo. The goal of this thesis was to contribute to the development of the sensor and, at the same time, to investigate the usefulness and practicability of the sensor under real use conditions.

The thesis summarizes how the sensor was developed, which components of the FuMo are crucial, and how they communicate with each other. The algorithms of image adjustments and measurements are explored to investigate how they influence the accuracy of photogrammetrically defined object points. Further components that influence the accuracy of photogrammetric measurements are explored. By performing the measurements in the test field, limitations of the system were investigated in order to achieve the best possible accuracy while measuring with the FuMo.

1.2 Introduction of the Terms

1.2.1 Bearing

The term bearing describes the movement of an object in motion. It is defined as the direction the FuMo is moving towards in respect to the geodetic north. The bearing of the sensor is presented in Figure 1.

1.2.2 Heading

Heading of the FuMo describes the direction the camera is pointing. The heading is expressed in respect to the geodetic north, as visualized in Figure 1.

1.2.3 Geodetic North Direction

The north direction serves as a reference direction for defining the bearing and heading. The north direction is defined with the respect to the ellipsoidal meridian, which is pointing along the Earth's surface towards the geographic North Pole. The geographic North Pole is defined by the point where the rotation axis meets the Earth's surface.

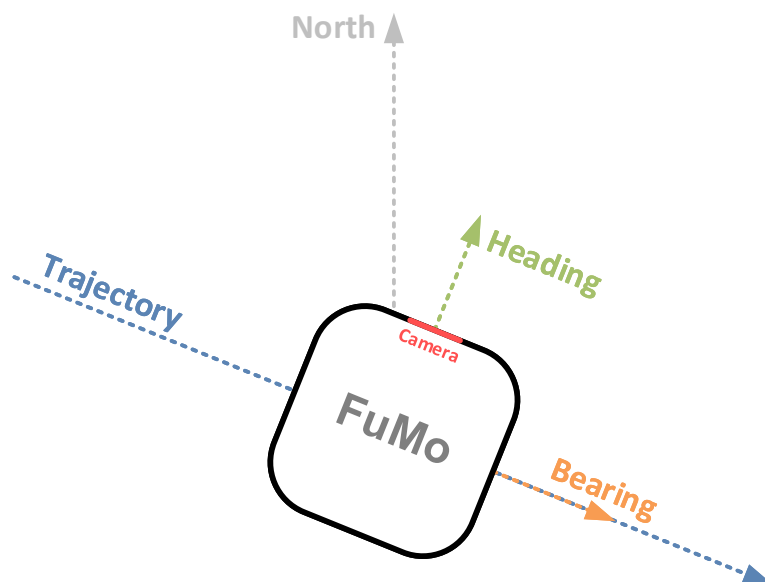


Figure 1: Heading and bearing of the FuMo

1.2.4 Attitude

The attitude describes how the FuMo is positioned in the space it is in. It is defined relative to the terrestrial coordinate system used for the measurements. The sensor is moving in the terrestrial coordinate system through translations and rotations. The attitude is described through three dimensional (3D) coordinates and 3D information of orientation. The reference point of the sensor's attitude is located at the antenna reference point (ARP).

The attitude of the sensor is defined through the GNSS and IMU measurements and it is used for defining initial camera poses.

1.2.5 Camera Pose

The camera pose from which an image was captured is defined using the sensor's attitude. The position and the orientation of captured images are determined by GNSS and IMU measurements. The position and the orientation together present the camera pose in the terrestrial coordinate system.

The reference point of the camera pose is defined in the perspective centre of the camera in the moment when the image was captured.

1.2.6 Epipolar Lines

The epipolar plane is a plane which is defined with the object point P and the perspective centres O' and O'' . The epipolar plane is depicted in Figure 2.

The epipolar line is a straight line that coincides with the line that presents the intersection of the epipolar plane with the image plane. When the image point p' is defined in the first image plane of the stereo pair, the image point p'' can be found in the second image plane along the epipolar line defined in the second image.

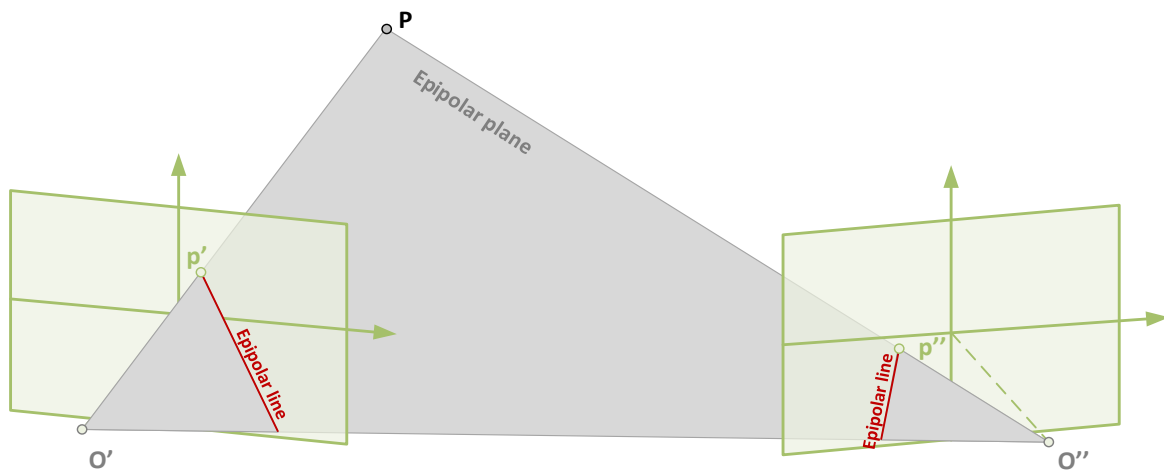


Figure 2: Epipolar line

1.2.7 Camera-to-Object Distance

While capturing images with the sensor, the camera-to-object distance represents the distance between the perspective centre of the camera and the measured object point. The camera-to-object distance is visualized in Figure 3.

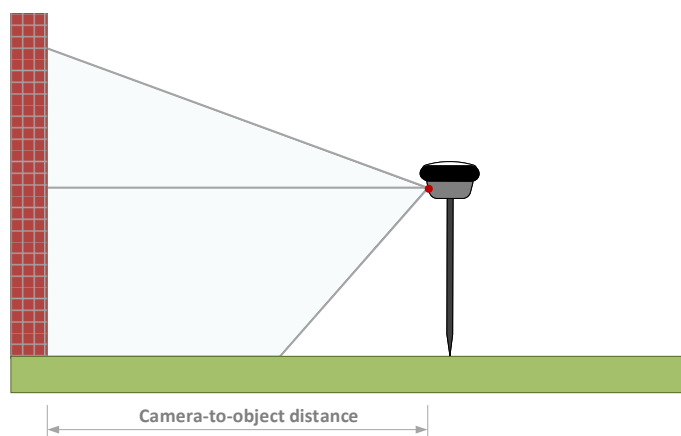


Figure 3: Camera-to-object distance

1.2.8 Object Point

The object point P is a point that is captured in the image as image point p (see Figure 4). The 3D coordinates of an object point can be reconstructed from 2D image points. The object point is defined in a terrestrial coordinate system with its 3D coordinates.

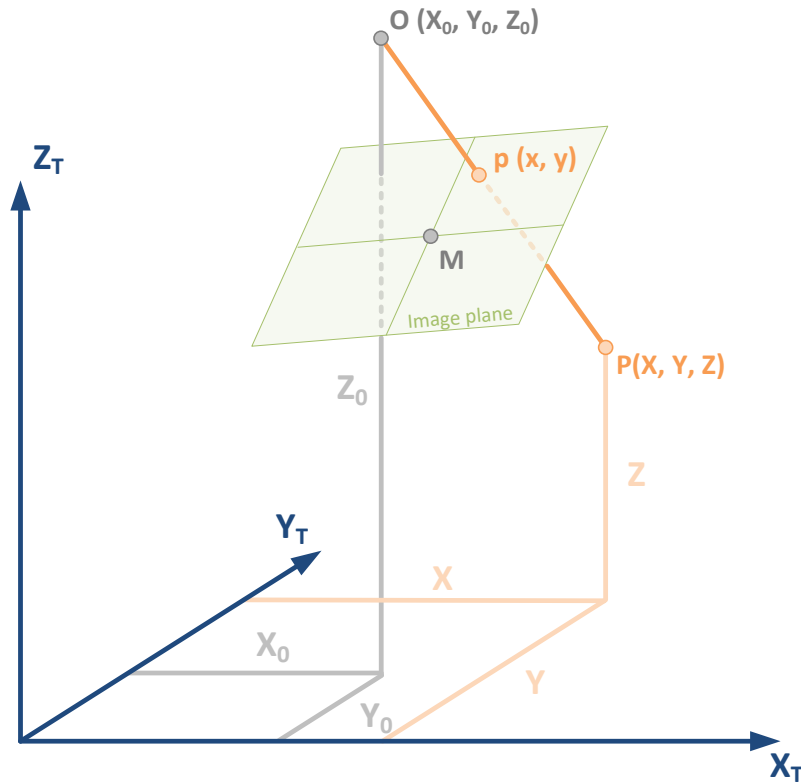


Figure 4: Object point P in a terrestrial coordinate system

1.2.9 Image Coordinate System

The image point is the object point captured in the image. An image point p is a point defined in the image coordinate system with a two dimensional (2D) Cartesian coordinates x and y . The origin of the image coordinate system is located at the centre of the image M . The image point p and the image coordinate system with its x and y axis are depicted in Figure 5.

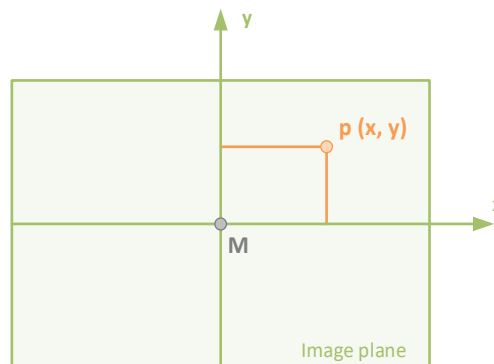


Figure 5: Image point p defined in the image coordinate system

1.2.10 Terrestrial Coordinate System

The terrestrial coordinate system is used to determine the location of object points on the Earth's surface. The location of object points is defined by 3D coordinates. A terrestrial coordinate system can be either local or global. It can be defined by the user.

1.2.11 Global Object Coordinate System

The global object coordinate system is defined with respect to the FuMo. It is used to define how the single components of the FuMo are located and oriented inside the sensor.

The origin of the global object coordinate system is located in the ARP and it is oriented as visualized in Figure 6. The axes are oriented as described below:

- X-Axis: pointing along the bottom of the sensor towards the side where the battery chamber is located
- Y-Axis: pointing along the bottom of the sensor towards the side where the camera is located
- Z-Axis: pointing towards the GNSS antenna, passing through the geometrical centre of the sensor

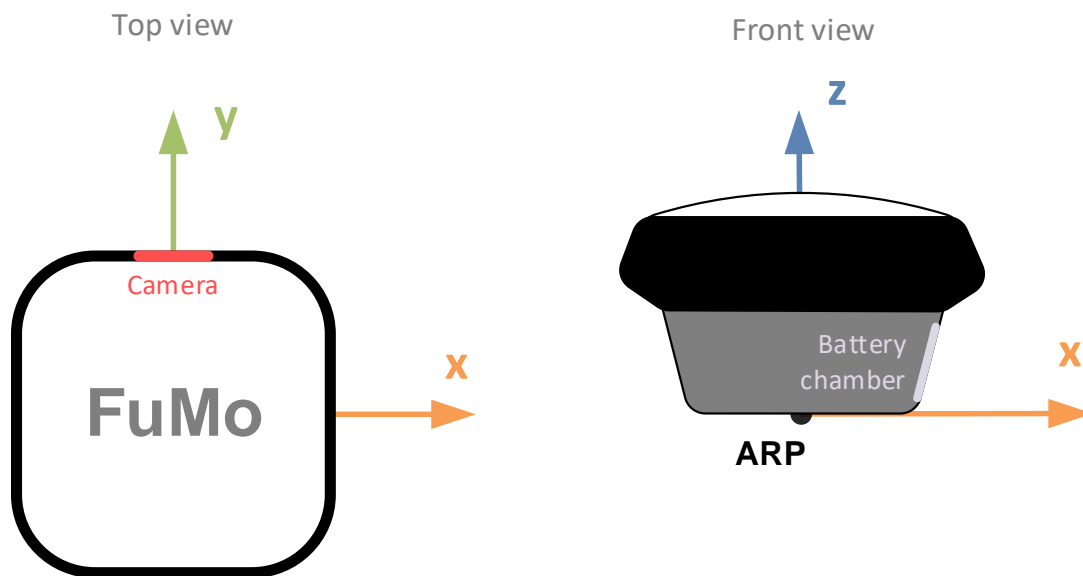


Figure 6: Global object coordinate system

1.3 Existing Knowledge

The fundamental principle of remote point measurements using photogrammetry is a known technique that has already been used in practice for decades. Numerous publications describing the use of close-range terrestrial photogrammetry have been published, e.g. Hagan (1980), Fussell (1982) and Hilton and Bales (1985). The methods for adjusting camera poses in space and the approaches for automatic feature-based object detection are already implemented in many photogrammetrically-based computer programmes.

A new approach that combines a near real-time photogrammetric adjustment of the images using GNSS and IMU measurements has been developed by Leica Geosystems AG. The FuMo uses remote point surveying to define new object points. The initial camera poses from which the images were captured are determined using a combination of IMU and GNSS measurements. An adjustment to determine the best approximation of camera poses is performed using algorithms implemented in the system. The technology is already developed and ready to be tested, therefore the measurements can already be carried out for detailed investigations.

2 State of the Art in Terrestrial Remote Point Measurements

Remote point measurements are of great importance in the field of surveying. The coordinates of object points and the dimensions of objects can be obtained through the measurements without a physical contact of a measuring device with the object. Terrestrial remote point measurements can be performed by means of photogrammetry, trigonometry or the combination of angular measurements with the electronic distance measurements. Many different systems that enable remote point measurements are already available on the market. Some of them are described in the following sections.

2.1 Remote Point Measurements Using Total Stations

A total station is an electro-optical instrument which is used for surveying. The total station is an electronic theodolite with an integrated electronic distance meter (EDM).

The advantage of total stations is that the remote point measurements can be performed with high accuracy and precision. The relative accuracy of the remote point measurements inside a local coordinate system can reach up to 1mm. Therefore, it can be used in the field of engineering surveying or civil engineering, where the highest accuracy and precision of point measurements is demanded.

On the other hand, a big disadvantage is time-consuming positioning and orienting of the total station, which has to be done before the measurements are taken. The instrument has to be set up at one point and the measurements can be performed from that point on only. If the instrument is moved in order to measure additional points that were not visible from the first set up, it has to be set up again before performing the measurements. In addition to that, the sensor alone can weigh 8 kg or more. There is also additional equipment needed in order to operate with the sensor. This makes it difficult to transport and difficult to set it up as well.

2.2 Remote Point Measurements Using Laser Scanners

Laser scanners can be used for remote point measurements as well. The sensor has to be set up so that the surrounding environment can be captured. At each measured horizontal and vertical angle, the distance to the object is obtained. The distance can be obtained by e.g. measuring the time needed for a laser beam to travel from the sensor to the object and back.

The laser scanners can record a great amount of data in a very short time period, which can be used for measuring the dimensions of the captured object or the surrounding environment. Laser scanners can also be positioned and oriented in a terrestrial coordinate system. Therefore, the coordinates of object points can be measured in the scan. However, the coordinates of the object points cannot be measured directly with the device. The scan has to be imported to the computer, where the data can be used to calculate coordinates from the measurements.

The scans can be used for calculating the volume of the objects. They can therefore be used in the fields of archaeology, architecture, civil engineering, monitoring, forensics, etc.

Laser scanners are not specially designed for single point measurements. In spite of this, the coordinates of single points can be obtained from the scan, but the point coordinates obtained from the scan can be determined with only a centimetre accuracy.

The laser scanners need to be stationary when performing the measurements. If additional measurements are required, the laser scanner has to be set up at another location. That can be a big disadvantage of a system, since the average laser scanner weigh about 6 kg. There is also additional equipment needed in order to operate with the sensor, which makes it difficult to transport and difficult to set it up as well.

2.3 Remote Point Measurements Using Photogrammetry

The object points can also be obtained photogrammetrically in a terrestrial coordinate system. Some systems enable capturing the images and simultaneously measuring the position of captured images. The position of the images can be defined:

- by capturing the images from the ground points with known coordinates,
- by defining the position of the sensor with geodetic methods (e.g. camera with an integrated GNSS antenna) or
- by determining the position of the images in post-processing.

Without regard to how the position of the images is determined, the images have to be processed afterwards in order to define the orientation of the images. The processing can be done manually or half-automatically with the help of the corresponding computer programmes. In many cases, the processing of captured images can be costly and time-consuming.

The advantage of the photogrammetric measurement is that the extra points of the captured object can be measured at any time in the future. There is also a lot of information captured in a short time interval, which makes field work much simpler.

In contrast to the total stations and laser scanners, the camera can be moved while capturing the images. The camera does not need to be set up at every point where an image is captured. This reduces the time spent in the field significantly.

The coordinates of object points can be measured with centimetre accuracy, and can therefore be used in numerous surveying applications, architecture, forensics, and so forth.

The size and the weight of such sensors vary a lot. There are some systems that can weigh up to 6 kg or more (e.g. Trimble V10 with the Trimble R10 and the Yuma tablet).

3 Functional Model

The FuMo (shown in Figure 7) developed by Leica Geosystems AG is a GNSS sensor with an integrated IMU and additional camera. The position of the device can be estimated with the help of GNSS measurements. The IMU provides the orientation information of the device in space. In addition to that, the global shutter camera captures a scene while the device moves along an object. That enables photogrammetric measurements of object points in the captured images.



Figure 7: FuMo consisting of GNSS antenna and receiver, IMU and camera

Due to the integrated IMU in the GNSS sensor, the information about the attitude of the sensor can be provided. In addition to that, the camera, in combination with the GNSS and IMU sensor, enables remote point measurements of object points located in the area where the GNSS sensor itself cannot ensure accurate measurements. The FuMo is designed to be used in an area where it is more convenient to measure in images.

3.1 Measurement Principle

The fundamental principle of capturing an object with the FuMo is depicted in Figure 8. While moving along a trajectory, the sensor captures one image at each epoch t_i . At the same time, the attitude of the sensor is defined through GNSS and IMU measurements.

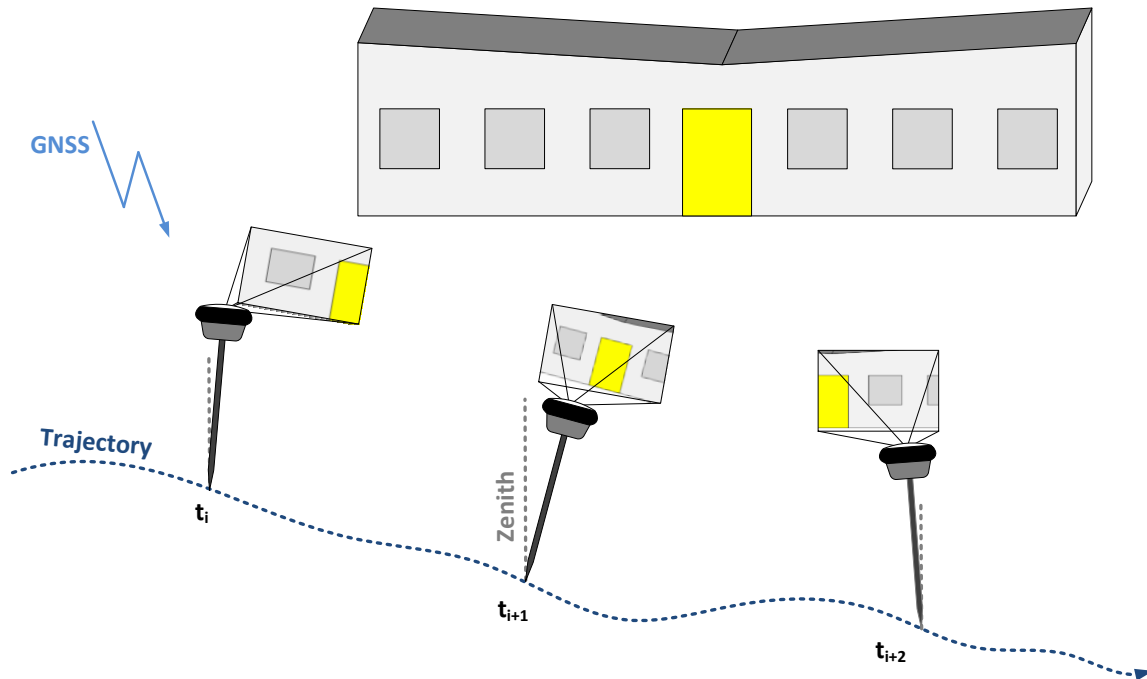


Figure 8: Measuring principle with the FuMo

To be able to perform photogrammetric measurements in the images, the camera poses have to be adjusted in space. In order to adjust camera poses, the attitude of the sensor is used to define initial camera poses. The adjustment of the camera poses is then processed automatically by the algorithms implemented in the system, so that the best possible geometry between the images is defined. The photogrammetric measurements of object points can be performed from the adjusted images right after the scene has been captured and the adjustment of the images has been done. Object points can be photogrammetrically measured in images with an uncertainty of 5 cm in addition to the GNSS measurement accuracy.

3.2 Application Areas

The idea of a new imaging sensor combined with a GNSS and an IMU sensor is to simplify surveying and to make measurements in difficult conditions more accessible (e.g. in areas where GNSS signal reception is not sufficient to perform accurate GNSS measurements). The imaging sensor is based on close-range terrestrial photogrammetry with a range from 0.5 m to 10 m. According to Luhmann et al. (2014, p. 14-17), close-range photogrammetry is potentially useful when:

- it is not certain what measurements are required;
- the use of direct measurements would influence the measured object;
- the measurement of a very large number of points is required.

While performing image based measurements, an enormous amount of data can be captured in a short time interval. This makes it possible to always have access to the captured scene. Therefore, extra points can be measured from the images at any time.

Due to the GNSS sensor with an integrated IMU and additional camera, the FuMo can be used to simplify the following tasks:

- measurements of objects of interest located on the façade of a building (e.g. doors, windows, etc.);
- measurements of points that are difficult to access (a pipeline, an open trench, points behind a fence, ect.);
- measurements of corner points of a building;
- measurements of points located under overhanging constructions;
- measurements of points located under a bridge;
- measurements of points located close to a forest;
- measurements of points located under a tree;
- reconstruction of traffic accidents;
- recording of ancient cities, where the physical contact is not appreciated or allowed;
- and many others.

3.2.1 Limitations of the System

Photogrammetric measurements taken with the FuMo are strongly connected to GNSS and IMU measurements, which provide information about the initial camera pose from which the images were captured. The position is defined using the GNSS measurements. Therefore, it is crucial that the sensor has a good GNSS signal reception during the whole period of video capturing.

While capturing the images with the sensor, it has to be moving constantly. Firstly, there is an algorithm implemented in the system that estimates the attitude of the sensor using GNSS and IMU data. On the basis of all the data, the algorithm additionally estimates the IMU error (e.g. bias of the sensor). As long as the sensor is moved around, the gyroscope and accelerometer bias can be estimated and therefore the heading drift is minimized. If the sensor is static for more than a few seconds, the algorithm cannot estimate and correct the drift anymore.

Secondly, photogrammetrically defined points can reach an optimal level of uncertainty when some conditions are fulfilled. For instance, as described in Section 4.3, the geometry of the captured images used for photogrammetric measurements plays a big role. The sensor does not take pictures from different standpoints, but it captures a video while constantly moving along a trajectory. That way it is ensured that the object is captured from different points of view. It is thus crucial that the sensor is moved along an object while capturing the images.

The algorithm, which is used for adjustment of the camera poses, is implemented in the system. It automatically recognizes features in the captured images. Due to this algorithm, there have to be enough distinguishable details recognized in the captured images in order to link the images with each other. The camera poses of the images which do not have enough recognisable features can for that reason not be adjusted and the remote point measurements can therefore not be performed. Based on this, it is crucial that the right amount of light is available while capturing images with the FuMo.

3.3 Main Components of the FuMo

The imaging sensor FuMo can calculate the coordinates of object points by using a combination of geodetic and photogrammetric methods. To ensure that all the data is provided, the three main components should be presented in a system. All the components have to communicate with each other to ensure the best possible solution of newly defined point coordinates. These components are as follows:

- **GNSS antenna and receiver** – it provides the position information of the sensor at each moment of measurements. The antenna receives the signals from the Galileo, GPS, GLONASS and BeiDou satellites. The GNSS receiver can process the correction data either from a local reference station or from a reference station network.
- **IMU** – it consists of accelerometers, gyroscopes, and magnetometers and provides information about the lateral and angular movement of the sensor, as well as the magnetic field of the FuMo. Together with GNSS data, the IMU provides the attitude of the sensor. The attitude of the sensor is used to define initial camera poses. The point coordinates defined from photogrammetric measurements can therefore be performed in a desired terrestrial coordinate system.
- **Camera Sensor** – with a fixed frequency of 10 Hz, it captures the images of the object during the defined period. The camera is based on the principle of the global shutter, which ensures that the captured images are not distorted (like by e.g. rolling shutter).

The algorithm implemented in the system starts estimating camera poses using the captured images and the attitude of the sensor already during the process of capturing of the images. The time for estimating the camera poses is dependent on the length of the capturing period. The estimation is finished several seconds after the capturing of the object is done. New object points of the captured scene can therefore be measured in the images in near real-time.

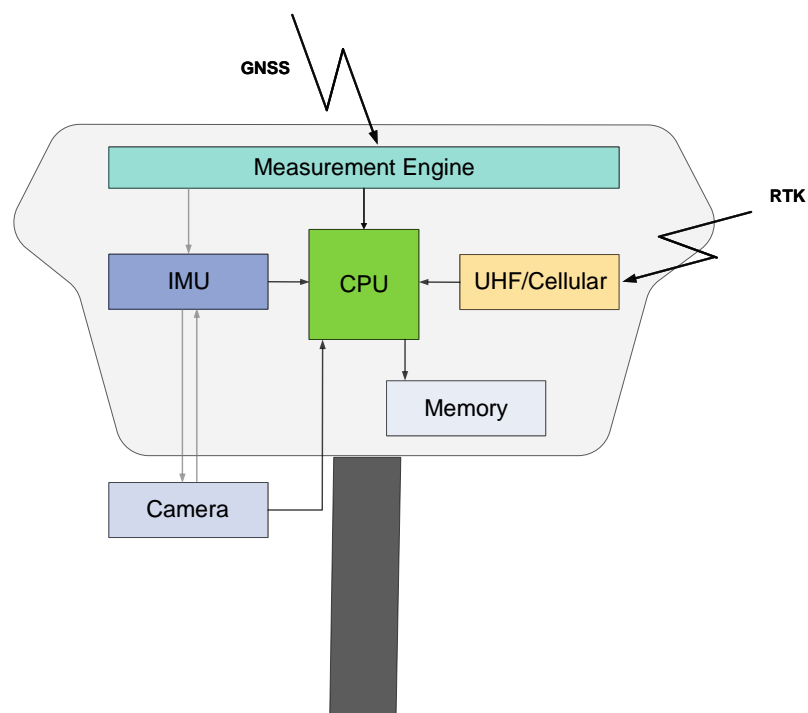


Figure 9: Main components of the FuMo

In Figure 9 it is visualized how all three main components of the FuMo communicate with each other and with the Central Processing Unit (CPU). At the same time the CPU receives RTK data from the Cellular Internet connection or UHF radio signal. The CPU is responsible for the processing of data. The measurements and the images taken with the FuMo are constantly saved to a SD card.

3.4 Camera specifications

When using images for photogrammetric measurements, it is crucial that there is minimal distortion presented in the captured images. A light-sensitive sensor that exposes light to all photosites simultaneously is suitable for remote point measurements in images. A photosite is a key element of each pixel. It is capable of registering red, blue or green colour. With the combination of one red, one blue, and two green photosites the true colour of one pixel is defined. The global shutter exposes light to all the photosites at once so it is ensured that the whole scene is captured at the same time. A camera using a global shutter is therefore integrated in the sensor, ensuring the best possible quality of captured images.

A Complementary Metal Oxide Semiconductor (CMOS) sensor is used to convert captured light into an electric charge and then process it into an electrical signal. Each pixel of a CMOS image sensor has its own amplifier and digitizer unit attached to it. The charge transfer can therefore be simultaneous, as individual sensor elements operate at the same time.

4 Photogrammetry

Photogrammetry is the science of making measurements from one or more images. According to Kraus (2007, p. 1), “the position, orientation, shape and size of objects can be reconstructed from pictures”. Reconstruction of an object using images can be done without physical contact with the object. The 3D position of an object point can be calculated from 2D coordinates of the same object point defined in different images. An example of two images that can be used for photogrammetric reconstruction of an object is shown in Figure 10.



Figure 10: Images used for photogrammetric measurements

4.1 Close-Range Terrestrial Photogrammetry

Photogrammetry as a science has been used in many different applications. When the measurements from the images that are taken on the ground are used for surveying, we are speaking about terrestrial photogrammetry. When those images are taken with a camera-to-object distance between 0.1 m and 100 m, the term close-range terrestrial photogrammetry can be used.

In order to define coordinates of object points remotely, the FuMo uses close-range terrestrial photogrammetry.

4.2 Fundamental Principle of Remote Point Capturing Using Images

Photogrammetry uses pairs of stereo images to measure 3D coordinates of new object points. According to Li et al. (2005, p. 36), the stereo pair “refers to two images of the same scene photographed at two slightly different places so that they have a certain degree of overlap.”

The position of an object that is measured from images involves estimating 3D coordinates of object points. Those points are defined using triangulation, as depicted in Figure 11. The images used for the photogrammetric measurements have to be correctly positioned and oriented in space. When this condition is met, new object coordinates can be defined through the intersection of image rays.

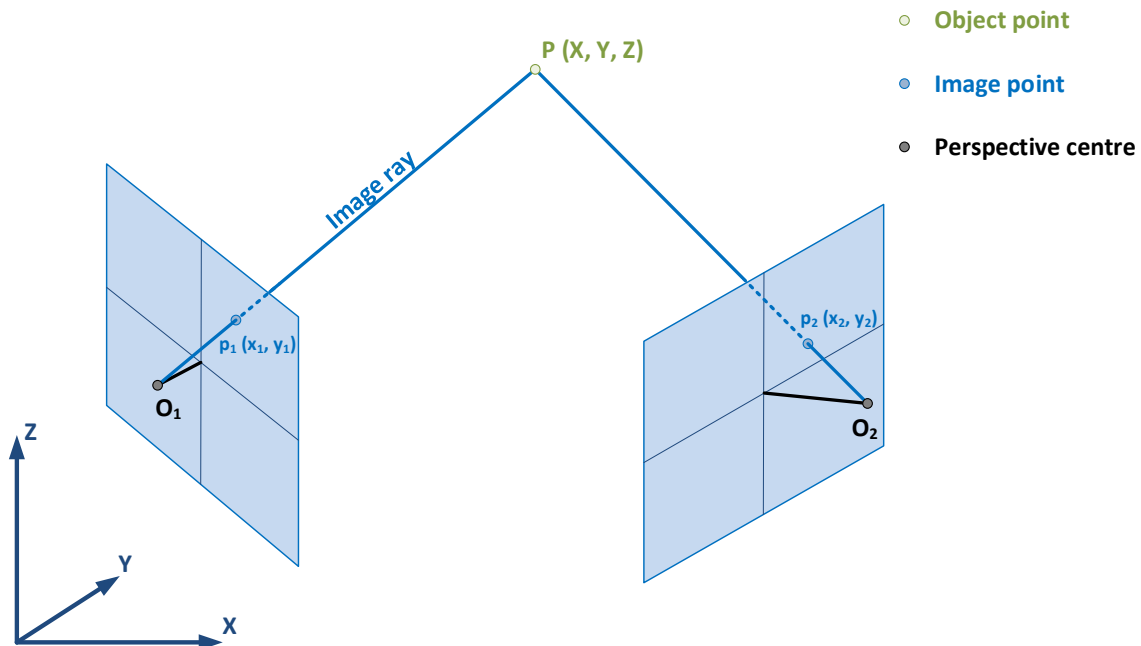


Figure 11: Fundamental principle of photogrammetry using a stereo pair

The image rays are developed to calculate object coordinates. Image rays are straight lines that pass through the image point p_i and the perspective centre O_i of each image i . At the intersection point, the object point P is reconstructed and defined by its 3D coordinates. That is how new object points are defined using photogrammetry.

4.2.1 Exterior Orientation

The exterior orientation consists of six parameters which describe the spatial position and orientation of the camera with respect to the global coordinate system (Luhmann, 2014). The global object coordinate system is described in Section 1.2.11.

As shown in Figure 12, the spatial position of the perspective centre O is defined by 3D coordinates (X_0, Y_0, Z_0) in the global object coordinate system. The three suitably defined angles ω , φ , κ are expressing the rotation of the image coordinate system with respect to the global object coordinate system (Luhmann, 2014).

The exterior orientation of the camera inside the FuMo is defined with respect to the global object coordinate system. The X_0 , Y_0 and Z_0 coordinates and ω , φ , κ angles present 6 Degrees of Freedom (DoF) and represent how the camera is positioned and oriented inside the FuMo.

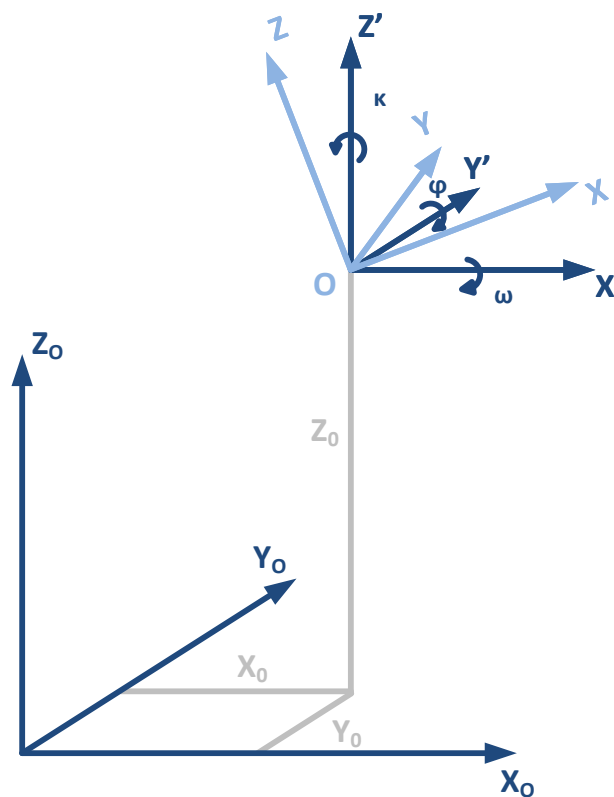


Figure 12: Exterior orientation of the camera in the global object coordinate system

4.2.2 Interior Orientation

The parameters of the interior orientation serve to establish the relationship between the global object coordinate system and the image coordinate system. The parameters that are known as elements of the interior orientation of a camera are the principal distance c and the image coordinates of the principal point PP (ξ_0, η_0). The parameters of the interior orientation are presented in Figure 13 in a terrestrial coordinate system. The internal parameters of a mathematical-geometric model intend to describe the internal geometry of a camera. The internal parameters are determined by camera calibration.

The **Principal point PP** represents the mathematically defined origin of the image coordinate system. The mathematical definition of the principal point is the basis of triangulation and cannot be defined optically. The point is defined with x_0 and y_0 coordinates, measured from the centre of the image M , as visualized in Figure 14.

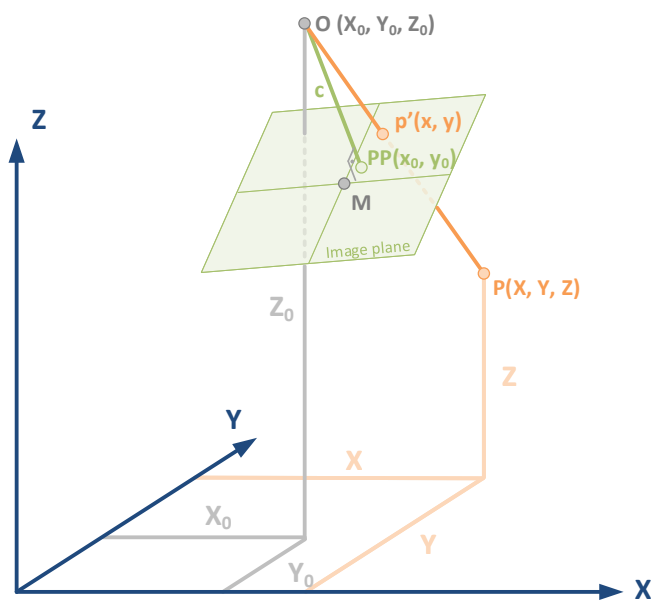


Figure 13: Relationship between the image and object coordinates in a terrestrial system

Principal distance c is the distance between the image plane and the perspective centre O . The position of the perspective centre is defined in the global object coordinate system. It is defined using X_0 , Y_0 and Z_0 coordinates as parameters of exterior orientation.

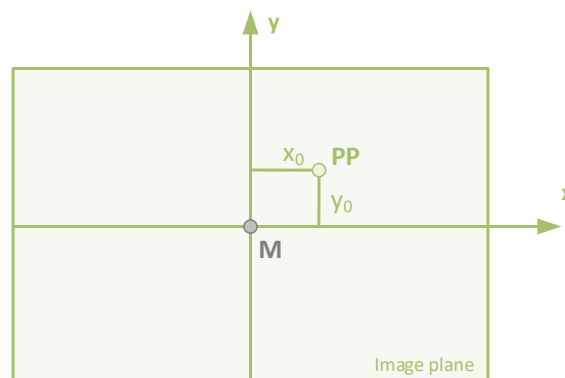


Figure 14: Principal point defined by two parameters of interior orientation

4.2.3 Structure from Motion (SfM)

According to Ullman (1979) and Szeliski (2010, p. 345), the locations of 3D points and camera poses can be estimated from multiple images, given a set of correspondences between image points. This process, which involves simultaneously estimating both 3D object points P (structure) and camera pose (motion), is commonly known as SfM.

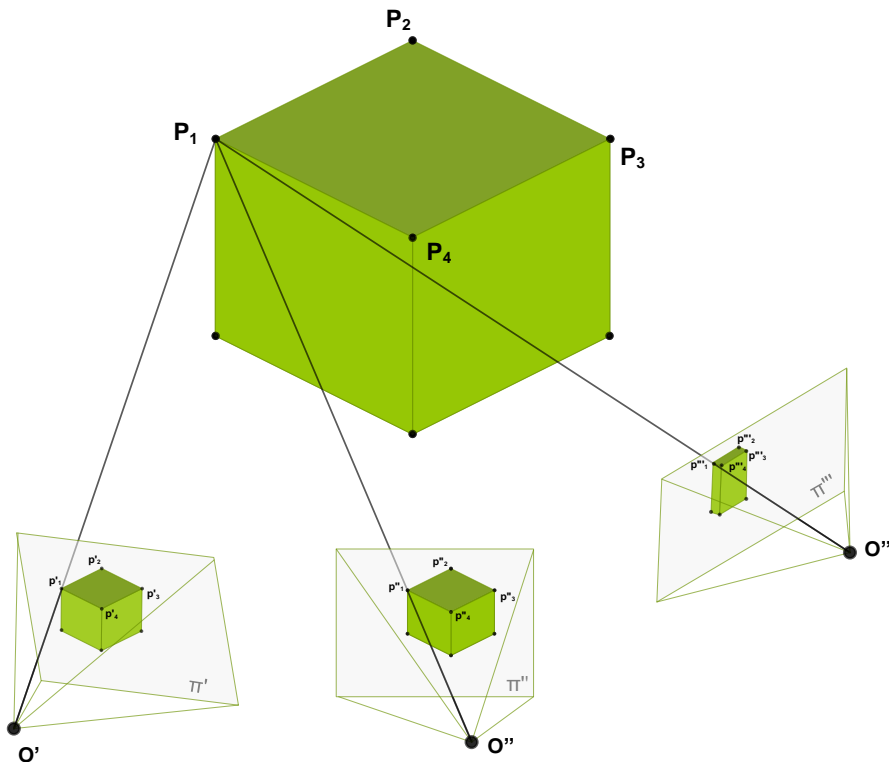


Figure 15: The principle of SfM algorithm

During the process of SfM the 3D object points are reconstructed and camera poses are determined. As visualized in Figure 15, the problem is solved in the following steps:

- the images of an object are taken from different perspectives;
- features p_j (e.g. edges, corners etc.) are identified in the first image π' ;
- the same features p_j are defined in other images π'' , $\pi''' \dots$;
- camera poses and object points P_i are calculated by intersecting the image rays of corresponding features.

Due to the measurement uncertainties and other effects that influence the measurements and captured images, the image rays can never intersect perfectly. Therefore, the defined camera poses and object points are not optimized to fit in the best possible way. In order to do so, the Bundle Adjustment algorithm optimizes camera poses and object points to meet the optimal intersection of image rays.

The processing of the Structure from Motion algorithm is explained using a practical example in Section 5.2.2.

4.2.4 Bundle Adjustment

Luhmann (2014, p. 322-323) describes Bundle Adjustment as “a method for the simultaneous numerical fit of an unlimited number of spatially distributed images (bundle of rays).” The Bundle Adjustment is an iterative method that can reconstruct a wide range of data. During the process, the optimal solution is found to intersect image rays with a minimum uncertainty presented.

The Bundle Adjustment uses features defined in single images and their corresponding object points to estimate the camera poses. During the process, the relation between single images and object point coordinates is iteratively optimized.

The processing of the Bundle Adjustment algorithm is explained using a practical example in Section 5.2.3.

4.3 Geometry

The geometry of the images is one of the most important factors while measuring object points photogrammetrically. With the appropriate geometry, the uncertainty of measured object points can be reduced and therefore much better accuracy can be estimated.

In order to measure object point coordinates, the image points of the object have to be determined in image planes. Each image point p is defined with its coordinates x, y and it also carries the information about its uncertainty (see Figure 16). The factors that influence the uncertainty of image points are discussed in Section 6.2.

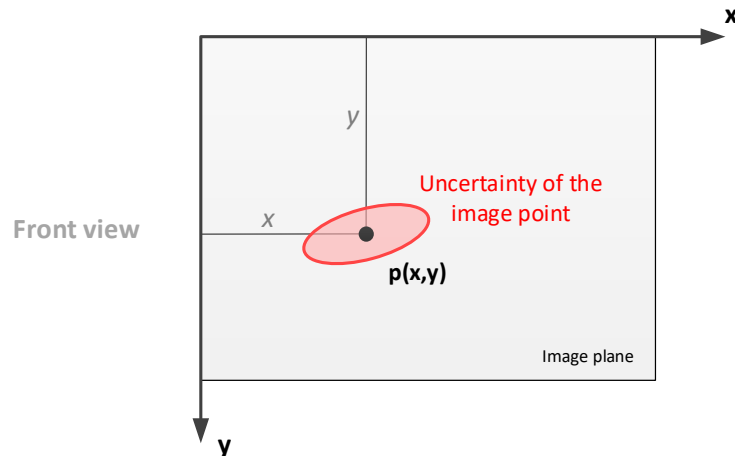


Figure 16: The coordinates and the uncertainty of the image point

An image ray is defined with an image point p and passes through the perspective centre O (see Figure 17). The position and the orientation of a perspective centre in a terrestrial coordinate system are defined with the camera pose (see Section 5.2). As visualized in Figure 17, the uncertainty of image point coordinates translates along the image ray.

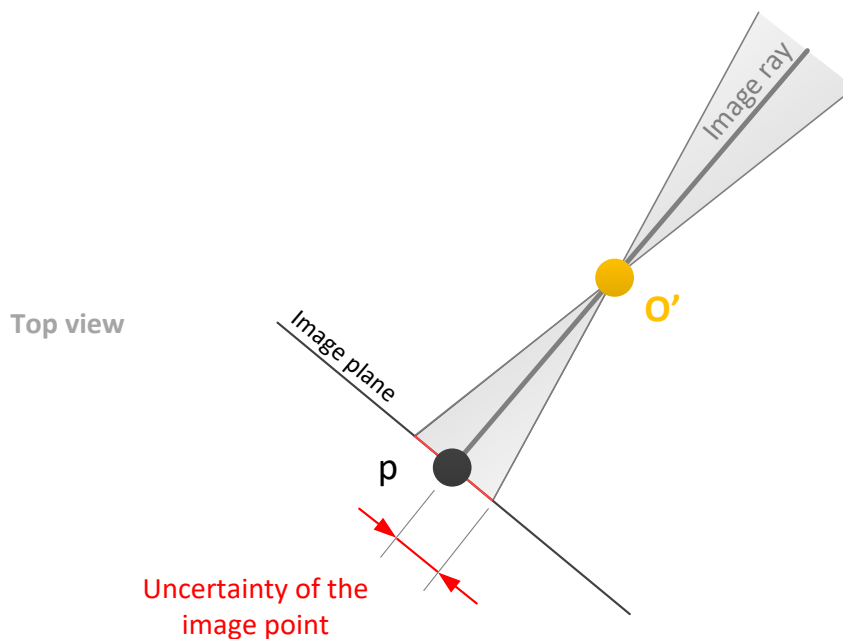


Figure 17: The uncertainty of the image point is translated along the image ray

Nevertheless, the perspective centre O is defined with its X_o, Y_o, Z_o coordinates in the terrestrial coordinate system. The perspective centre also carries the information about its uncertainty (see Figure 18). The factors that influence the uncertainty of the perspective centre are listed in Section 6.1. The uncertainty of an image point and the uncertainty of a perspective centre are translated along the image ray as visualized in Figure 18 and Figure 19.

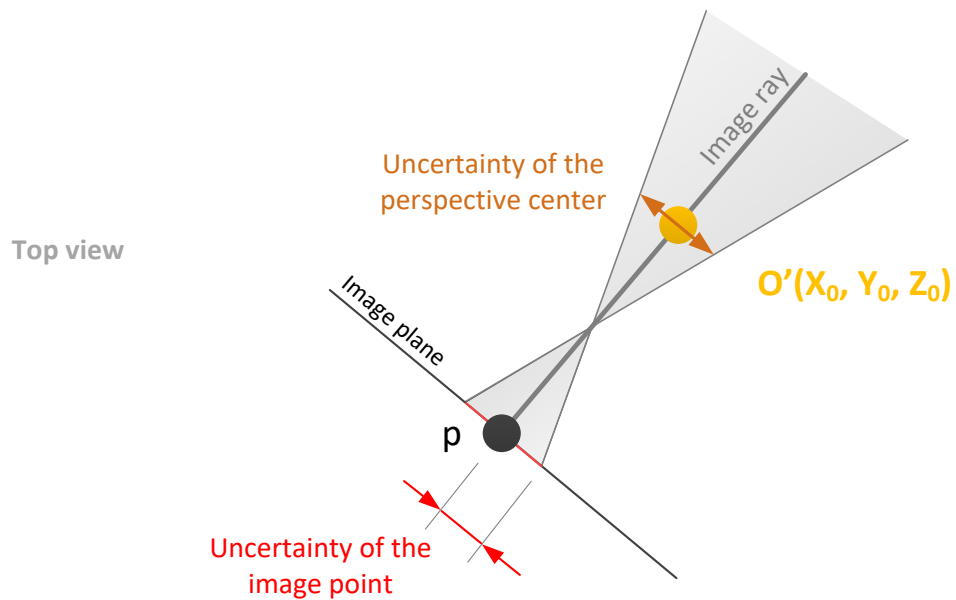


Figure 18: The uncertainty of the perspective centre

At the intersection point of image rays, the object point P is defined with its space coordinates X_p, Y_p, Z_p . The object point P also carries the information about its uncertainty, which is defined by the intersection of the uncertainties of two or more image rays (see Figure 19).

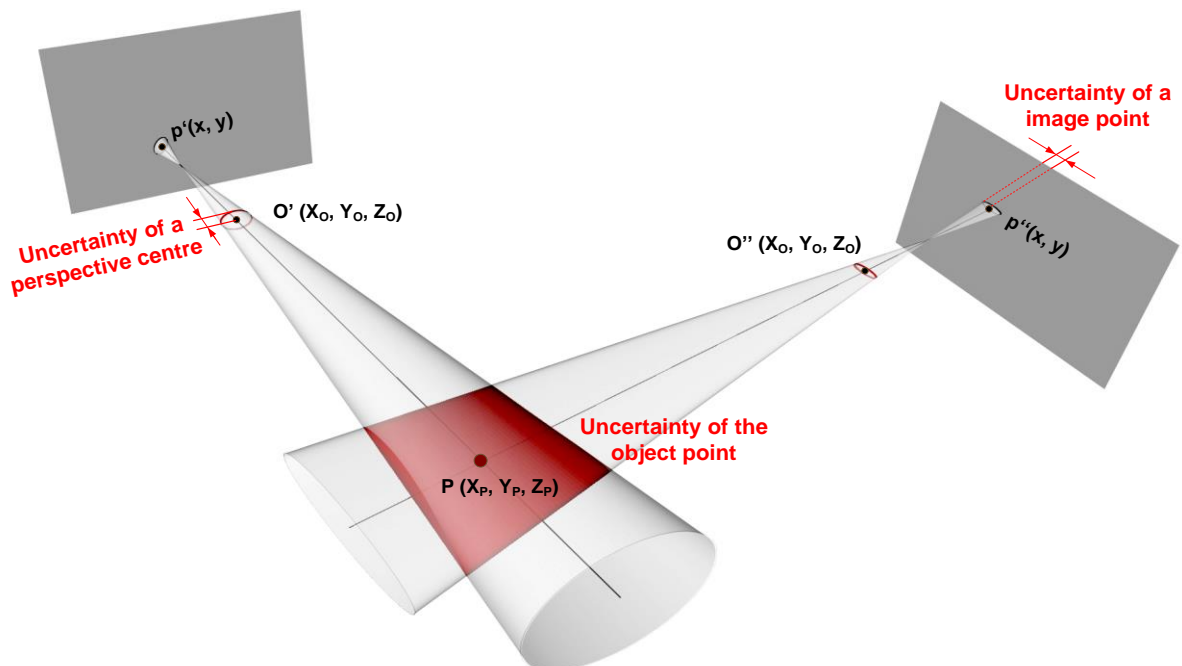


Figure 19: Space intersection of two image rays and their uncertainties

The uncertainty of the object point P depends on the uncertainty of the perspective centre O and the uncertainty of the image point p . While measuring with the FuMo, the uncertainty of the reconstructed object point P can be reduced by the factors described in Section 6.1 and in Section 6.2.

In addition to that, with appropriate geometry, the uncertainty of object points can be reduced while performing measurements with the sensor. The uncertainty of the object point can be reduced by optimizing the angle between two images and the measured object point. The distances from both cameras to the measured object point also contribute to the uncertainty of measured object points. The accuracy of the measured object point P can additionally be reduced also by increasing the number of images taken from different standpoints. In the following sections it is described how the uncertainty of the object point P can be reduced through the optimal geometry between the camera poses and the object point.

For better interpretation, the schemas in the following sections are visualized from the top view only.

4.3.1 Intersection Angle

Every object point P carries the information about its uncertainty. The uncertainty of the object point P is defined by the intersection of uncertainties of both image rays. As visualized on the left side of Figure 20, good intersection geometry is achieved when the rays are intersected at 90° . In this case, the intersection of uncertainties of image rays defines the smallest uncertainty of the object point. The more the angle between the two images and the measured point differs from the optimal angle of 90° , the bigger the uncertainty of the object point P is presented. Poor intersection geometry is visualized on the right side of Figure 20.

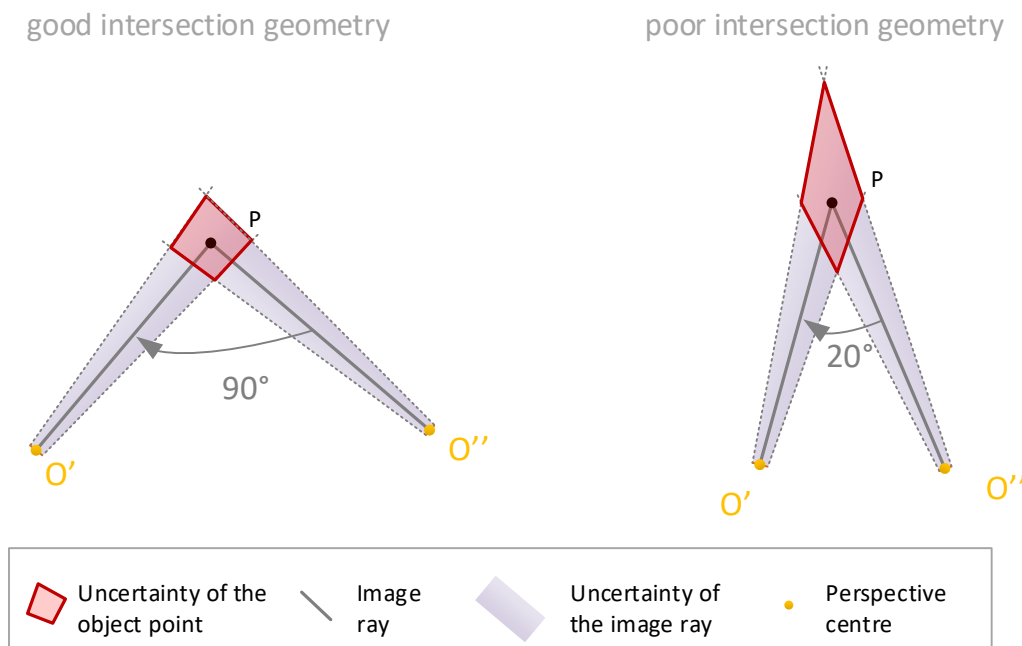


Figure 20: The influence of the angle between both images and the object point on the accuracy of photogrammetric measurements

4.3.2 Camera-to-Object Distance

The distance between both cameras and the measured point has a big influence on the accuracy of the measurements as well. As depicted in Figure 21, the bigger the distance between one camera and the object is, the bigger the level of uncertainty of the object point. The uncertainty of the object point P can therefore be improved by reducing the distance between the object point and the camera capturing the images.

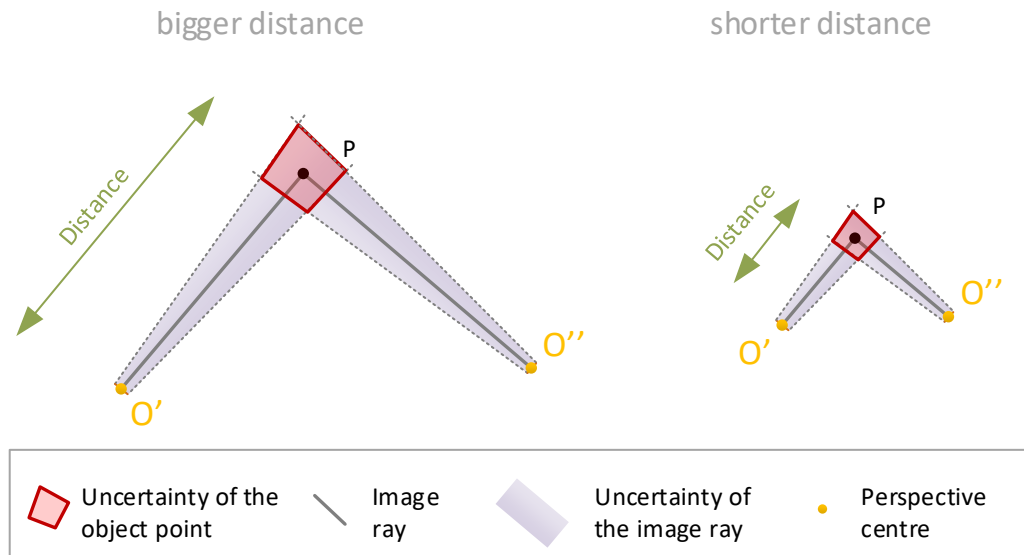


Figure 21: Influence of the camera-to-object distance on the accuracy of photogrammetric measurements

4.3.3 Number of Images

By increasing the number of images taken from different standpoints, the uncertainty of an object point measured from the images can be improved. All the image rays intersect at object point P , along with the uncertainty of the image rays. As shown in Figure 22, each ray with its uncertainty contributes to reducing the uncertainty of the object point P . This means that by increasing the number of images taken from different locations, which are used to define new object points, a smaller uncertainty of the object point P will be achieved.

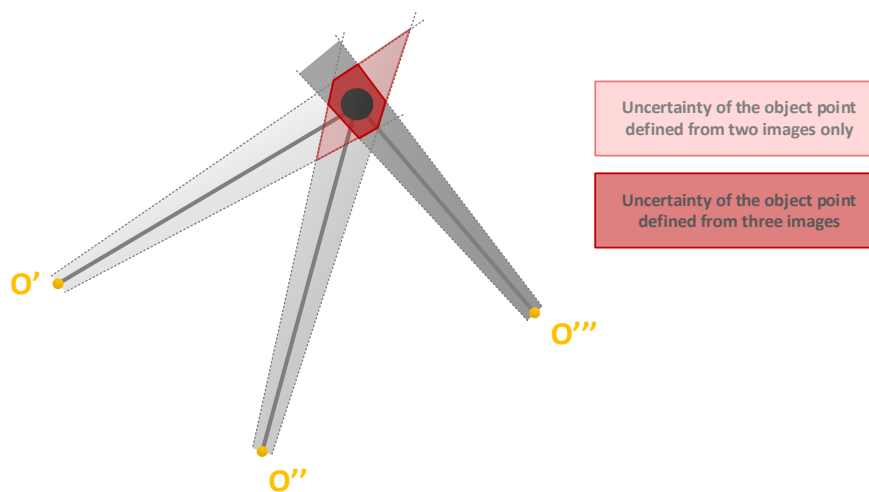


Figure 22: Improved accuracy of photogrammetric measurements through the measurements in multiple images

5 Processing of the Data

The images are captured with the FuMo, while the position and orientation of the sensor are being measured. In order to accurately determine the attitude of the sensor at every moment when an image is captured, the camera has to be synchronized with the GNSS sensor and the IMU. The attitude of the sensor is then used by the algorithms to determine the camera poses from which the images were captured. After the camera poses are determined, the coordinates of object points can be measured in the images.

5.1 Communication between Main Components

As visualized in Figure 23, the FuMo consists of three main sensors that take measurements or capture images. All three sensors are connected to each other. At the same time, they communicate with the CPU as well.

As described in Section 5.2.2, the initial camera poses from which the images were captured, are defined using processed GNSS and IMU measurements. Therefore, it is of great importance that the measurements taken with the GNSS and IMU sensors are synchronized with the time stamp of the images taken with the camera.

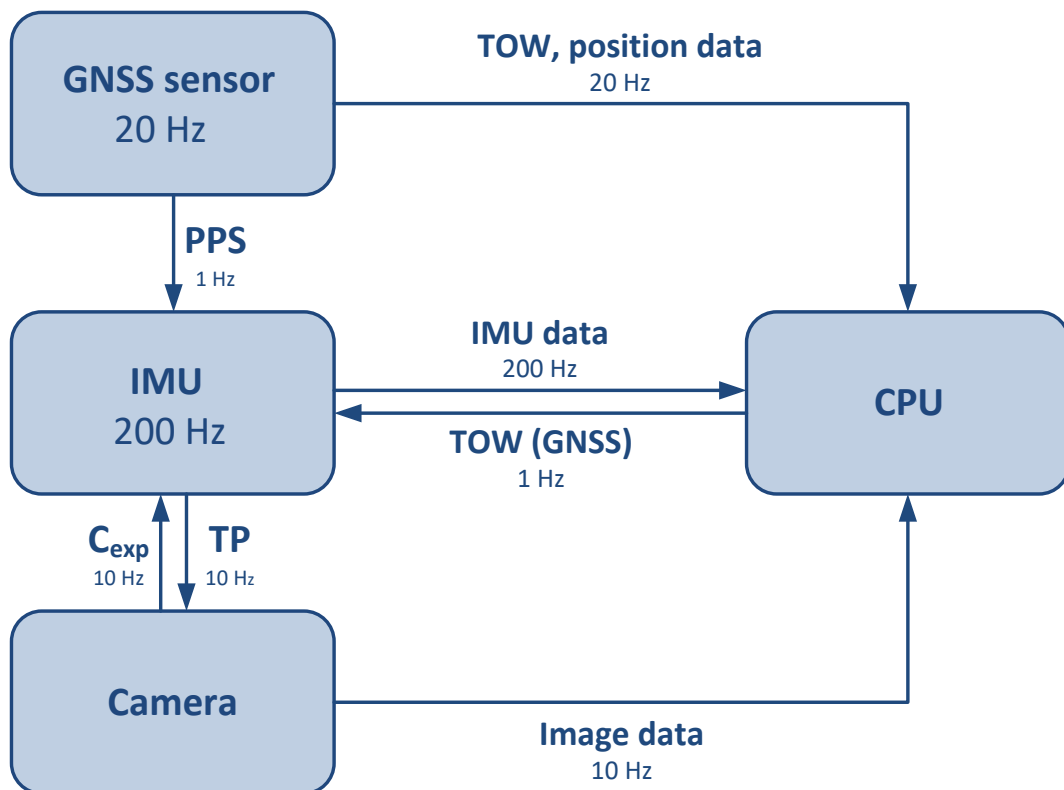


Figure 23: Data flow between GNSS sensor, IMU, Camera and CPU

As depicted in Figure 23 and Figure 24, the GNSS sensor takes measurements with the frequency of 20 Hz. The time stamp of the GNSS measurements is defined with the Time of Week (ToW). Every full ToW second, the Pulse Per Second (PPS) is sent from the GNSS sensor to the IMU. The PPS is sent to synchronize the IMU and the GNSS measurements.

The GNSS sensor simultaneously sends its position with a ToW time stamp to the CPU. Each second the CPU sends the information about the exact ToW time stamp to the IMU. Information about the ToW is needed in order to define absolute time stamps of the inertial measurements.

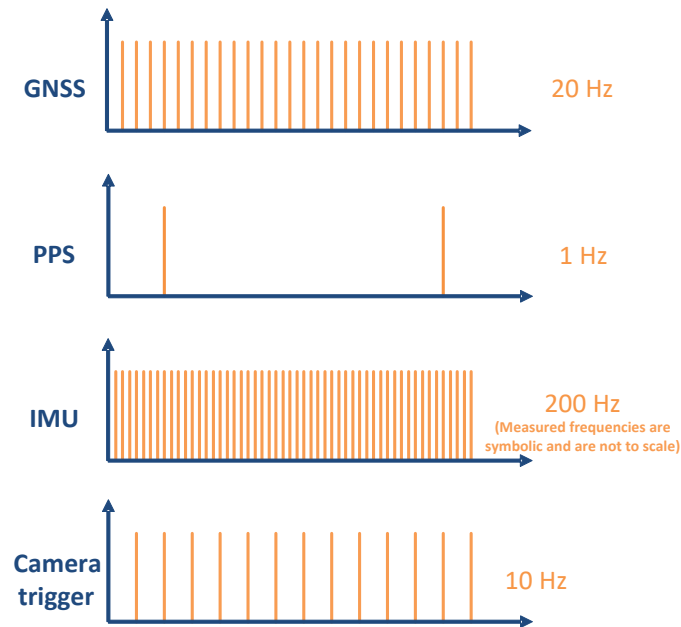


Figure 24: GNSS and IMU measurements taken with different frequency as images captured with the camera

The IMU measures the sensor's specific force, the angular rate and the heading of the sensor with a frequency of 200 Hz. The IMU also triggers the camera with the triggering pulse (TP) that is synchronized with the PPS. The camera triggered by the IMU starts taking a picture in the moment when the triggering pulse is sent. The exposure time C_{exp} of the image depends on light conditions. Information about exposure time is sent back to the IMU, which forwards the information to the CPU for further processing.

Figure 25 shows the relation between the triggering pulse, camera exposure time and the image time stamp.

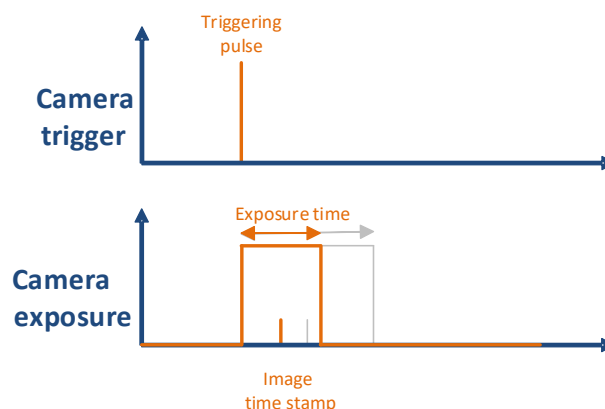


Figure 25: Time stamps of images taken with the FuMo camera

As mentioned before, the camera is triggered with the triggering pulse. At that moment, the camera starts taking the image. The time length when the sensor inside the camera is exposed to light is called the exposure time. The exposure time of the camera depends on the light conditions. At a brighter scene, a shorter exposure time is needed and therefore a better sharpness of the image is achieved while the camera is moving. To ensure a good image quality at walking speed and at short camera-to-object distances, the maximum exposure time of the FuMo camera is limited to 5 ms.

As visualized in Figure 25, the image time stamp is not synchronised with the triggering pulse. Consequently, the image time stamp differs from the time stamps of GNSS and IMU measurements.

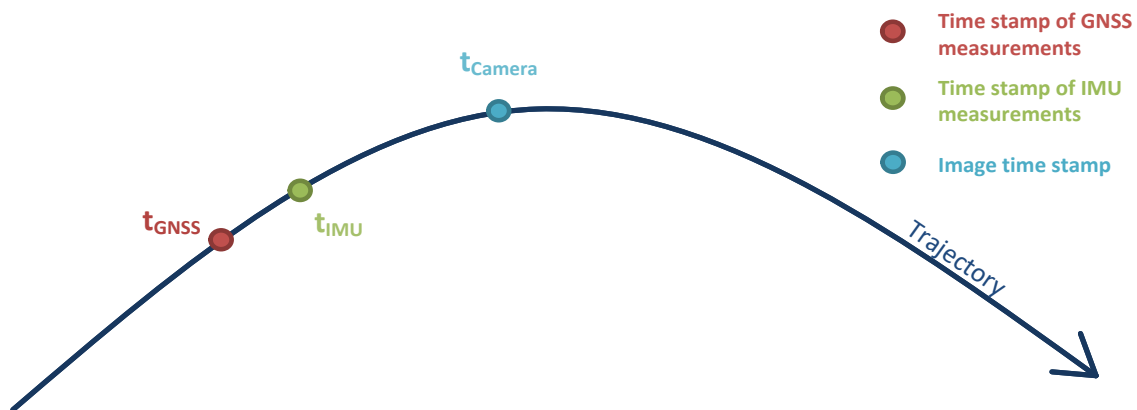


Figure 26: Measurements with FuMo taken at different time stamps, at different places along the trajectory

As shown in Figure 26, while moving the sensors, the GNSS and IMU measurements are taken at different places along the trajectory as the captured image. In order to define the optimal initial camera poses, the GNSS and IMU measurements are linearly interpolated for the corresponding image time stamp.

5.2 Determining the Camera Pose from Which the Images Were Captured

The camera implemented in the FuMo captures images with a frequency of 10 Hz. The sensor takes GNSS and inertial measurements at the same time to compute the sensor's attitude. The initial camera pose can be defined for each image using the computed attitude of the sensor. To measure the position of the captured images, the RTK based GNSS measurements are carried out with the sensor during the video capturing. Nevertheless, the GNSS measurements performed with the RTK are not accurate enough to precisely define the camera poses. Therefore, the camera poses have to be adjusted in the post-processing to improve the accuracy of photogrammetric measurements.

The camera implemented in the sensor captures images with a frequency of 10 Hz. Every 5th image is saved as a key frame. All the other images are called intermediate frames and are used for feature tracking only, which is described in Section 5.2.1.

The adjustment of camera poses is processed in three steps as shown in Figure 27. At first the algorithm generates the features from captured images. The same features found at different key frames are linked together and sent to the SfM algorithm. The SfM algorithm uses the generated features and the sensor's attitude to define the camera poses from which the key frames were captured. The camera poses defined with SfM algorithm are optimized through the Bundle Adjustment algorithm, so that the optimal geometry between the key frames is found.

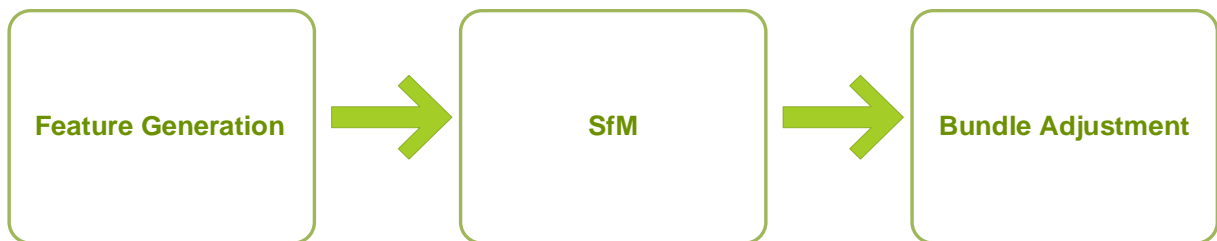


Figure 27: Adjustment of camera poses

5.2.1 Feature Generation

The goal of the feature generation algorithm is to generate features in the images captured with the FuMo. The feature presents the same object point found in different images. The features are generated to establish the geometric connection between the images.

The detailed process of the feature generation and feature tracking algorithm is visualized in Figure 28. In the first step, each captured image is determined as a key frame or as an intermediate frame. The key frames are the images that were captured with the frequency of 2 Hz. As visualized in Figure 28, the first captured image and each fifth captured image are recognised as keyframes. All the other images are recognised as intermediate frames. The intermediate frames are used for the feature generation algorithm only and are deleted after the processing is done.

As visualized in Figure 28, the feature generation algorithm at first generates features in the first captured image, which is recognised as the key frame *KF0*. The features generated in the *KF0* are tracked in following intermediate frames *IF*. The same features are tracked in the next key frame *KF1*, too. Because the camera is moving along the object while capturing the images, one part of the object that is captured in the *KF0* is not captured in the *KF1*. Therefore, not all the features from the *KF0* can be tracked in the *KF1*. The tracked features are found on one side of the key frame *KF1* only. On the other side of the key frame there are no tracked features found. Therefore, new features are generated in the next step only on the side of the key frame, where no features were tracked. All the features

generated or tracked in KF1 are then tracked in the next four intermediate frames and in the next key frame *KF2*. The described process is repeated until all the captured images are processed.

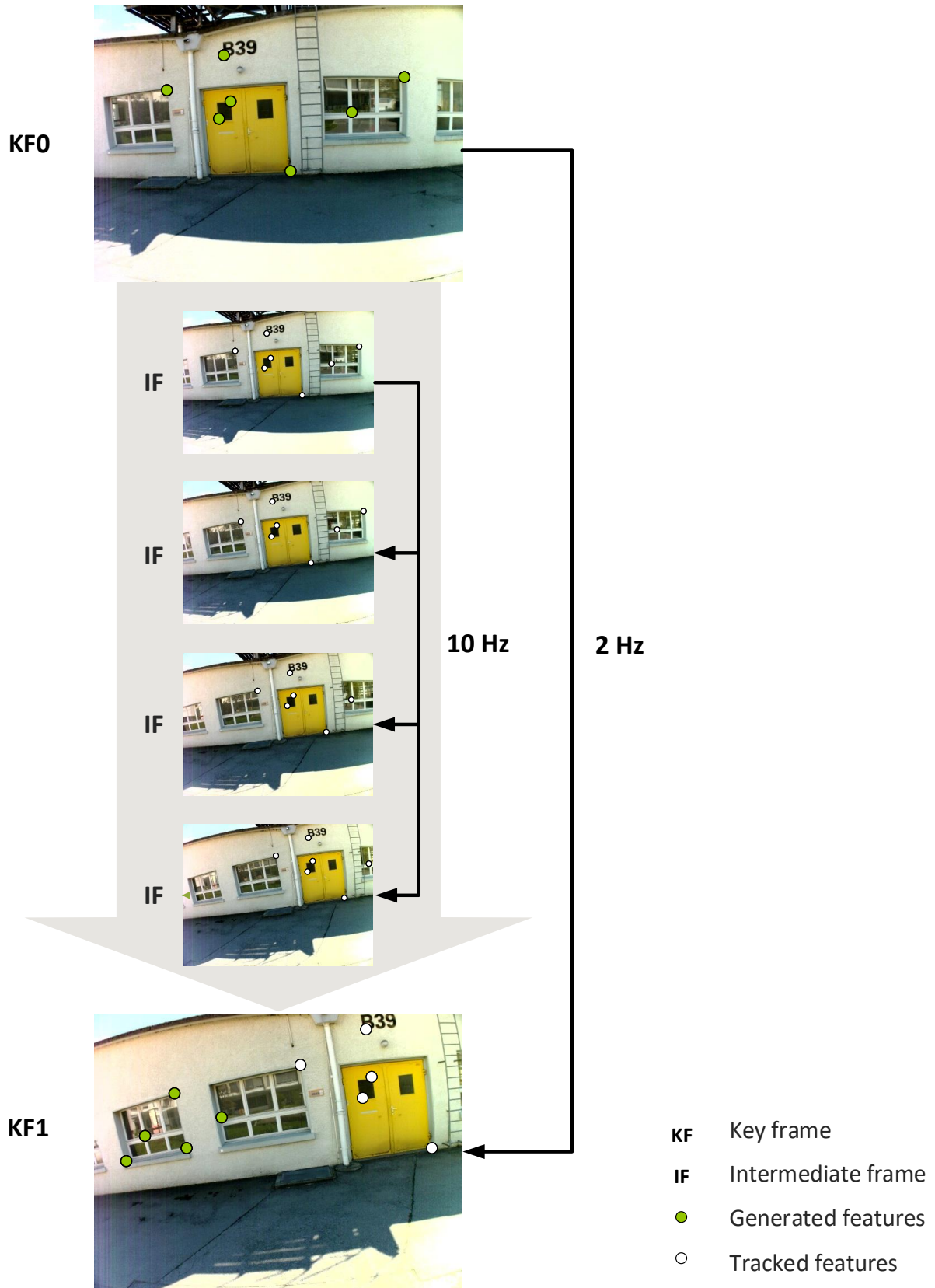


Figure 28: Feature generation and feature tracking algorithm

As visualized in Figure 29, all the images captured with the frequency of 10 Hz are sent to the feature generation algorithm. The images are processed so that the algorithm generates and tracks the features in images. The output of the algorithm are the key frames and the generated features with their properties. Those are the ID of one feature, its pixel coordinates and the link to other key frames where those features were generated. The properties of features 10, 20, 30 and 40 are listed in Figure 30.

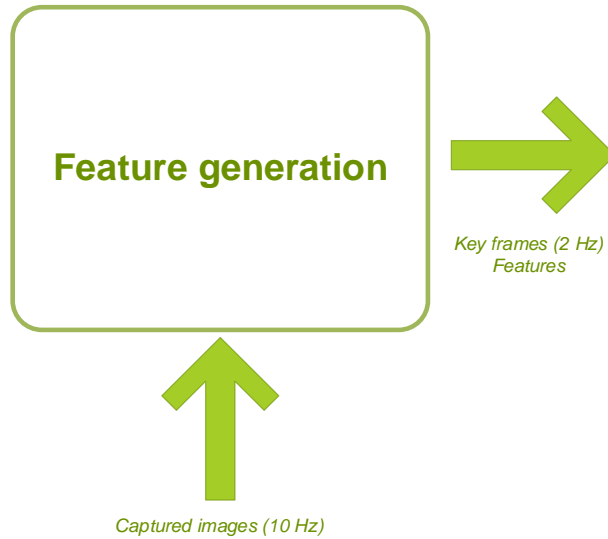


Figure 29: Feature generation and feature tracking algorithm

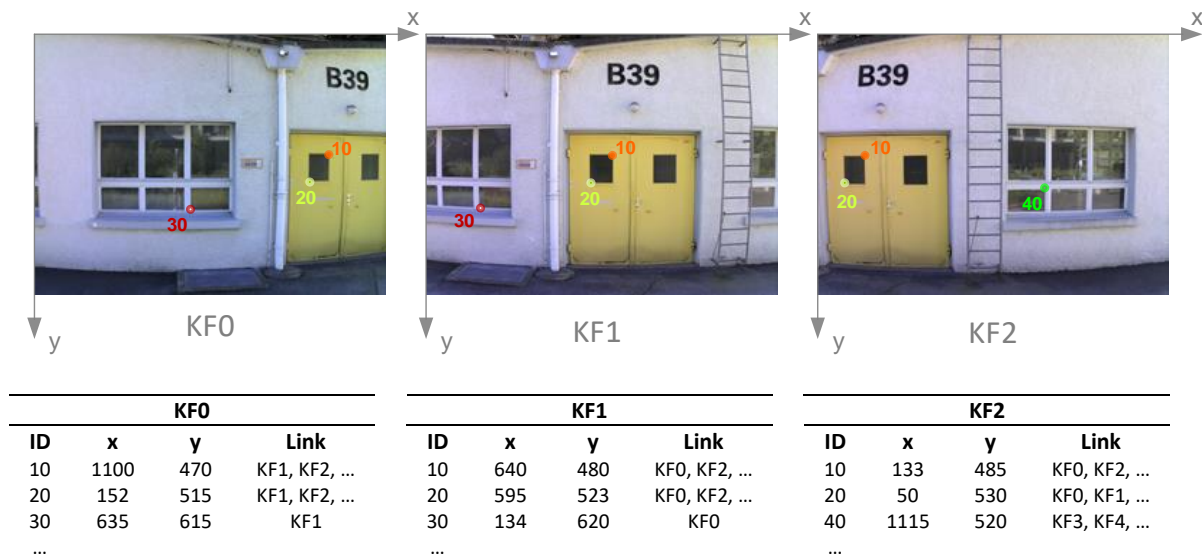


Figure 30: Properties of features

5.2.2 Structure from Motion (SfM)

As described in Section 4.2.3, the SfM estimates both the locations of features in the terrestrial coordinate system and the camera poses from which the key frames were captured.

As visualized in Figure 31, the SfM algorithm implemented in the FuMo uses the attitude of the sensor to define relatively accurate camera poses from which the key frames were taken. The algorithm also requires the set of correspondences between the same features generated in different key frames to improve the geometry between the key frames.

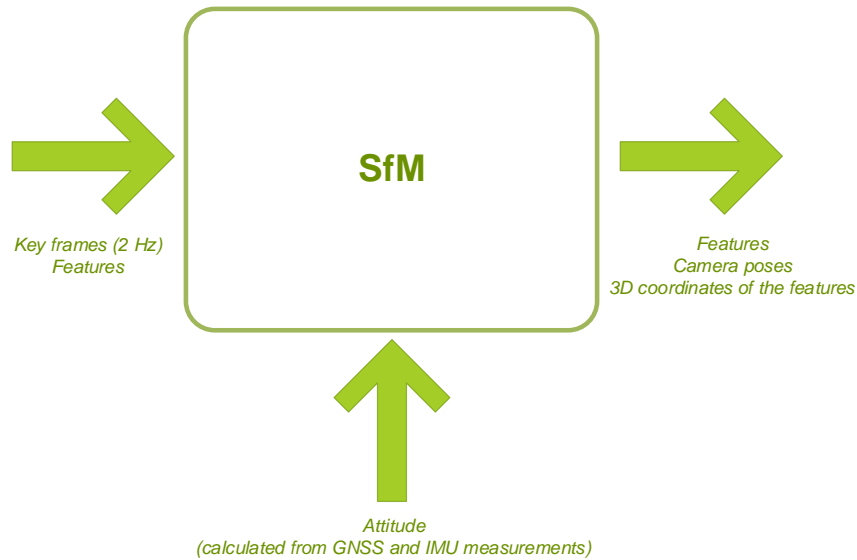


Figure 31: SfM algorithm

The features are defined in images with their image coordinates. As shown in Figure 32, the features are defined through the SfM algorithm with their 3D coordinates of the features $P_i (X_i, Y_i, Z_i)$ in the terrestrial coordinate system.

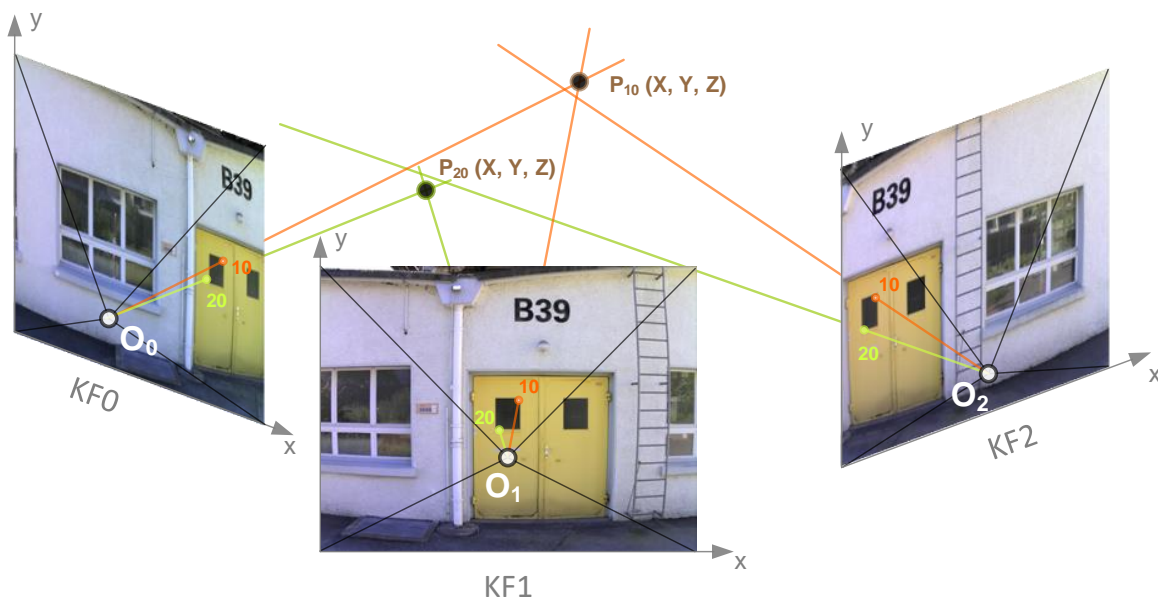


Figure 32: Camera poses and object points defined by the SfM algorithm

Figure 32 shows the principle of the SfM process. Features P_{10} and P_{20} are estimated in the terrestrial coordinate system using image coordinates of features 10 and 20, which were generated in the $KF0$ and the $KF1$. At the same time, the camera poses from which the $KF0$ and the $KF1$ were captured are calculated by the resection of image rays. The camera pose from which the $KF2$ was captured is determined in the next step. The camera pose is determined on the basis of already calculated 3D coordinates of the features P_{10} and P_{20} and the features 10 and 20 generated in the $KF2$. The values of $KF0$ and $KF1$ camera poses stay unchanged, no matter how good the image rays determined in the $KF2$ intersect with object points P_{10} and P_{20} . That way all the camera poses are sequentially computed and saved. The camera poses that are already estimated do not change anymore during the SfM algorithm. In order to make a better fit of all camera poses and 3D coordinates of the features, the camera poses are adjusted later by Bundle Adjustment algorithm.

5.2.3 Bundle Adjustment

The generated features, the computed camera poses, and the computed 3D coordinates of the features are sent to the Bundle Adjustment algorithm together with the GNSS position information. As described in Section 4.2.4, the Bundle Adjustment algorithm iteratively optimizes the camera poses and the object points, so that the optimal geometry between the camera poses and the object points is established.

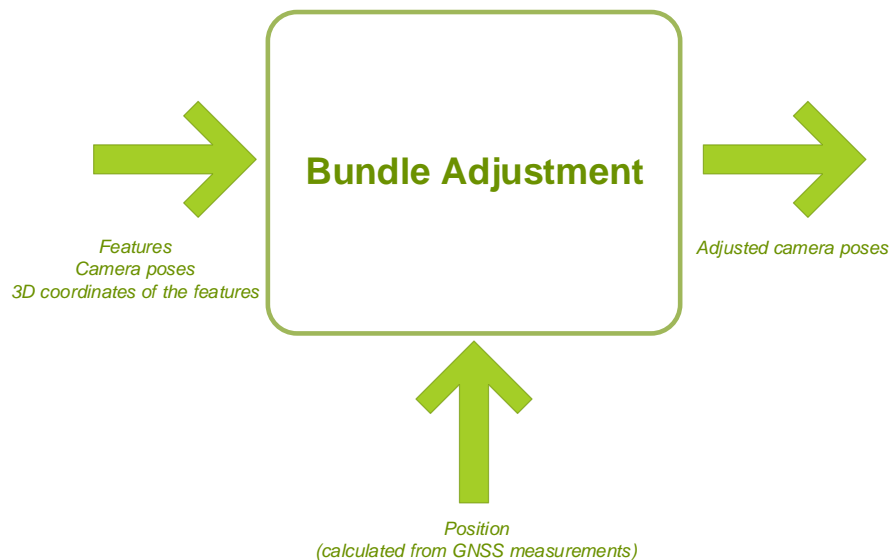


Figure 33: Bundle Adjustment

The Bundle Adjustment calculates the optimal fit of the camera poses in space and therefore enables photogrammetric measurements with a minor measurement uncertainty presented. As depicted in Figure 34, the camera poses and the 3D coordinates of the features are optimized during the Bundle Adjustment to ensure the optimal intersection of bundle rays. The intersection of image rays is improved. However, perfect intersection of image rays can never be achieved.

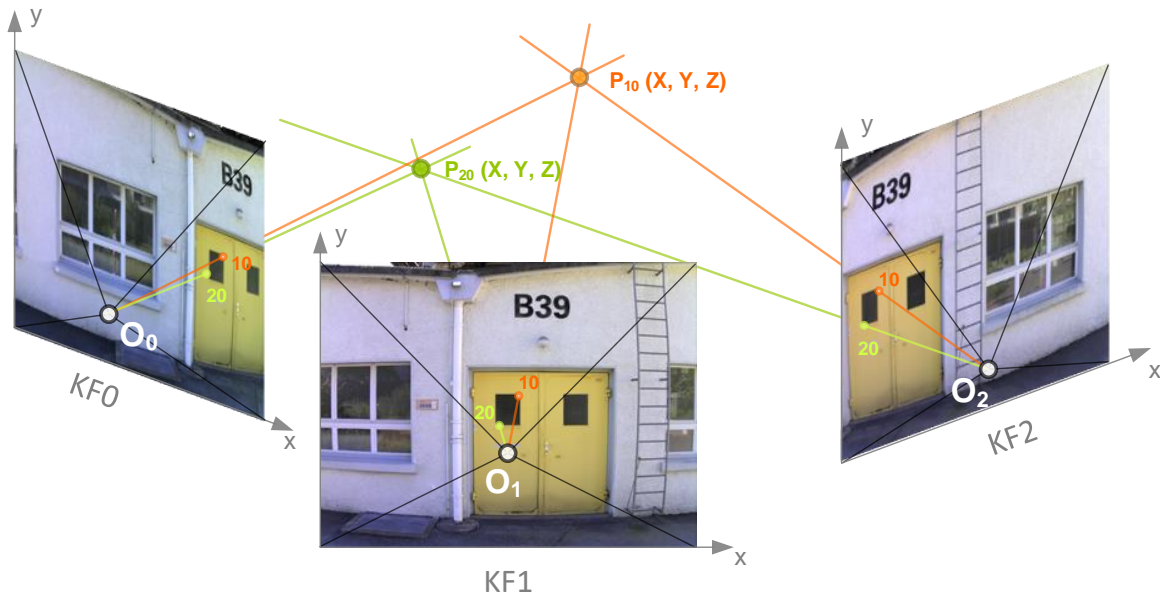


Figure 34: Camera poses and object points optimized after the Bundle Adjustment

5.2.4 Summary

As visualized in Figure 35, the camera poses are defined in three steps. At first the features are generated and linked together with the key frames where they were generated. The outputs of the feature generation algorithm, together with the sensor's attitude, are sent to the SfM algorithm. The SfM algorithm defines the camera poses and the 3D coordinates of the features. The output data of the SfM algorithm and the GNSS position information is then sent to the Bundle Adjustment algorithm. The algorithm adjusts the camera poses so that the optimal geometry between camera poses and object points is found. As an output, the adjusted camera poses are defined for each key frame. Photogrammetric measurements with a minimal measurement uncertainty can then be performed.

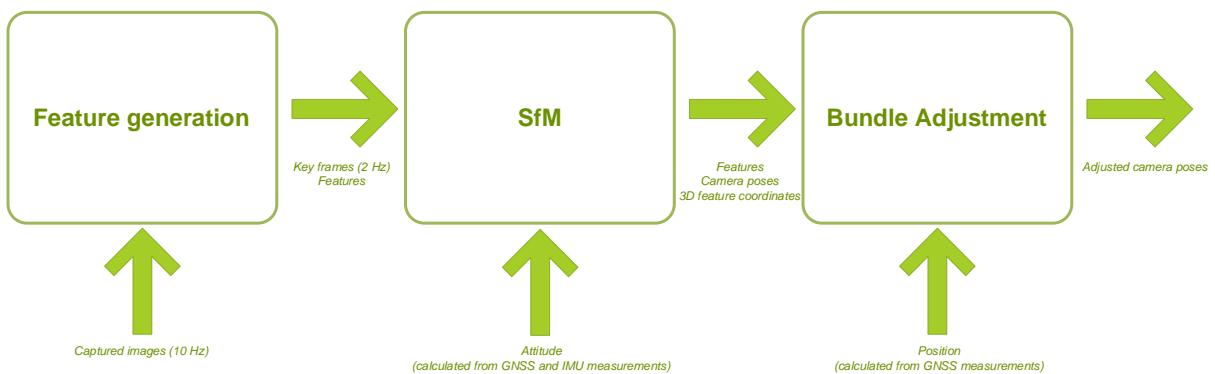


Figure 35: Detailed adjustment of camera poses

5.3 Measuring the Coordinates of the Object Point

After the camera poses of the images are defined, the objects point can be measured in the images. Image coordinates of one object point are defined in one image by the user. The reference matrix is determined around the defined image point as visualized in Figure 36.



Figure 36: The reference matrix defined around the image point

The algorithm places the epipolar lines in other images. The epipolar line in an image presents the line along which the same object point should be depicted in the other image. By calculating the correlations, the algorithm searches for the best match of the reference matrix along the epipolar lines in other images. As visualized in Figure 37, where the best match is found, the target is determined in other images with its image coordinates.

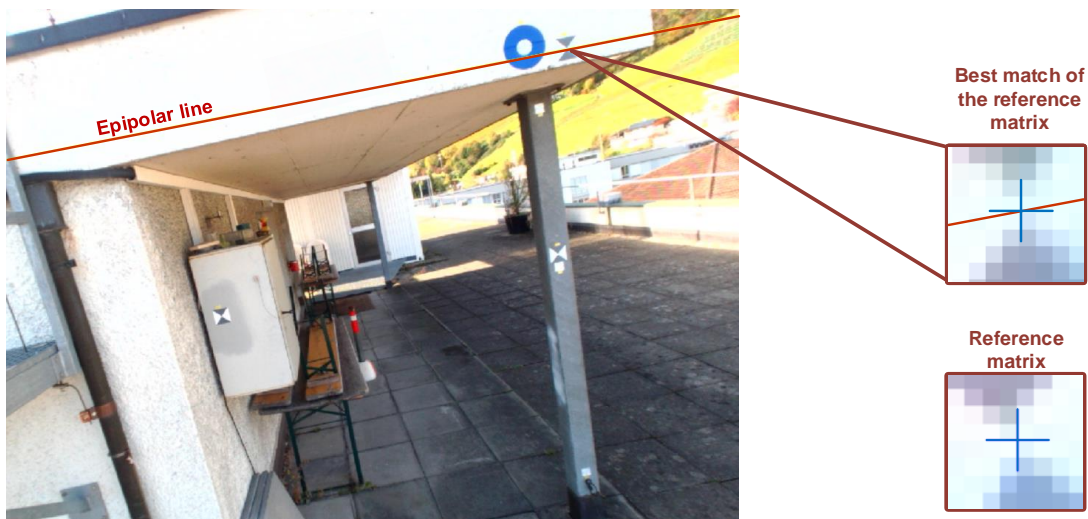


Figure 37: Best match of the matrix found along the epipolar line

The coordinates of the object point are then determined in a terrestrial coordinate system using image coordinates of the object of interest.

When the reference matrix is not unique, the algorithm cannot find the matching matrix along the epipolar line in other images. In such case, image points can still be manually determined in other images by the user. This way the coordinates of the object point can also be determined in the terrestrial coordinate system.

6 Uncertainty of Photogrammetric Measurements

Measurements taken with the FuMo are based on GNSS and IMU measurements and on the images taken with the camera. The uncertainties presented in GNSS and IMU measurements influence the accuracy of the photogrammetrically measured object points. The synchronisation and the calibration uncertainties have a big influence on the accuracy as well. In addition to that, the quality of the images contributes to the accuracy of the photogrammetric measurements.

The influences on the uncertainty of measured object points can be divided into three groups. They are schematically visualized in Figure 38 and depicted in Figure 19. The accuracy of an object point is highly dependent on:

- the geometry of the captured images,
- the uncertainties of image points that are used to define the object point, and
- the uncertainties of the perspective centres of the images, which are used to define the object point.

The uncertainty of an object point occurs due to the uncertainty of the perspective centres and due to the uncertainty of the image points. The uncertainty that occurs due to the components described in Section 6.1 and Section 6.2 can be improved by the appropriate geometry of the camera poses from which the images are taken.

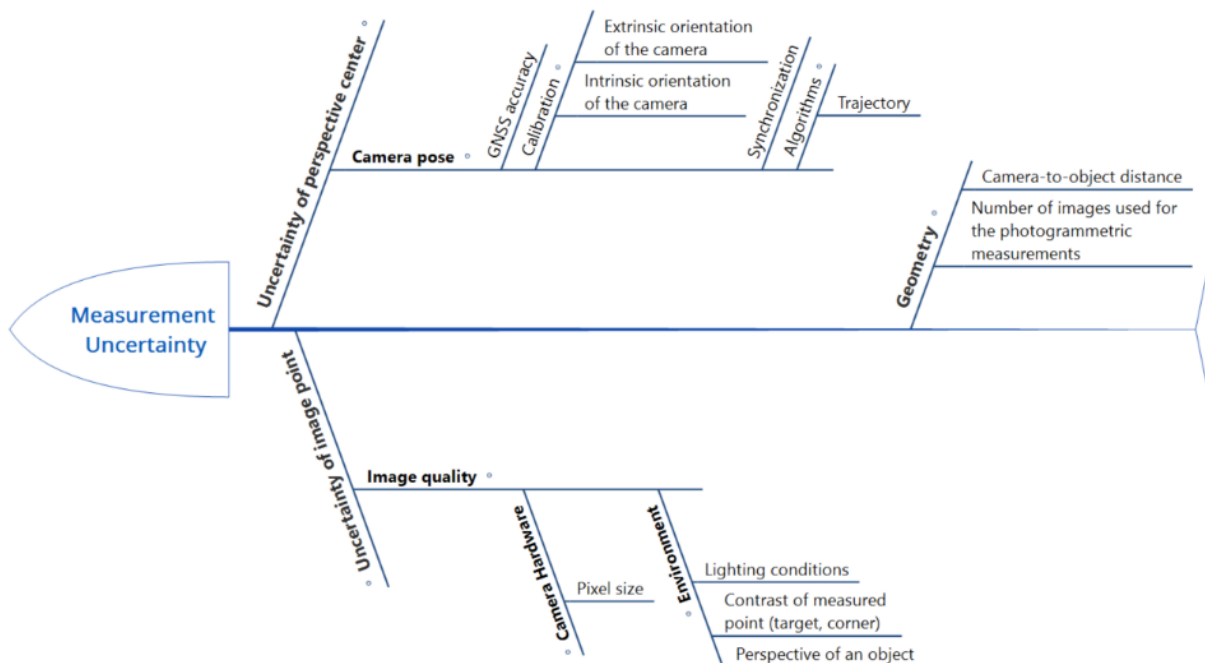


Figure 38: The components that influence the uncertainty of the measurements taken with the FuMo

6.1 Influences on the Uncertainty of Perspective Centre

6.1.1 Uncertainty of the GNSS Measurements

The uncertainty of the GNSS measurements is highly dependent on the environmental conditions in which the sensor is in the moment of measurements. The uncertainty can be improved by measuring in the area where an open view to the sky is available. It can also be improved by measuring in the area where the effect of the multipath minimally affects the position measurements.

6.1.2 Calibration

The FuMo sensor should be calibrated before starting to perform measurements with it. During the calibration, the intrinsic orientation of the camera in the sensor is determined. It is determined together with the position and orientation of the camera within the housing of the FuMo. Calibration values are accurately determined. Nevertheless, there is always an uncertainty presented in the calibrated values, too. The uncertainty of the calibration values contributes to the uncertainty of the initial camera pose. Consequently, they contribute to the uncertainty of the perspective centre.

6.1.3 Synchronization of Main Components

The quality of the synchronization of the measurements performed with the main components (see Section 5.1) influences the accuracy of photogrammetric measurements as well. The time stamp of the measurements taken with the GNSS and the IMU sensor and the time stamp of captured images do not coincide. The linear interpolation is therefore used to compute the initial camera poses for the time stamps of the images. Due to the uncertainty presented in the camera poses computed with the linear interpolation, the uncertainty of the perspective centre is influenced.

6.1.4 Trajectory

The uncertainty of the perspective centre is affected due to the algorithms processing the camera poses from which the images were taken. Depending on the trajectory along which the images were captured, the algorithms can correspondingly minimize the uncertainty of the perspective centre successfully (see Section 8.2.3). The influence of the trajectory on the uncertainty presented in measured object points is analysed in Section 10.2 and in Section 10.3.

6.2 Influences on the Uncertainty of the Image Point

6.2.1 Lighting Conditions

The amount of light is one of the most important factors while capturing the images with the FuMo. The maximal exposure time in which the CMOS sensor is exposed to the light is set to 5 ms. If there is not enough light available while capturing the images with the FuMo, the details may not be recognisable in the images. The same happens if there is too much light available while capturing the images. Image point coordinates defined from such images contain bigger uncertainty than the image points that are defined in the images taken in optimal lighting conditions. In worst case scenario, it can happen that the algorithms cannot adjust the images in the space and the processing fails entirely.

6.2.2 Perspective of an Object

The perspective of an object point is of a great importance while taking measurements with the FuMo. When the image coordinates of an object are defined in the images that are captured from large oblique angles, the coordinates can be influenced by bigger errors. Namely, small uncertainty in the image point coordinates leads to a big uncertainty of the measured object point (see Figure 39).

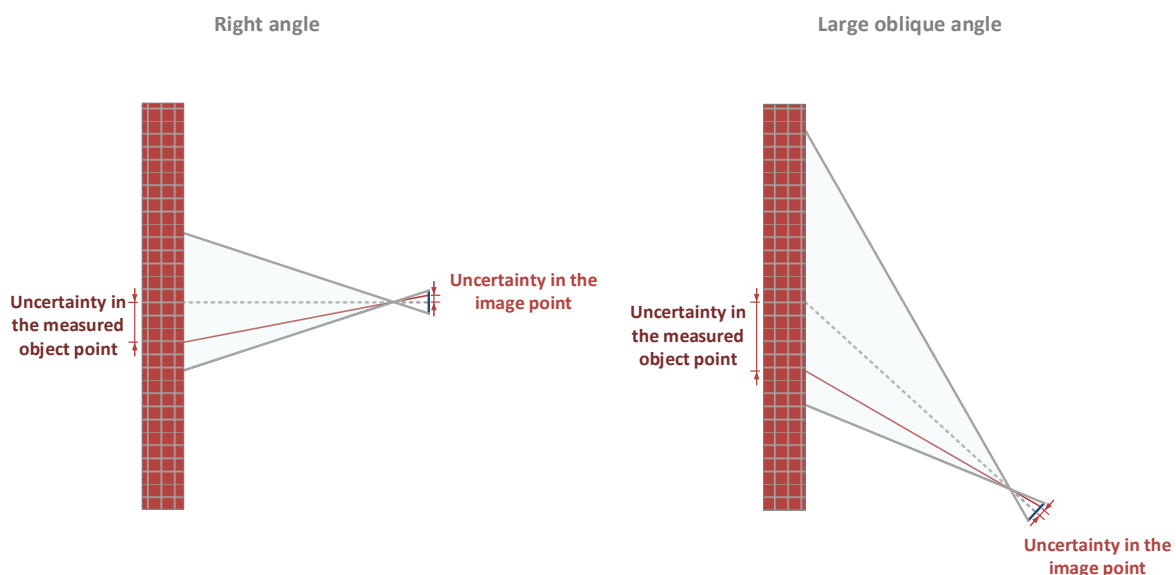


Figure 39: Uncertainty of the image coordinates translated to the uncertainty of the defined object point

6.2.3 Contrast of Measured Object Point

The measured object point should be recognisable in the images to be able to define its coordinates. The object point is defined in one of the images by the user. The algorithm searches for the same point in other images. The point is found along the epipolar line using a feature recognition algorithm (see Section 5.3). Therefore, the accuracy of image points that are difficult to recognize in the images is more influenced by the measurement uncertainty.

6.2.4 Pixel Size

The size of the area that is captured in one pixel contributes to the sharpness of the images and therefore contributes to the uncertainty of the object point. When capturing the images from shorter camera-to-object distances, a smaller area of an object is captured in one pixel. When the images are captured from bigger camera-to-object distances, a bigger area of an object is captured in one pixel (see Figure 40).

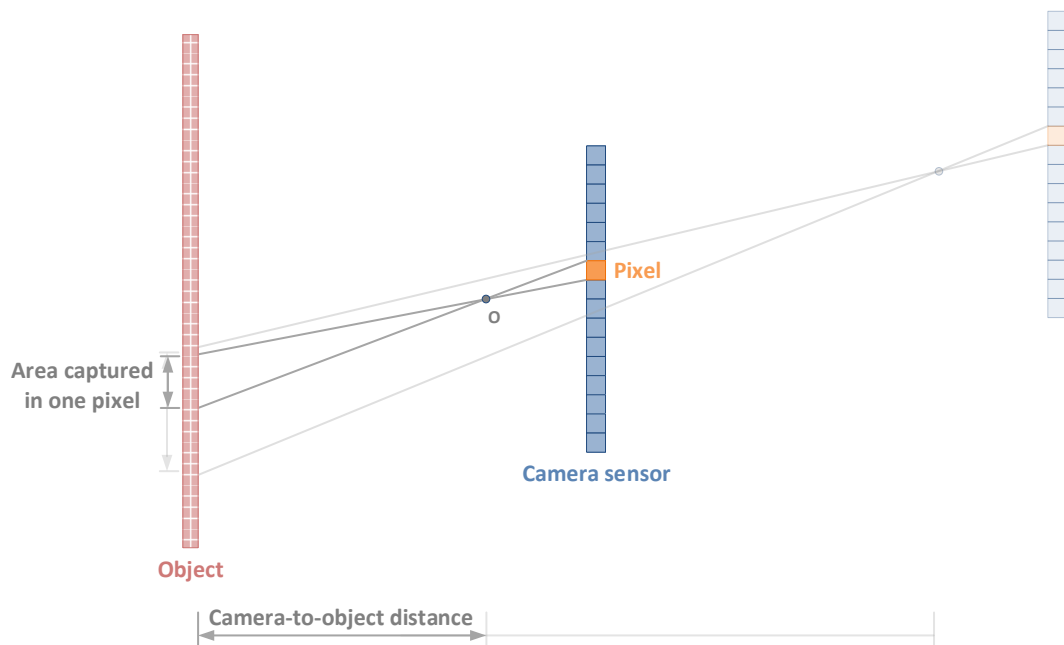


Figure 40: The size of the area captured in one pixel from different camera-to-object distances

The smaller the area captured in one pixel is, the smaller the uncertainty of the image point is presented. In order to assure minimal uncertainty presented in the defined image point, good quality and sharpness of the images should be ensured.

The sizes of the object areas that are captured in one pixel compared for different camera-to-object distances are listed in Table 1. The principle of calculating the area captured in one pixel is described in Appendix A.

Table 1: The size of area captured in one pixel in dependence on different camera-to-object distances

Camera-to-object Distance [m]	Area captured in one pixel	
	Hz [mm]	V [mm]
0.5	0.7	0.7
5	7.1	7.4
10	14.1	14.7

7 Test Field

In order to investigate the capability and the limitations of the FuMo, the test field had to be established. While choosing the location of the test field, the conditions listed in the Section 7.5 had to be met. By locating the test field on the roof of the Leica Geosystems AG building B26, all the conditions were met. The part of the building shown in Figure 41 was chosen for the test field, where the objects of interest were determined and the targets were established.



Figure 41: Part of the Leica Geosystems B26 building used to establish the test field

The objects of interest were chosen in the test field to investigate the limitations of the FuMo. They are described in Section 7.4. Additional optical targets described in Section 7.3 were established in the test field. The coordinates of the targets determined with the FuMo were compared to the reference coordinates of the targets in order to investigate the capability of the system.

The reference coordinates of both the targets and the objects of interest were measured with the Leica MS60. They were defined in reference to the local geodetic network, which is described in Section 7.2. The targets and the objects of interest were measured in the local Swiss coordinate system. Then they were transformed into the WGS84 Cartesian coordinates with the assumed accuracy of 10 mm. Hereby the reference coordinates were provided for the photogrammetric measurements performed with the FuMo.

7.1 Goal of the Measurements in the Test Field

The goal of the measurements performed in the test field was to investigate how the accuracy of photogrammetric measurements varies depending on different camera-to-object distances. The targets visualized in Figure 45 were used as a reference to determine the capability of the photogrammetric measurements taken with the FuMo. In addition, the objects of interest visualized in Figure 46 served for defining the limitations of the system.

The test field was designed as shown in Figure 42. The images were captured with the FuMo along the green and the orange lines. The green lines represent “I-trajectories” placed at different distances to the object wall along which the images were captured. The orange lines represent “U-trajectories” placed at different distances to the wall of the object, along which the images were captured. The properties of the “I-trajectory” and the “U-trajectory” are described in Section 8.1.

To determine the capability of the system, the measurements with the FuMo were taken in the optimal environmental conditions, which are described in Section 7.5. The target coordinates measured photogrammetrically with the FuMo were compared to the reference target coordinates described in Section 7.3. As a result of the measurements, the capability of the system is described in Section 10.

At the same time, the measurements of the objects of interest were performed. The measurements were based on the real-use conditions. The corners of the building and other objects of interest that are visualized in Figure 46 were measured in images. As a result, the additional limitations of the FuMo were determined and described in Section 11.

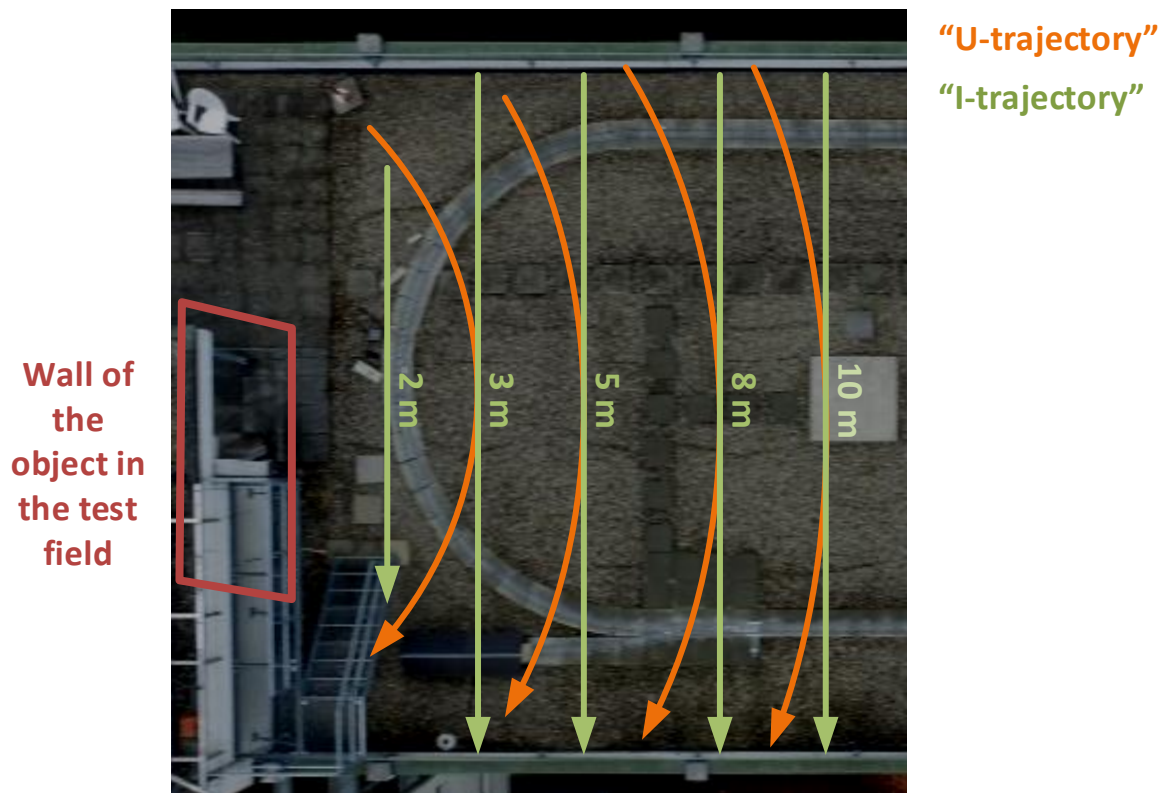


Figure 42: Trajectories along which the measurements were taken in the test field

7.2 Local Geodetic Network

The local geodetic network was established in the area depicted in Figure 43. At first the static GNSS measurements were performed at the GNSS points. The raw data was processed so that the coordinates of the GNSS points were defined in the local Swiss coordinate system LV95.

After the static GNSS measurements were processed, the Leica MS60 was force centred on the tripod at point GNSS_B26. On the other three tripods that were located at GNSS points, the prisms were force centred. The network adjustment was performed between the GNSS points.

After the network adjustment, the coordinates of the prisms P1 to P5 were measured. The prisms P1 to P5 were permanently mounted in the surrounding area.



Figure 43: Local geodetic network

The coordinates of the prisms and the GNSS_B26 point were defined in the reference frame, which is aligned to the International Terrestrial Reference Frame 2008 (ITRF2008). The reference frame of the coordinates is Igb08 epoch 2015-12-22.

The coordinates were defined in the local Swiss coordinate system LV95 with the properties listed in Table 2 and Table 3.

Table 2: Properties of the local Swiss coordinate system used for the measurements

Coordinate system	Swiss_Testbed
Transformation	LV95 Parameter
Projection	Swiss95
Geoid Model	Geoid2004_03+

Table 3: Properties of the LV95 Parameter transformation

Transformation	LV95 Parameter
Model	Bursa Wolf
Δx	-674.3740 m
Δy	-15.0560 m
Δz	-405.3460 m
Rx	0.00 "
Ry	0.00 "
Rz	0.00 "
Scale	1.0000000000

The ground point GNSS_B26 and the prisms P1 to P5 were used to define the coordinates of the targets and the coordinates of the objects of interest in the test field. The ground point GNSS_B26 was used as a standpoint. The coordinates of the prisms P1 to P5 were used to set up the Leica MS60 using the method "Multiple backgrounds". The coordinates of the ground point GNSS_B26 and prisms P1 to P5 are listed in Table 4.

Table 4: The coordinates of the local geodetic network defined in the WGS84 coordinate system

Point	X [m]	Y [m]	Z [m]
GNSS_B26	4263861.932	722616.388	4672985.512
P1	4263828.851	722704.376	4673001.434
P2	4264041.804	722572.160	4672821.198
P3	4264111.098	722372.593	4672785.791
P4	4263864.936	722187.952	4673061.635
P5	4263735.721	722481.168	4673183.465

7.3 Targets

The targets that were used to establish the test field are visualized in Figure 44. There were two different types of targets used to establish the test field. It was investigated how the size, the shape, and the colour contrast of measured points influence the accuracy of photogrammetric measurements.

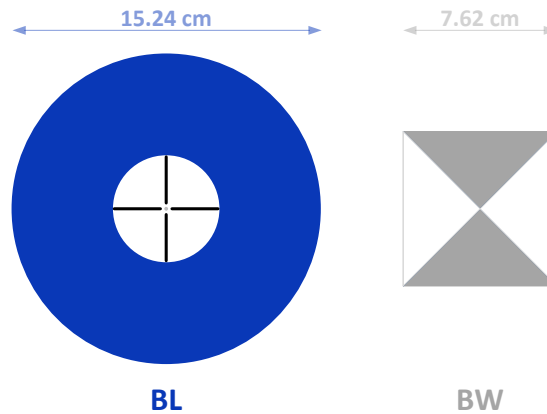


Figure 44: Blue and black-and-white targets

The targets were distributed in the test field, as shown in Figure 45. They were placed at different heights, so that the influence of the height of the target in the image could be investigated. The investigation was made in the images captured from the camera-to-object distance of 2 m. Namely, when the images are captured from shorter distances, the targets are equally captured at different heights in the images. In addition to that, the influence of different angles from which the photogrammetric measurements can be taken was investigated. The results of the investigation are analysed in Section 10.1.

Furthermore, the coordinates of the targets were also used as a reference for defining the error of the coordinates measured photogrammetrically with the FuMo. The results of the investigation are described in Sections 10.2 and 10.3.



Figure 45: The blue and the black-and-white targets in the test field

The reference coordinates of the targets were measured with the Leica MS60 Multistation. They were determined with reference to the local network that was established as described in Section 7.2. The coordinates of the targets were measured in the local Swiss coordinate system LV95. They were transformed afterwards to the WGS84 coordinate system. The reference coordinates in Table 5 are listed with a centimetre accuracy.

Table 5: Reference coordinates of the targets measured with the Leica MS60, defined with WGS84 Cartesian coordinates

Point ID	X [m]	Y [m]	Z [m]
BL01	4263864.553	722599.226	4672988.780
BL02	4263866.863	722599.441	4672986.662
BL03	4263865.365	722599.117	4672985.043
BW01	4263864.422	722599.210	4672988.854
BW02	4263863.876	722598.670	4672988.336
BW03	4263865.108	722598.724	4672987.256
BW04	4263865.365	722599.800	4672986.908
BW05	4263866.749	722599.429	4672986.782
BW06	4263865.764	722600.322	4672986.460
BW07	4263865.270	722599.114	4672985.166

The reference coordinates were determined in the WGS84 coordinate system, because the coordinates of the targets measured with the FuMo are also determined with the WGS84 Cartesian coordinates.

7.4 Objects of Interest

The objects of interest that were defined in the test field are shown in Figure 46. Selected were typical objects used for surveying tasks like corner points of the building. They were used to determine the limitations of the FuMo, which are described in Section 11. The coordinates of the objects of interest were measured with the Leica MS60 in the local Swiss coordinate system LV95. Afterwards they were transformed to the WGS84 coordinate system. The reference coordinates of the objects of interest are listed in Table 6 with a centimetre accuracy.



Figure 46: The objects of interest in the test field

Table 6: Reference coordinates of the objects of interest measured with the Leica MS60, defined with WGS84 Cartesian coordinates

Point ID	X [m]	Y [m]	Z [m]
CO01	4263864.467	722599.260	4672989.393
CO02	4263864.168	722599.185	4672989.033
CO03	4263862.979	722598.521	4672987.431
CO04	4263865.121	722598.737	4672987.665
CO05	4263864.634	722598.653	4672987.131
CO06	4263863.998	722599.934	4672986.039
CO07	4263865.030	722599.118	4672986.341
CO08	4263866.504	722599.263	4672984.960
CO09	4263865.088	722601.202	4672984.864
CO10	4263865.226	722600.190	4672984.893
CO11	4263866.474	722599.507	4672987.195
CO12	4263867.550	722599.608	4672986.203
CO13	4263868.077	722599.652	4672985.722

7.5 Conditions of the Test Field

7.5.1 GNSS Reception

The position of the image capturing sensor is defined with the GNSS measurements. Therefore, it is of great importance that the sensor has a good GNSS reception while performing test measurements. The factors that are listed below have the biggest influence on the accuracy of GNSS measurements. In order to test the capability of the FuMo, the best possible accuracy of GNSS measurements has to be achieved. Therefore, the factors listed below were of big importance while selecting the test field.

Location of the Measuring Sensor

A GNSS receiver needs a clear line of sight to the satellites that are being tracked. That means that the GNSS receiver measures the position best when an open view to the sky is available. As the test field had to be located on the northern hemisphere, the majority of the satellites can be found on the southern part of the observable sky. For that reason, the test field had to be located somewhere where the open view to the southern part of the observable sky was available. By locating the test field on the roof of the building, a clear line of sight to the tracked satellites was assured.

Surrounding Environment

Surrounding buildings and vegetation can lead to the effect of the multipath of the GNSS signal. Due to the effect of multipath, the signal from the satellites arrives to the sensor by different ways and at different times, which affects the position accuracy of GNSS measurements.

While establishing the test field for the measurements with the FuMo, it was of great importance to locate the test field somewhere where GNSS measurements are the least affected by the multipath. By defining the test field on the roof of the building B26, this condition was met. Namely, there are no trees or buildings higher than the test field in the surrounding area.

7.5.2 Geometry

The test field was constructed so that the images could be taken under optimal geometrical conditions for the measurements taken up to 5 m camera-to-object distance. As described in Section 4.3.1, the intersection angle of two image rays should equal 90° in order to measure points with the highest accuracy. As visualized in Figure 47, the optimal intersection angle in the test field is assured for the measurement taken up to 5m camera-to-object distance.

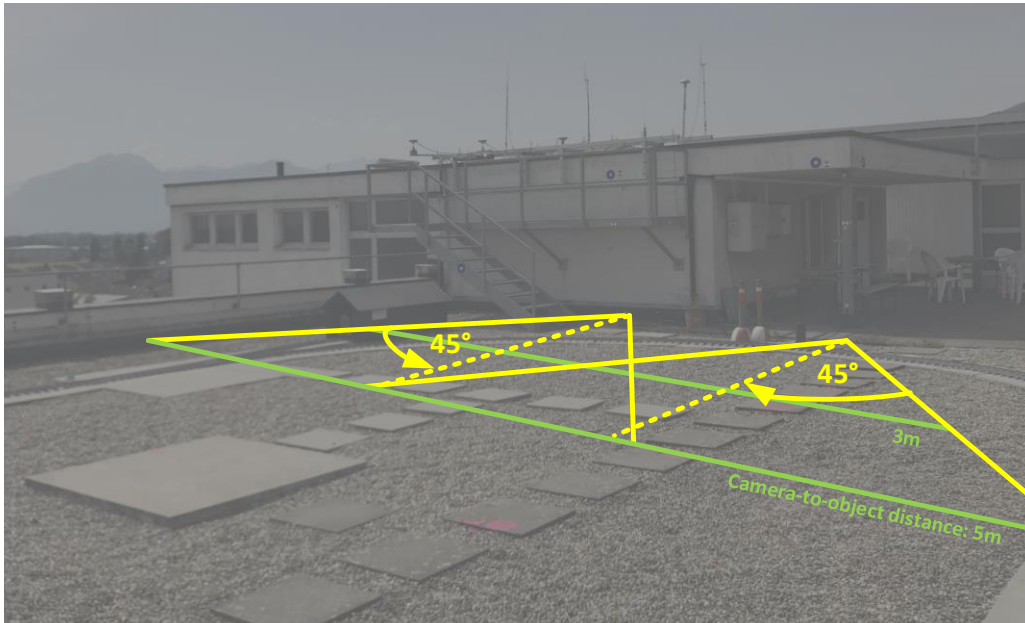


Figure 47: Optimal intersection angle in the test field

7.5.3 Structure of the Object

As described in Section 5.2.1, the algorithm implemented in the sensor adjusts camera poses from which the images were taken. For the processing of the data, the algorithm needs to recognize enough unique details, which can be linked together in different images. Therefore, it is of great importance that the recorded object has as many recognizable details as possible.

The test field was established in the area where many details can be recognised in the images. The feature generation algorithm was therefore able to generate enough features to link the images with each other.

8 Subject of the Research

While performing the test measurements with the FuMo in the test field the images were captured along the trajectories shown in Figure 42. The coordinates of the targets located in the test field were determined in captured images and the error of the coordinates was computed. The error was determined by comparing the measured target coordinates to the reference target coordinates as described in Section 9.2.

The error was at first investigated for the targets measured in the images that were captured along the “I-trajectory” placed in the test field at 2 m camera-to-object distance. It was investigated how the height of a target in the images influences the error of the measurements. It was also investigated how the perspective of the camera according to the object influences the error of the measurements. In addition, it was investigated how the size, the shape, and the colour contrast of measured points influence the error. The results are described in Section 10.1.

Secondly, it was investigated how the type of trajectory influences the error of the measurements in the following three directions:

- in the direction parallel to the wall of the object,
- in the direction perpendicular to the wall of the object and
- in the height direction.

To define the error in each of the three directions, the coordinates of measured targets were transformed from WGS84 coordinate system to a local coordinate system. The transformation was applied as described in Section 9.1. It was investigated how the type of trajectory influences the error in each direction. The expectations are described in Section 8.2. The results are analysed in Section 10.2.

Furthermore, it was investigated how the 3D error of target coordinates is influenced by:

- **the type of trajectory along which the images are captured** – the measurements performed in the test field were taken along “I-trajectory” and “U-trajectory”. Both types of trajectories are described in Section 8.1. It was investigated how the geometry of captured images influences the error of measured target coordinates.
- **the camera-to-object distance** – test measurements were performed along the trajectories which were placed at different distances from the wall of the object. It was investigated how the error is influenced by the distance from which the images were captured. The influence of the camera-to-object distance on the error of measured point coordinates is described in Section 4.3.2.

The results of the investigation of the 3D error on the measurements taken along different trajectories and from different distances are described in Section 10.3.

8.1 Impact of Trajectory

A trajectory is the line along which the sensor moves through space as a function of time. While capturing the images, the FuMo moves along the trajectory. While performing the test measurements, it was investigated how the type of trajectory influences the errors of measured coordinates. Both types of trajectory are described in following sections 8.1.1 and 8.1.2.

8.1.1 “I-Trajectory”

While capturing the images along “I-trajectory” the sensor moves along a straight line. As visualized in Figure 48, the images are captured along the trajectory at epochs i , $i+1$, $i+2$, . . . The sensor moves parallel to the wall of the object so that the camera-to-object distance remains constant. The optical axes of the camera at each camera pose from which the images were captured remain parallel to each other.

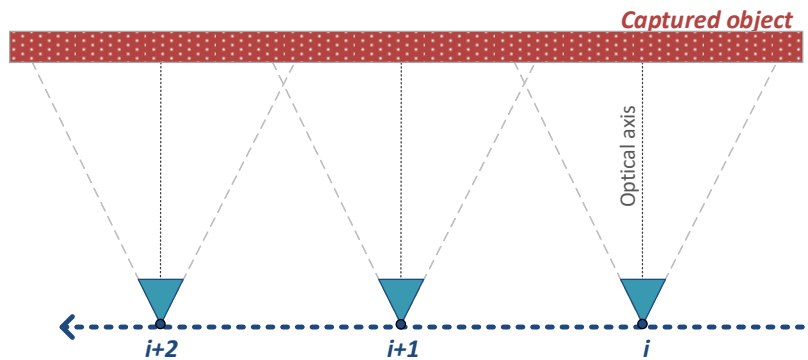


Figure 48: Top view of the sensor capturing images along the “I-trajectory”

8.1.2 “U-trajectory”

The “U-trajectory” presents a curved line along which the sensor moves while capturing the images. As visualized in Figure 49, the images are captured along the trajectory at epochs i , $i+1$, $i+2$, . . . The optical axes of the camera at each camera pose from which the images were captured are not parallel to each other.

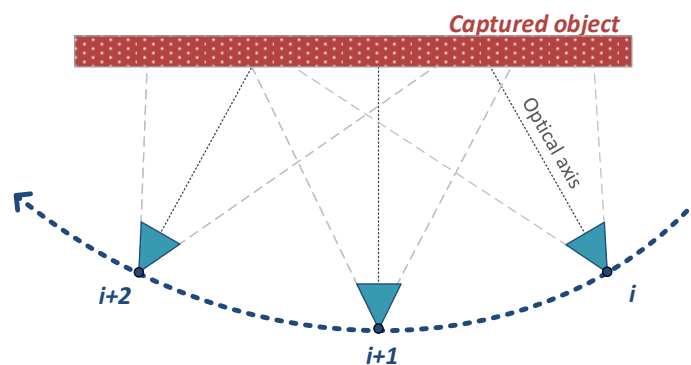


Figure 49: Top view of the sensor capturing the images along the “U-trajectory”

The “U-trajectory” can be placed in a horizontal plane, as visualized in Figure 49. The “U-trajectory” can also be tilted or placed in the vertical plane. However, for better interpretation, the trajectories placed in the horizontal plane will be the subject of the research.

While capturing the images along the “U-trajectory”, a better geometry of the images is provided. Therefore it is expected that the object points measured in those images are determined with higher accuracy.

8.2 Error Considerations

While capturing the images with the FuMo along a trajectory, the initial camera poses are determined for each captured image. The initial camera poses are computed using the GNSS and IMU measurements. As each initial camera pose is influenced by the uncertainty of the GNSS and IMU measurements, the initial camera poses have to be adjusted. To minimize the uncertainty, the initial camera poses are adjusted by the feature generation, Structure from Motion, and Bundle Adjustment algorithms (see Section 5.2). Adjusted camera poses should present the actual position and orientation of captured images. The uncertainty is reduced after the adjustment, but it is still present even in the adjusted camera poses.

The object points can be measured in images which are defined with the adjusted camera poses. When measuring in the images, the uncertainty presented in the adjusted camera poses is transferred to the measured object point coordinates (see Section 4.3). The uncertainty of object point coordinates can be expressed with an error. This error can be calculated by subtracting the coordinates of the targets measured with the FuMo from the reference coordinates of the targets.

As mentioned in the introduction of Section 8, the error of measured target coordinates was investigated in three directions, which are depicted in Figure 50. The coordinates of the targets measured with the FuMo were therefore transformed from the WGS84 coordinate system to the local coordinate system as described in Section 9.1. The local coordinate system was established so that the error of each coordinate of the target presented the error of the measurements in one of the directions as follows:

- error in the direction parallel to the wall of the object (X coordinate),
- error in the direction perpendicular to the wall of the object (Y coordinate) and
- error in the height direction (Z coordinate).

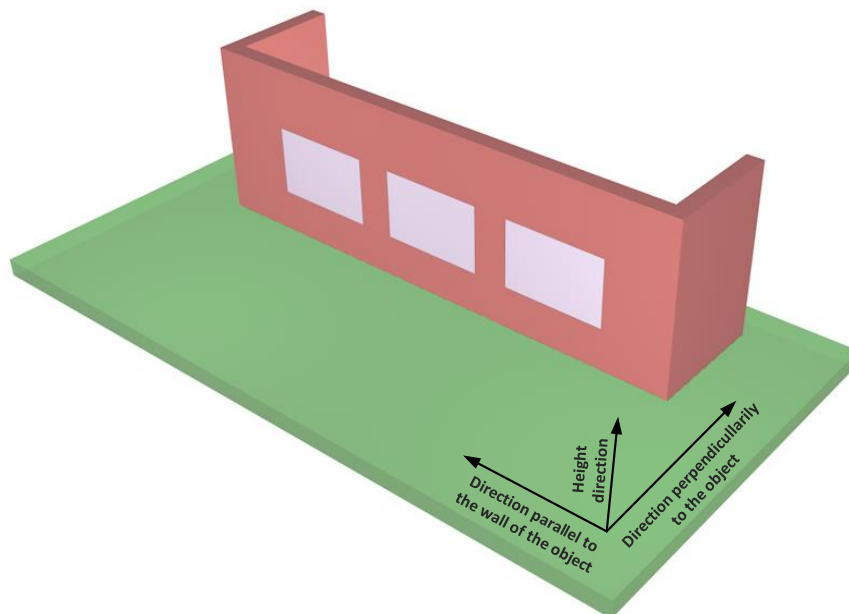


Figure 50: The directions in which the error of the measurements was computed

8.2.1 Error in the Direction Parallel to the Wall of the Object

It was expected that the error in the direction parallel to the wall of the object is not influenced by the type of trajectory along which the images were captured. As visualized in Figure 51, the error of the X coordinate can be equally small when the measurements are taken along the “I-trajectory” and the “U-trajectory”.

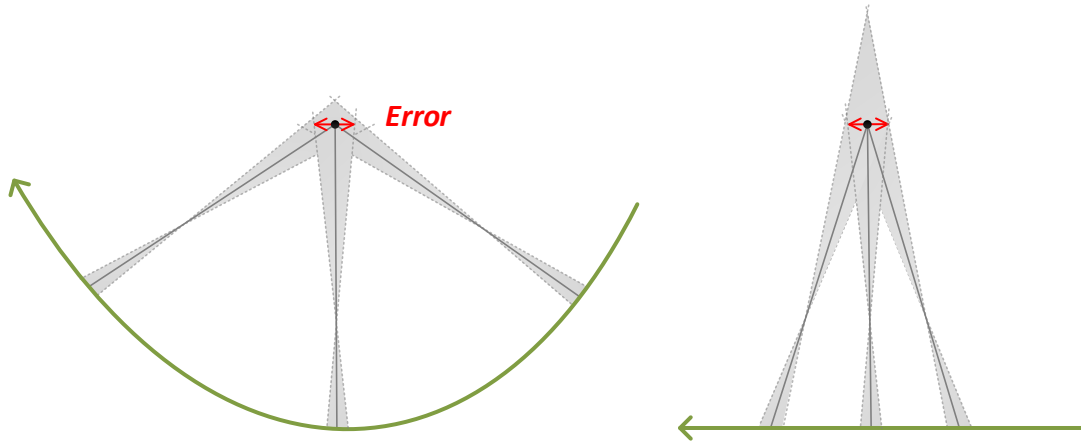


Figure 51: Error in the direction parallel to the wall of the object presented from the top view

8.2.2 Error in the Direction Perpendicular to the Object

The measurement error in the direction perpendicular to the wall of the object is expected to be smaller when the coordinates of the targets are measured in the images that were captured along the “U-trajectory”. While capturing the images along the “I-trajectory”, the intersection angles of image rays are much smaller. As visualized in Figure 52, the error of the Y coordinate can be improved with the optimal geometry of the captured images.

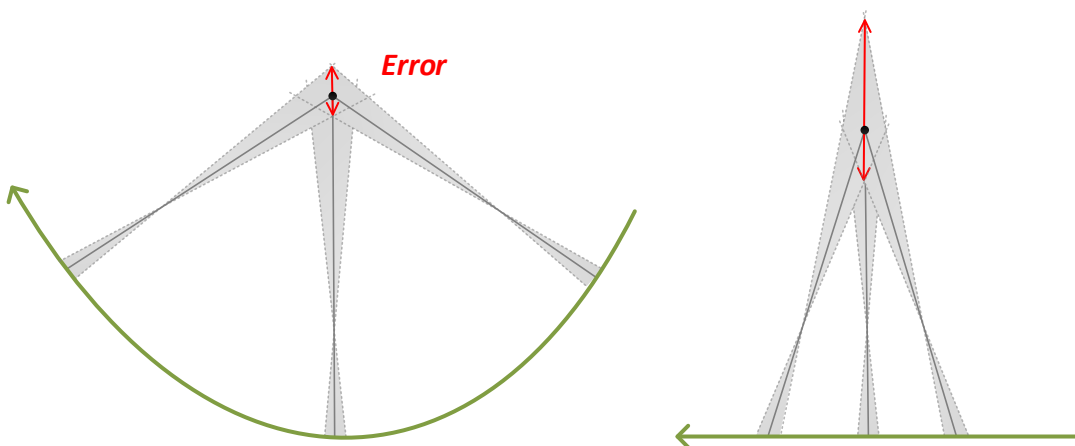


Figure 52: Measurement error in the direction perpendicular to the wall of the object presented from the top view

8.2.3 Error in the Height Direction

The initial camera poses are adjusted using the features generated in the images. The relative orientation (and position) of the images is highly accurate after the adjustment. Despite this, the absolute orientation of the images in the terrestrial coordinate system is less accurate and is highly related to the geometry of captured images. The uncertainty of adjusted camera poses is highly related to the geometry of the captured images because the camera poses are defined by the absolute orientation of the images in the terrestrial coordinate system. Therefore better geometry is provided and a smaller uncertainty is presented in the camera poses when the images are taken along the “U-trajectory”.

The smaller the uncertainties of the camera poses are, the smaller the errors in measurements are presented. The error in the height direction was therefore expected to be smaller while measuring the points in the images that were captured along the “U-trajectory”.

To understand how the error in height direction is influenced by the geometry of captured images, let us define the roll angle of captured images. The roll angle presents the vertical angle between the horizontal line and the optical axis of the camera at each camera pose from which the image was captured. The horizontal line presents the projection of the optical axis on the horizontal plane, which passes through the origin of the camera pose. The horizontal line, the optical axis, and the roll angle are visualized in Figure 53.

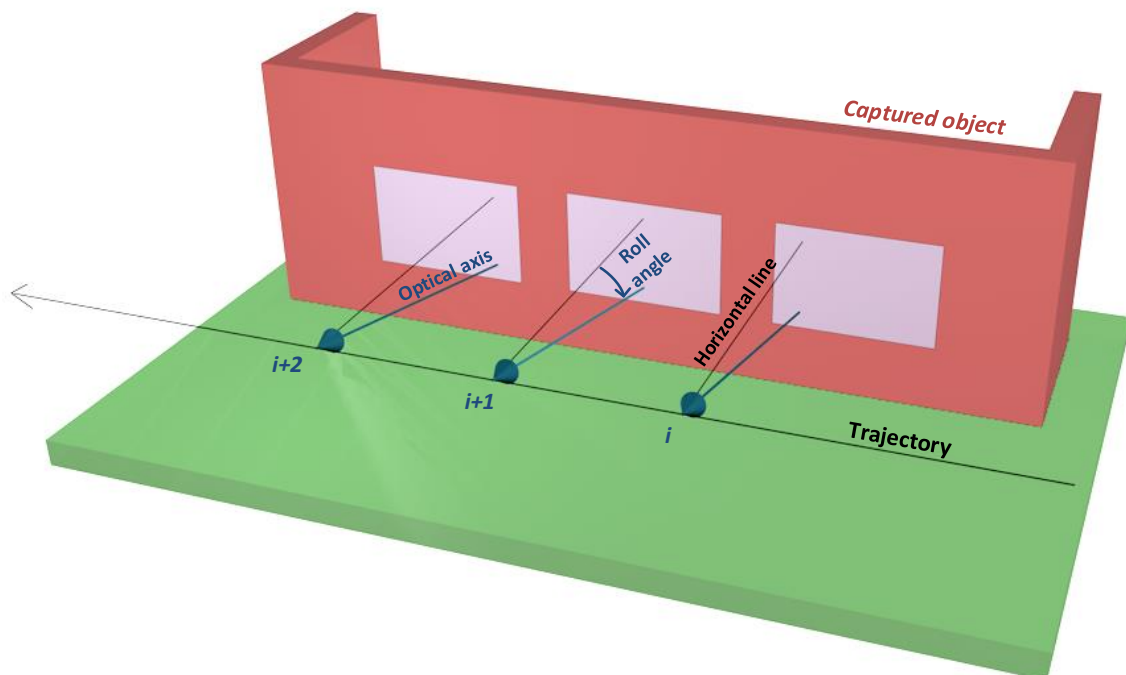


Figure 53: Roll angle of defined camera poses

For better understanding, the examples are explained for the measurements taken along the trajectories placed on the horizontal plane.

When the images are captured, the roll angle of the camera is defined by the inertial measurements taken with the IMU. The uncertainty presented in the initial camera poses is adjusted by the algorithms defined in Section 5.2. For better interpretation about how the camera poses are adjusted, let us fix the trajectory plane through the origins of each camera pose from which the images were taken. The trajectory plane should be defined by the horizontal lines of each camera pose, as visualized in Figure 54.

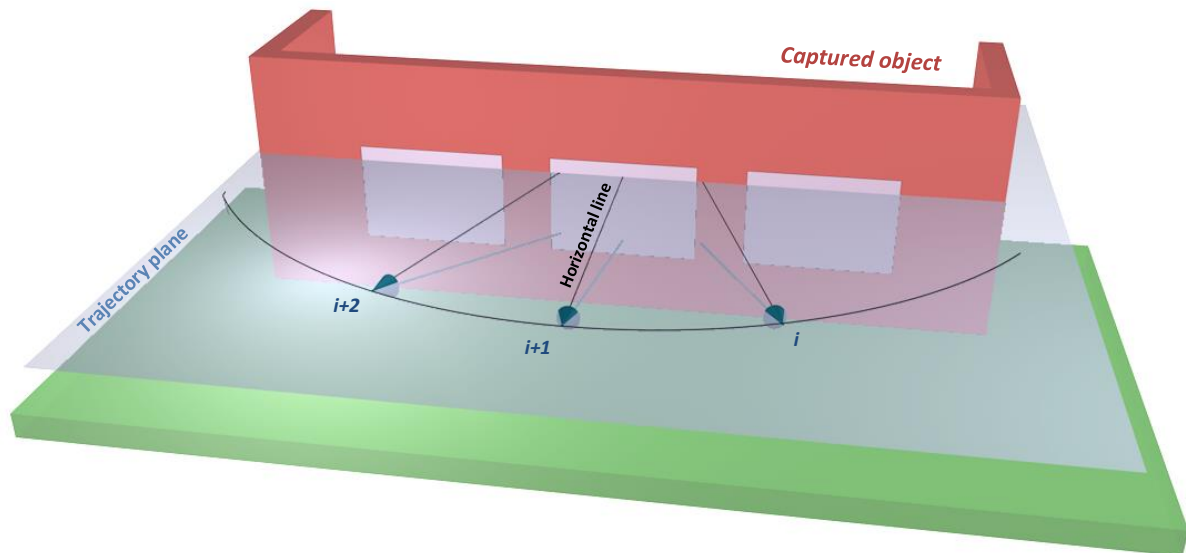


Figure 54: Trajectory plane defined while capturing the images along the “U-trajectory”

Assuming that the sensor is held horizontally while capturing the images along the trajectory, the roll angle should equal 12° downwards with respect to the horizontal line. The camera of the FuMo is namely tilted 12° downwards.

On one hand, while capturing the images along the “U-trajectory”, the trajectory plane can be defined unambiguously. The origins of the camera poses are namely not collinear. Due to a defined trajectory plane, the uncertainty in the roll angle of camera poses can be minimized by the Structure from Motion and Bundle Adjustment algorithms.

On the other hand, while capturing the images along the “I-trajectory”, the trajectory plane cannot be defined due to the collinearity of the origins of the camera poses. The uncertainty in the roll angle of the initial camera poses can therefore not be adjusted optimally through the Structure from Motion and Bundle Adjustment algorithms.

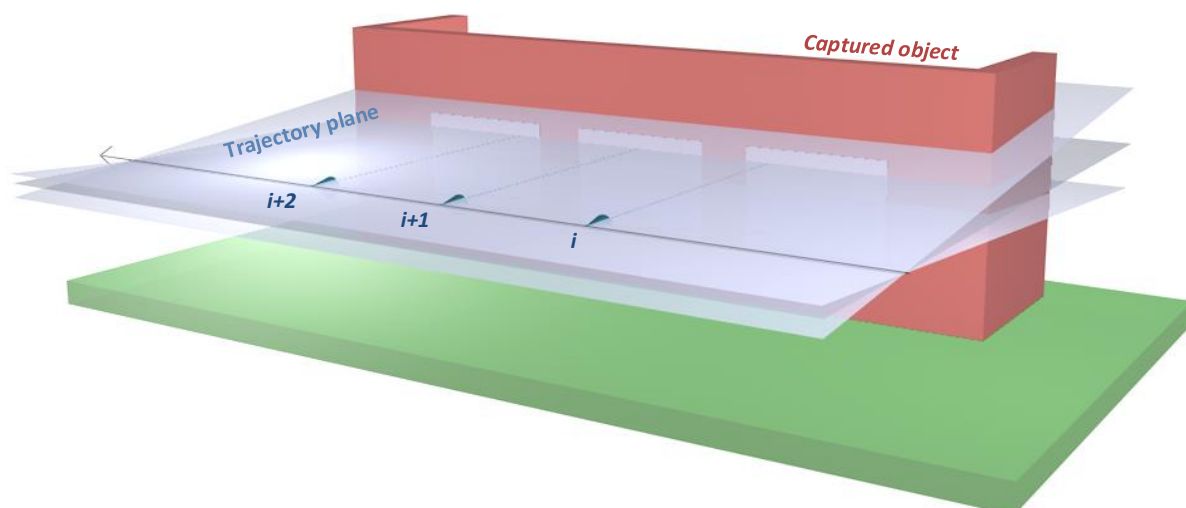


Figure 55: Undefined trajectory plane while capturing the images along the “I-trajectory”

The trajectory plane is actually not defined through the Structure from Motion and Bundle Adjustment algorithms. It was used in this section only for better interpretation of the problem.

The examples were explained for the trajectories that are placed in the horizontal plane. The uncertainty of the roll angle of camera poses can also be minimized by capturing the images along the “U-trajectory” that is tilted or placed in the vertical plane. The “U-trajectory” placed in the vertical plane is visualized in Figure 56.

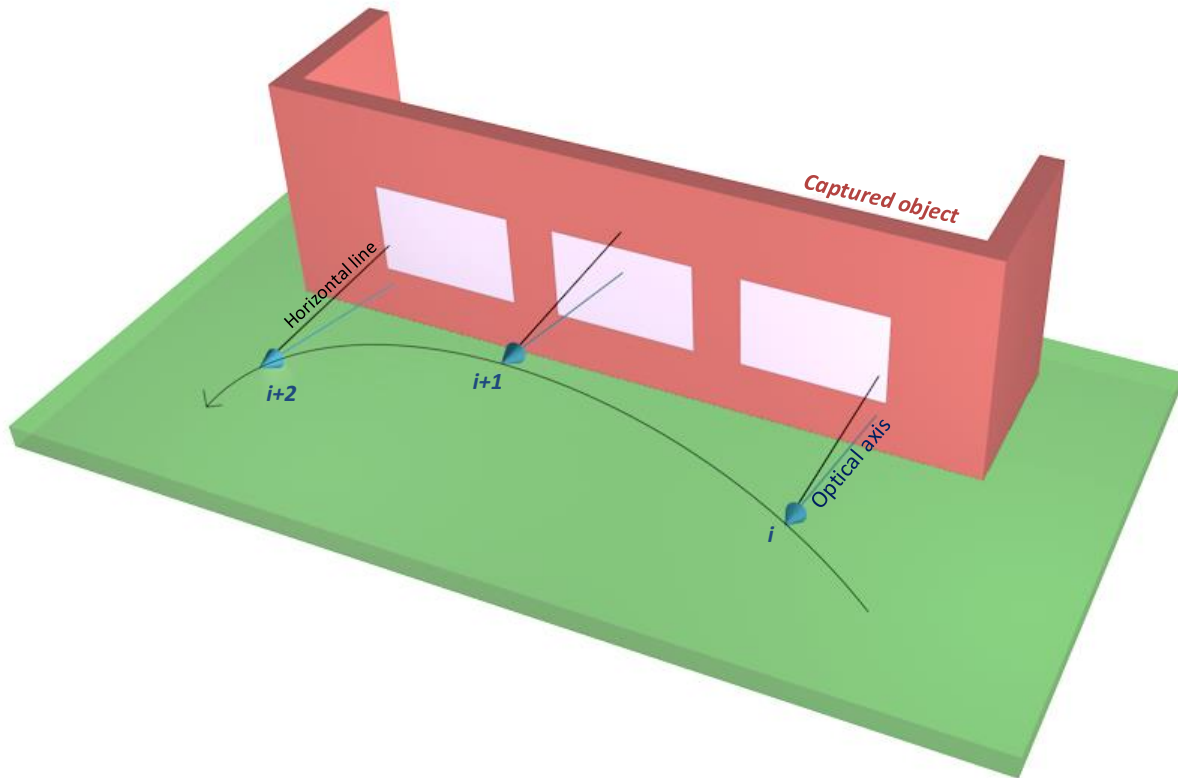


Figure 56: “U-trajectory” placed in vertical plane

To analyse the influence of the type of trajectory on the measurement error, the measurements were performed multiple times, as described in Section 9. The results of the measurements are analysed and interpreted in Section 10.2.

9 Measurements and Data Processing

The measurements taken with the FuMo were performed in the test field that is described in Section 7. They were taken repeatedly along the trajectories, which are visualized in Figure 42. The measurements with the FuMo were performed as shown in Table 7, where each measurement is presented with *x*.

The coordinates of the targets and the coordinates of the objects of interest were measured in captured images. All the coordinates obtained from one measurement are listed in a common data set. Each data set is defined with the properties of its measurement. Therefore, each data set in Table 7 can also be presented with *x*.

The data is then divided into measurement groups, which are marked in Table 7 with orange squares. All the data within one measurement group is processed together, as described in Section 9.2.

Table 7: Date and properties of the measurements in the test field

Date	Distance to the wall of the object										
	2 m		3 m		5 m		8 m		10 m		
	I	U	I	U	I	U	I	U	I	U	
18.09.2017			x	x	x	x					
19.09.2017					x	x	x	x	x	x	
20.09.2017			x		x	x	x	x	x	x	
22.09.2017				x	x	x	x	x	x	x	
18.10.2017	x		x	x			x	x	x	x	
19.10.2017			x	x							
24.10.2017	x		x	x	x						
30.30.2017	x		x	x					x	x	
31.10.2017	x										

x - processed measurements/data set
 - measurement group

The measurements were at taken different dates along the trajectories visualized in Figure 42. As seen in Table 7, the measurements did not take place along all the trajectories at every day listed in the table. Some data gaps are presented also because some measurements could not be processed. Due to the bumps and fast rotations of the FuMo that occurred during the measurements, the camera poses could not be adjusted (see Section 11.6).

The coordinates of the targets and the coordinates of the objects of interest that are measured with the FuMo are determined with the WGS84 Cartesian coordinates. In order to compute the error in the three desired directions, the coordinates of the targets can be transformed to a local coordinate system as described in Section 9.1. The error of the X coordinate in the local coordinate system presents the error in the direction parallel to the wall of the object located in the test field. The error of the Y coordinate presents the error in the direction perpendicular to the object wall. The error of the Z coordinate presents the error in the height direction.

The errors of the coordinates and the 3D errors are computed after the transformation as described in Section 9.2.

9.1 Transformation of the Coordinates

The coordinates of the targets measured with the FuMo are estimated in the WGS84 coordinate system. The reference coordinates of the targets were measured with the Leica MS60 in the local Swiss coordinate system LV95 and also determined in the WGS84 coordinate system. In order to determine the error in the three directions described in Section 8.2, the coordinates of the targets should be determined in a local coordinate system. The reference target coordinates and the target coordinates measured with the FuMo were therefore transformed from the WGS84 coordinate system to the local coordinate system. The local horizontal coordinate system LCS was therefore established as visualized in Figure 57.

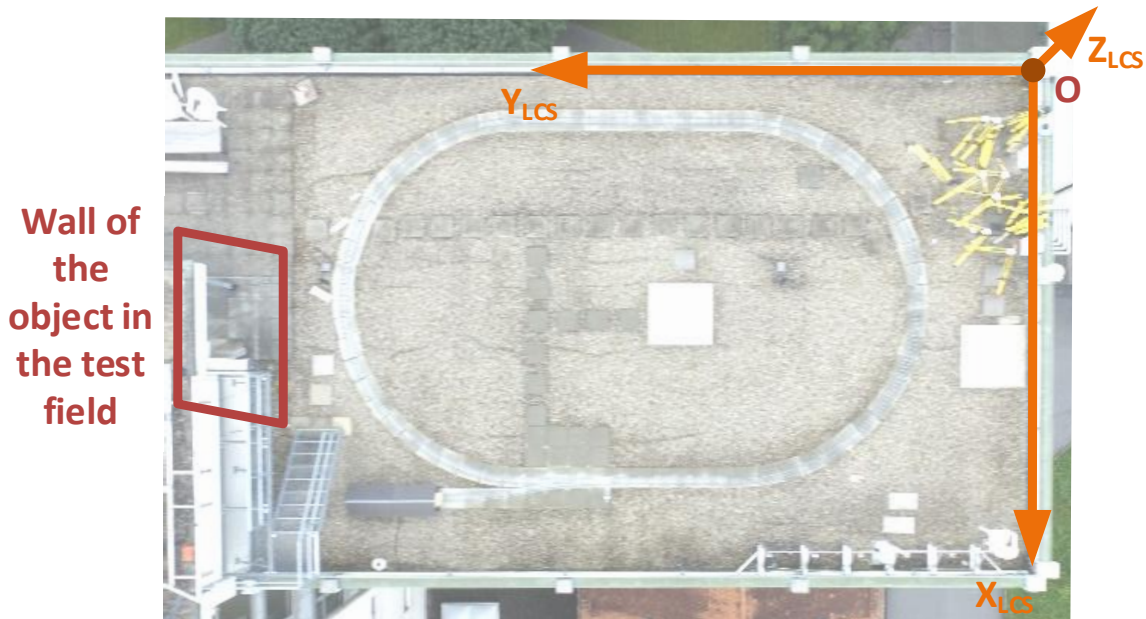


Figure 57: Local coordinate system in the test field

The origin of the local coordinate system is located in point O, which is placed on the roof in the north-east corner of the Leica Geosystems building B26. The WGS84 Cartesian and ellipsoidal coordinates of the point O are listed in Table 8. The X_{LCS} axis of the local coordinate system is oriented in the direction parallel to the wall of the object in the test field. The Y_{LCS} axis is oriented in the direction perpendicular to the wall. The Z_{LCS} axis is placed perpendicular to the X_{LCS} and Y_{LCS} axes, so that it coincides with the ellipsoid normal with the positive end outward of the ellipsoid.

Table 8: The WGS84 Cartesian and ellipsoidal coordinates of the origin of the local coordinate system

WGS84 Cartesian coordinates	WGS84 ellipsoidal coordinates
$X_o = 4263857.1101$	$\varphi_o = 47^{\circ} 24' 31.73668''$
$Y_o = 722616.8075$	$\lambda_o = 9^{\circ} 37' 7.68895''$
$Z_o = 4672989.7716$	$h_o = 471.3311$

In order to transform target coordinates from the WGS84 coordinate system to the local coordinate system LCS, the transformation should be applied in two steps. First, the transformation between the WGS84 coordinate system and the local coordinate system LCS1 is applied. In the second step, the coordinates should be transformed from the local coordinate systems LCS1 to the local coordinate system LCS.

The transformation between the WGS84 coordinate system and the local coordinate system LCS1 is applied as described in Leick (1995). As shown in Figure 58, the local coordinate system LCS1 is defined with its origin in the point O. The axes X_{LCS1} and Y_{LCS1} define the plane that is perpendicular to the ellipsoidal normal through the surface point O. The X_{LCS1} axis is pointed towards the North and the Y_{LCS1} axis is pointed towards the East. The Z_{LCS1} axis coincides with the ellipsoid normal with the positive end outward of the ellipsoid.

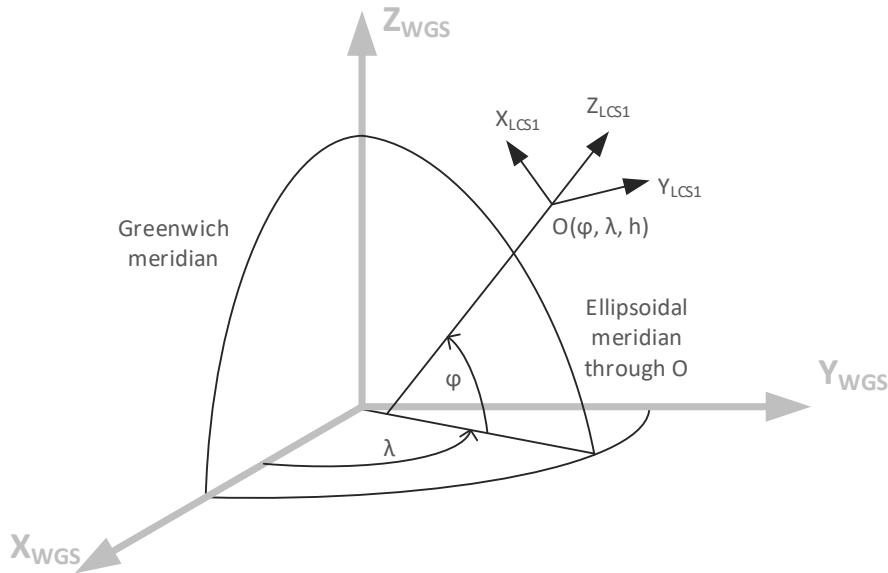


Figure 58: The local coordinate system and the WGS84 coordinate system

The transformation of the target point coordinates from the WGS84 coordinate system to the local coordinate system LCS1 is computed as described in Leick (1995):

$$\begin{bmatrix} X_T \\ Y_T \\ Z_T \end{bmatrix}^{LCS1} = P_Y \cdot R_Y(\varphi - 90^\circ) \cdot R_Z(\lambda - 180^\circ) \cdot \begin{bmatrix} X_O \\ Y_O \\ Z_O \end{bmatrix}^{WGS84} - \begin{bmatrix} X_T \\ Y_T \\ Z_T \end{bmatrix}^{WGS84} \quad (9.1)$$

Where

$\begin{bmatrix} X_O \\ Y_O \\ Z_O \end{bmatrix}^{WGS84}$ presents the translation vector between the coordinate systems. The vector is defined with the Cartesian coordinates of the point O in the WGS84 coordinate system (see Table 8).

$\begin{bmatrix} X_T \\ Y_T \\ Z_T \end{bmatrix}^{WGS84}$ presents the WGS84 Cartesian coordinates of the targets which are transformed to the local coordinate system LCS1.

$\begin{bmatrix} X_T \\ Y_T \\ Z_T \end{bmatrix}^{LCS1}$ presents the coordinates of the targets in the local coordinate system LCS1.

λ the longitude of the point O in the WGS84 coordinate system defines the rotation of the coordinate system around the Z_{WGS} axis.

φ the latitude of the point O in the WGS84 coordinate system defines the rotation of the coordinate system around the Y_{WGS} axis.

The transformation is realised by the rotation matrices R_Y and R_Z and the reflection matrix P_Y , which are shown in equations (9.2) to (9.4).

$$R_Y = \begin{bmatrix} \cos(\varphi) & 0 & -\sin(\varphi) \\ 0 & 1 & 0 \\ \sin(\varphi) & 0 & \cos(\varphi) \end{bmatrix}, \quad (9.2)$$

$$R_Z = \begin{bmatrix} \cos(\varphi) & \sin(\varphi) & 0 \\ -\sin(\varphi) & \cos(\varphi) & 0 \\ 0 & 0 & 1 \end{bmatrix}, \quad (9.3)$$

$$P_Y = \begin{bmatrix} 1 & 0 & 0 \\ 0 & -1 & 0 \\ 0 & 0 & 1 \end{bmatrix}. \quad (9.4)$$

After the transformation, the X_{LCS1} and Y_{LCS1} axes of the local coordinate system LCS1 point towards the North and towards the East. The Z_{LCS1} axis coincides with the ellipsoid normal with the positive end outward of the ellipsoid.

The final coordinate system LCS should be defined with the X_{LCS} and Y_{LCS} axes as visualized in Figure 59. The Z_{LCS} axis coincides with the Z_{LCS1} axis. In order to determine the coordinates in the local coordinate system LCS, the local coordinate system LCS1 has to be rotated around the Z_{LCS1} axis for the angle δ .

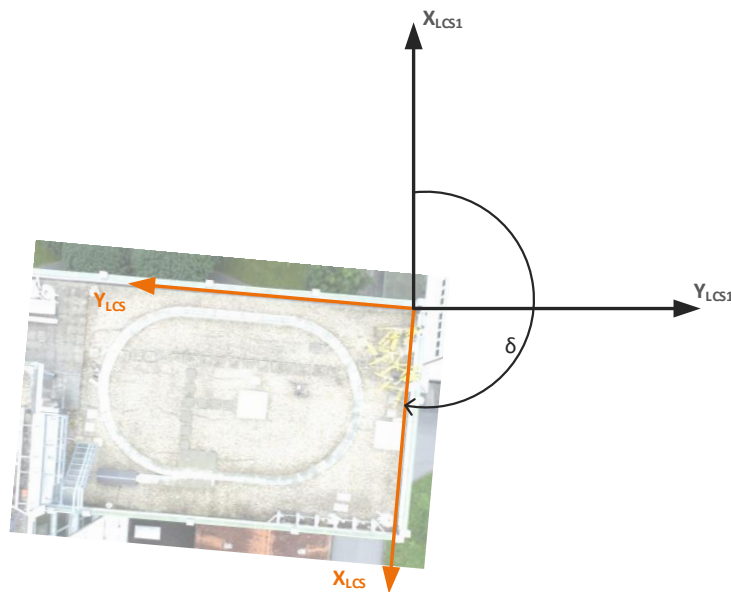


Figure 59: Rotation of the local coordinate system around the Z_1 axis

In order to calculate the angle δ , an orientation point should be defined along the X_{LCS} axis. The orientation point was determined with WGS84 Cartesian coordinates listed in Table 9.

Table 9: The WGS84 Cartesian coordinates of the orientation point

WGS84 Cartesian coordinates
$X_N = 4263865.3670$
$Y_N = 722617.5735$
$Z_N = 4672982.1707$

The orientation point should be transformed to the local coordinate system LCS1. The angle δ is computed using the X_N and the Y_N coordinates of the orientation point in the local coordinate system LCS1. The relation between the coordinates X_N and Y_N and the angle δ are visualized in Figure 60.

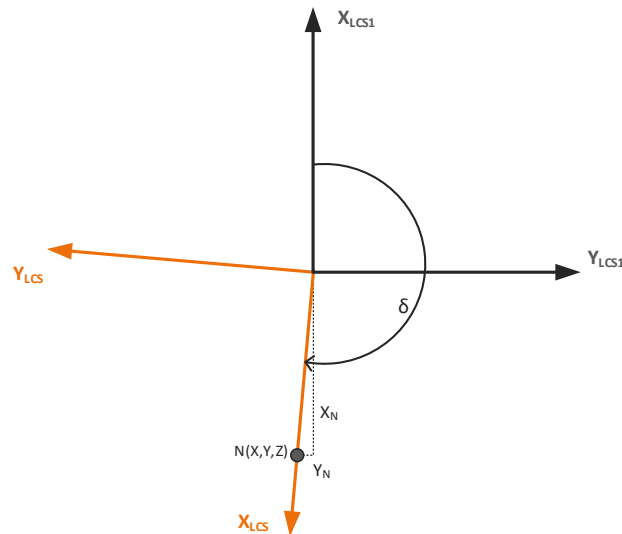


Figure 60: The transformation between local coordinate systems LCS1 and LCS

The angle δ is computed in the local coordinate system LCS1 as shown in Equation (9.5).

$$\delta = \text{atan}\left(\frac{X_N}{Y_N}\right) + 180^\circ \quad (9.5)$$

The rotation around the Z_L axis is applied as shown in Equation (9.9).

$$\begin{bmatrix} X_P \\ Y_P \\ Z_P \end{bmatrix}^{LCS} = R_{Z1} \cdot \begin{bmatrix} X_P \\ Y_P \\ Z_P \end{bmatrix}^{LCS1} \quad (9.6)$$

Where the R_{z1} is defined as follows:

$$R_{Z1} = \begin{bmatrix} \cos(\delta) & \sin(\delta) & 0 \\ -\sin(\delta) & \cos(\delta) & 0 \\ 0 & 0 & 1 \end{bmatrix}. \quad (9.7)$$

The reference coordinates of the targets determined in the local coordinate system LCS with the Leica MS60 are listed in Table 10.

Table 10: Reference coordinates of targets defined in the local coordinate system

Point ID	X [m]	Y [m]	Z [m]
BL01	4.9362	18.3322	2.2483
BL02	8.0773	18.3319	2.2547
BL03	8.0497	18.4027	0.0263
BW01	4.7889	18.3342	2.2139
BW02	4.7010	18.7812	1.4070
BW03	6.3388	18.8428	1.4393
BW04	6.8360	17.7951	1.4769
BW05	7.9119	18.3333	2.2650
BW06	7.4676	17.3116	1.4718
BW07	7.8970	18.3978	0.0532

9.2 Computation

The measurements with the FuMo were taken as listed in Table 7. In order to investigate the capability of the FuMo, the errors of the target coordinates should be computed. The error can be computed either separately for the X, Y and Z coordinates of measured targets or it can be computed as a 3D error of measured targets. All the errors in this section are computed with respect to the local coordinate system LCS, described in Section 9.1.

The error represents the difference between the coordinates measured with the FuMo and the reference coordinates described in Section 7. The measured coordinates of the targets were determined in the images captured with the FuMo. The reference coordinates of the targets were determined with the Leica MS60 as described in Section 7.3. The error of the measured coordinates of one target can be computed for each measured target as follows:

$$X_{\text{error,target}} = X_{\text{meas,target}} - X_{\text{ref,target}} \quad (9.8)$$

$$Y_{\text{error,target}} = Y_{\text{meas,target}} - Y_{\text{ref,target}} \quad (9.9)$$

$$Z_{\text{error,target}} = Z_{\text{meas,target}} - Z_{\text{ref,target}} \quad (9.10)$$

Where $X_{\text{meas,target}}$, $Y_{\text{meas,target}}$ and $Z_{\text{meas,target}}$ are the coordinates of a target, measured photogrammetrically with the FuMo. The reference coordinates of the target are indicated as $X_{\text{ref,target}}$, $Y_{\text{ref,target}}$ and $Z_{\text{ref,target}}$.

9.2.1 Mean Coordinate Errors of the Measurement Group

The mean error can be computed for each measurement group listed in Table 7. It can be computed using the errors of the target coordinates, which are computed as shown in equations (9.8) to (9.10). The mean error of each coordinate is computed as an average error of the target coordinates that are listed within one measurement group. It is computed as follows:

$$\bar{X}_{\text{error}} = \frac{1}{n} \sum_{i=1}^n X_{i\text{error}} \quad (9.11)$$

$$\bar{Y}_{\text{error}} = \frac{1}{n} \sum_{i=1}^n Y_{i\text{error}} \quad (9.12)$$

$$\bar{Z}_{\text{error}} = \frac{1}{n} \sum_{i=1}^n Z_{i\text{error}} \quad (9.13)$$

Where i presents the i -th evaluated error of the target coordinate that was measured within one measurement group. The same targets which were measured multiple times within one measurement group, were treated as independent measurements.

9.2.2 3D Error of the Measured Target

The 3D error of the measured target is computed as a distance between the measured target and the reference target. It is computed using the errors of the target coordinates, as shown in equations (9.8) to (9.10). The 3D error is computed as shown in Equation (9.14).

$$3D_{\text{error,target}} = \sqrt{X_{\text{error,target}}^2 + Y_{\text{error,target}}^2 + Z_{\text{error,target}}^2} \quad (9.14)$$

9.2.3 Accuracy of the Measurement group

The accuracy of the measurements can be computed separately for each measurement group listed in Table 7. The accuracy can be computed as an average of 3D errors of all targets measured in one measurement group. The 3D error of a target is computed as shown in Equation (9.14). The accuracy of the measurement group is computed as follows:

$$\text{Accuracy} = \frac{1}{n} \sum_{i=1}^n 3D_{i,\text{error,target}} \quad (9.15)$$

Where i presents the i -th evaluated 3D error of the target that was measured within one measurement group. The same targets which were measured multiple times within one measurement group, were treated as independent measurements.

10 Evaluation

Test measurements were taken with the FuMo as described in Section 9. The coordinates of the targets that are visualized in Figure 45 were determined in the images. The errors of the target coordinates were then computed as described in Section 9.2. It was investigated how the measurements are influenced by various factors that are described in Section 8.

10.1 3D Error of the Targets

The 3D error was computed for the target coordinates that were measured in the images which were taken along “I-trajectory” placed at the distance 2 m from the wall. The 3D error was computed as described in Section 9.2.2.

By computing the 3D error, the influence of the height of the targets in the images was investigated. The 3D error was computed for the targets measured in the images that were taken from the distance of 2 m. This way it was assured that the targets were captured not only along the middle line of the images, but also close to the top and the bottom edge of the images.

The 3D error of the target coordinates was computed from the measurements taken along the “I-trajectory” only. As the influence of the perspective of the camera according to the targets (see Section 6.2.2) was investigated, the measurement sets taken along the “U-trajectory” could not be used.

Furthermore, it was investigated how the size, the shape, and the colour contrast of measured targets influences the measurement error. Two different types of targets were therefore used to establish the test field and to determine their coordinates in the images captured with the FuMo.

10.1.1 Influence of the Target Height on the 3D Error

The influence of the height of the targets in captured images was investigated. The motivation for the research was to determine how the distortion of the images influences the 3D error of measured targets. Namely, each image captured by the FuMo is distorted. The distortion is caused by the optical design of the lens of the camera. As visualized in Figure 61, the distortion is much bigger on the edges of the image than it is close to the principal point of the image. To ensure the best possible quality of the images for the photogrammetric measurements, the distortion of the images is corrected, as shown in Figure 62.

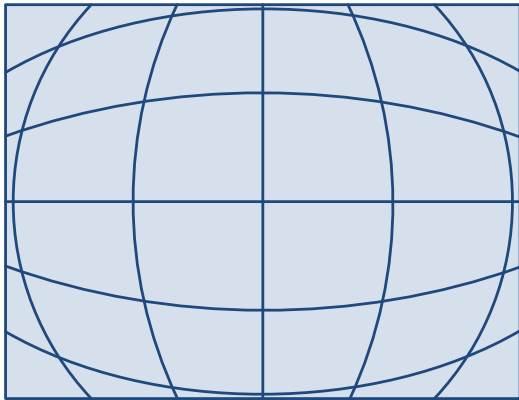


Figure 61: Captured image with distortion

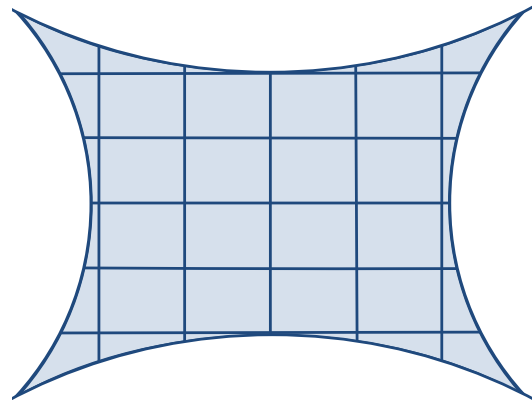


Figure 62: Processed image without distortion

In order to investigate if the distortion is still present in the images after the correction, the 3D error of the BW01 and BW02 targets was compared. As visualized in Figure 63, the targets were located on approximately the same horizontal position in the local coordinate system. The height of the coordinates differed for approximately 0.8 m. The coordinates of the targets in the local coordinate system are listed in Table 11.



Figure 63: Targets BW01 and BW02 located on different heights of the image

Table 11: Reference coordinates of the BW01 and BW02 targets determined in the local coordinate system LCS

Point ID	X [m]	Y [m]	Z [m]
BW01	4.7889	18.3342	2.2139
BW02	4.7010	18.7812	1.4070

To investigate the distortion that might be present in the images, one target had to be captured along the middle horizontal line of the images. Another target had to be captured close to the top edge of the image. In order to assure such distribution of the captured targets in the images, the measurements were taken from the camera-to-object distance of 2 m. The BW01 and the BW02 targets were captured in the images as shown in Figure 63.

It was expected that the BW01 target captured close to the top edge of the image has a bigger 3D error as the BW02 target captured along the middle horizontal line.

The difference between the 3D error of the BW01 and BW02 targets is visualized in Figure 64. The 3D errors of both targets are visualized together for the targets listed the same data set. The blue bars present the 3D error of the BW01 target and the green bars present the 3D error of the BW02 target.

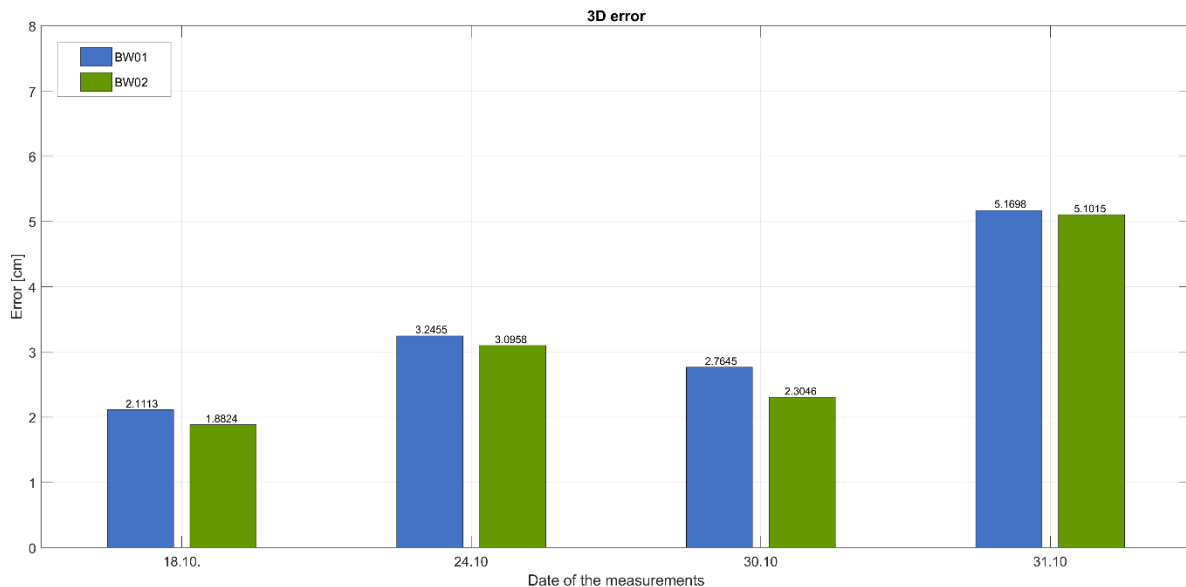


Figure 64: 3D error of the BW01 and BW02 targets

As expected, the 3D error of the BW02 target is smaller than the error of the BW01 target. This means that, after the correction, there is still some distortion present in the images. However, the difference between the errors of both targets was never bigger than 3 mm. The influence of other components on the 3D error is much bigger than the influence of the height of the targets in the images. Therefore, it is not of big importance where the targets are captured in the images.

The measurements were taken at different dates, but in similar light conditions and along the same trajectory. Despite that, the 3D error of one target measured at different dates varies for a few centimetres. The varying error of the targets can be seen in Figure 64 and Figure 66. The 3D error of measured targets is namely highly influenced by the accuracy of GNSS measurements. The accuracy of the GNSS measurements varies with the time and the day. It is influenced by the number and angle of the satellites from which the signal is accepted, by atmospheric signal interference, etc. As these conditions cannot be constant during different measurement periods, the coordinates of the targets cannot be defined with the same 3D error.

10.1.2 Influence of the Perspective of the Camera According to the Target on the 3D Error

The influence of the perspective of the camera according to the target was investigated as well. The motivation for the investigation is described in Section 6.2.2. Namely, the uncertainty translated from the image point to the measured object point can be much bigger when the images of the targets are taken from larger oblique angles.

In order to investigate how big of an influence the perspective of the camera has according to the target, the 3D error of the BW03, BW04, and BW06 targets was compared. As visualized in Figure 65, the targets were located at approximately the same height in the local coordinate system (see Section 9.1). The height difference between the targets was approximately 4 cm. The coordinates of the targets in the local coordinate system are listed in Table 12.



Figure 65: Targets BW03, BW04, and BW06 placed in the test field under different angles

Table 12: Reference coordinates of the BW03, BW04, and BW06 targets in the local coordinate system LCS

Point ID	X [m]	Y [m]	Z [m]
BW03	6.3388	18.8428	1.4393
BW04	6.8360	17.7951	1.4769
BW06	7.4676	17.3116	1.4718

To investigate the influence of the perspective of the camera according to the target, the target BW04 was captured in images from high oblique angles. The targets BW03 and BW06 were captured from much smaller oblique angles. In order to assure that the target BW04 is captured in each image from a higher oblique angle as the targets BW03 and BW06, the images were taken along the “I-trajectory” only. The perspective of the targets as seen from one image is shown in Figure 65.

It was expected that the BW04 target captured from larger oblique angles has a bigger 3D error as the BW03 and BW06 targets captured from smaller oblique angles.

The difference between the 3D error of the BW03, BW04, and BW06 targets is visualized in Figure 66. The 3D error is visualized together for the targets listed in the same data set. The blue bars represent the 3D error of the BW03 target, the green bars of the BW04 target and the grey bars represent the 3D error of the BW06 target.

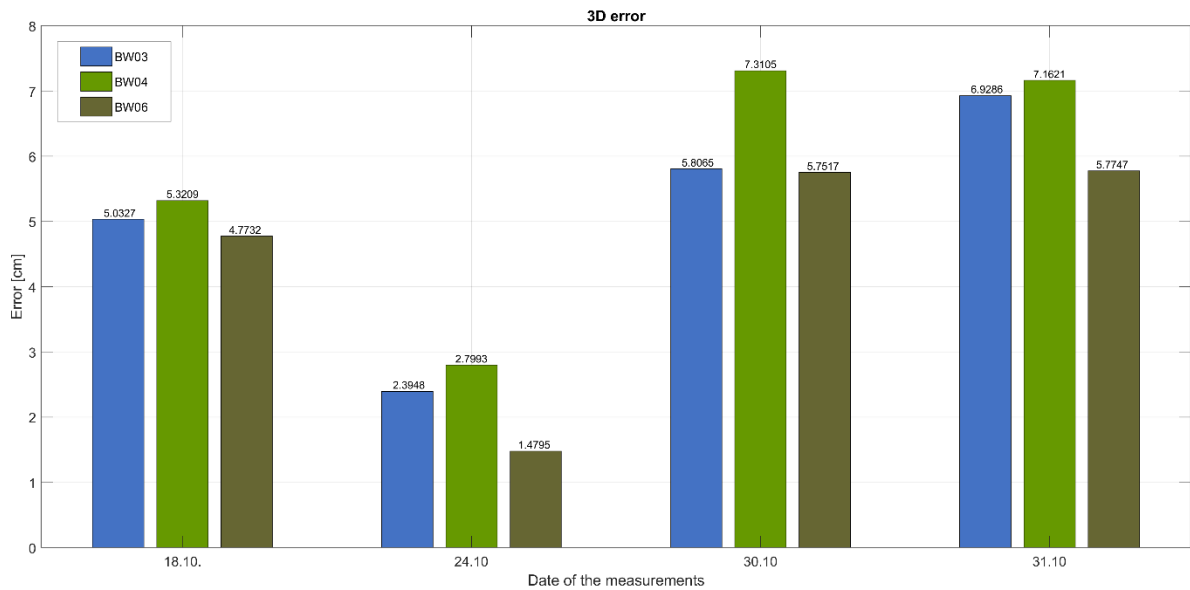


Figure 66: 3D error of the BW03, BW04, and BW06 targets

As expected, the 3D error of the BW04 target is bigger as the 3D error of the BW03 and BW06 targets. This means that the perspective of the camera according to the captured object does influence the 3D error of the target coordinates.

There was also another influence presented in the error of the target coordinates, which are visualized in Figure 66. The 3D error of the BW06 target was smaller than the 3D error of the BW03 target in all data sets. The camera-to-object distance difference between the BW03 and BW06 targets was approximately 1 m. The BW06 target was measured from shorter camera-to-object distances as the BW03 target. Smaller uncertainties were therefore translated from image points and the projective centre to the BW06 target.

As described in Section 10.1.1, the 3D error of one target measured at different dates varies for few centimetres. The varying error of the targets can be seen in Figure 64 and Figure 66. The 3D error of measured targets is namely highly influenced by the accuracy of GNSS measurements, which varies with the time and the day.

10.1.3 Influence of the Target Type on the 3D Error

Two different target types were used for test measurements in order to investigate how the size, the shape, and the colour contrast of measured targets influence the 3D error of photogrammetric measurements.

The blue and the black-and-white targets that are shown in Figure 44 were used for the investigation. There were three pairs of blue and black-and-white targets placed in the test field. As visualized in Figure 67, the BL01 and the BW01 targets were placed close to each other. As visualized in Figure 68, the BL02 and BW05 targets were placed close to each other, as well as the BL03 and BW07 targets. The coordinates of the targets are listed in the local coordinate system in Table 11.



Figure 67: Two different types of targets, BL01 and BW01



Figure 68: Two different types of targets, BL02 and BW05, BL03 and BW07

Table 13: Reference coordinates of the BL01, BL02, BL03, BW01, BW05, and BW07 targets in the local coordinate system

Point ID	X [m]	Y [m]	Z [m]
BL01	4.9362	18.3322	2.2483
BW01	4.7889	18.3342	2.2139
BL02	8.0773	18.3319	2.2547
BW05	7.9119	18.3333	2.2650
BL03	8.0497	18.4027	0.0263
BW07	7.8970	18.3978	0.0532

Calculated from the coordinates listed in Table 11, the targets of each pair were placed approximately 16 cm apart. The targets were therefore captured in images close to each other. By placing the targets close to one another it was ensured that other influences on the 3D error were of minority.

Image coordinates of the targets were determined in images. As described in Section 5.3, the image coordinates of a target are defined in one image by user. The image coordinates of the BL01 and the BW01 targets were defined by the user in one of the images, as shown in Figure 69.



Figure 69: Image coordinates of BL01 and BW01 defined by the user in one image

The same target should be found automatically by the algorithm in other images. The algorithm searched for the same target along the epipolar line in other images. As shown in Figure 73, the target BW01 was found in the other image and the coordinates of the target were determined. The image coordinates of the BL01 target could not be determined. The algorithm searched where the matching of the reference matrix along the epipolar line in the other images was the biggest. Because there was too much light presented when capturing the images with the FuMo, the black cross in the middle of the blue target was not captured in the images. The reference matrix defined in the first image was therefore not unique and could not be found in other images. The coordinates of the target could therefore not be determined in the local coordinate system.



Figure 70: Image coordinates of the BL01 not found in other images

The same problem occurred while defining the coordinates of the BL02 and the BL03 targets in the images taken from the distance of 2 m. The comparison of the 3D measurement error was therefore not possible.

The problem could be solved by taking the measurements from bigger camera-to-object distance. The targets captured in images taken from bigger distances appear much smaller in the images. The reference matrix would then be unique enough to match images with one another.

10.2 Mean Error of the Measurement Class

The mean error of each measurement group was visualized separately for each of the three directions. The measurements of each measurement group took place as listed in Table 7.

At first the distribution of the errors of target coordinates measured within the measurement groups was investigated. The distribution of the errors of the target coordinates measured in images taken along the “I-trajectory” is visualized in Figure 71. The distribution of the errors of the coordinates measured in images taken along the “U-trajectory” is visualized in Figure 72.

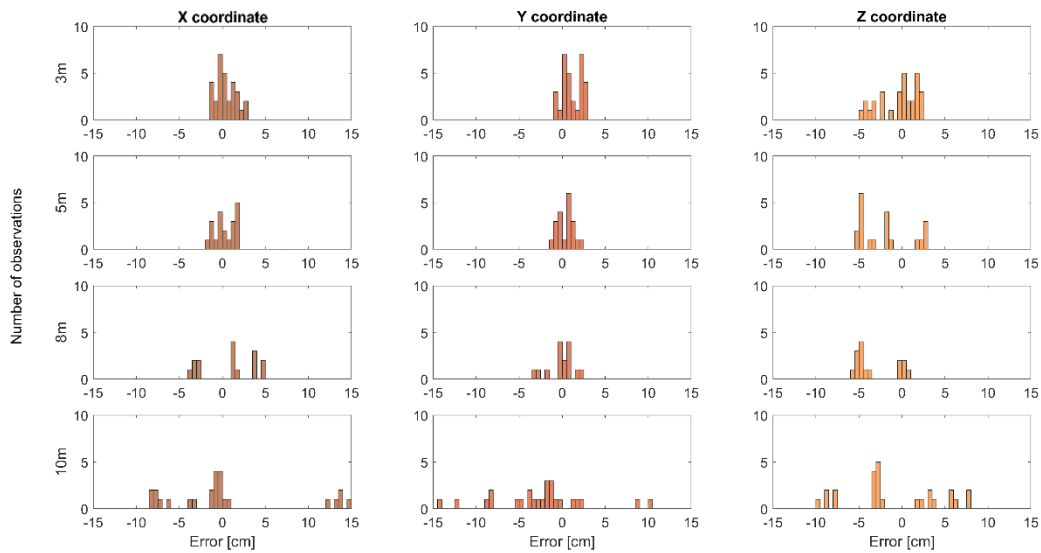


Figure 71: Distribution of the errors of the measurements taken along the “I-trajectory”

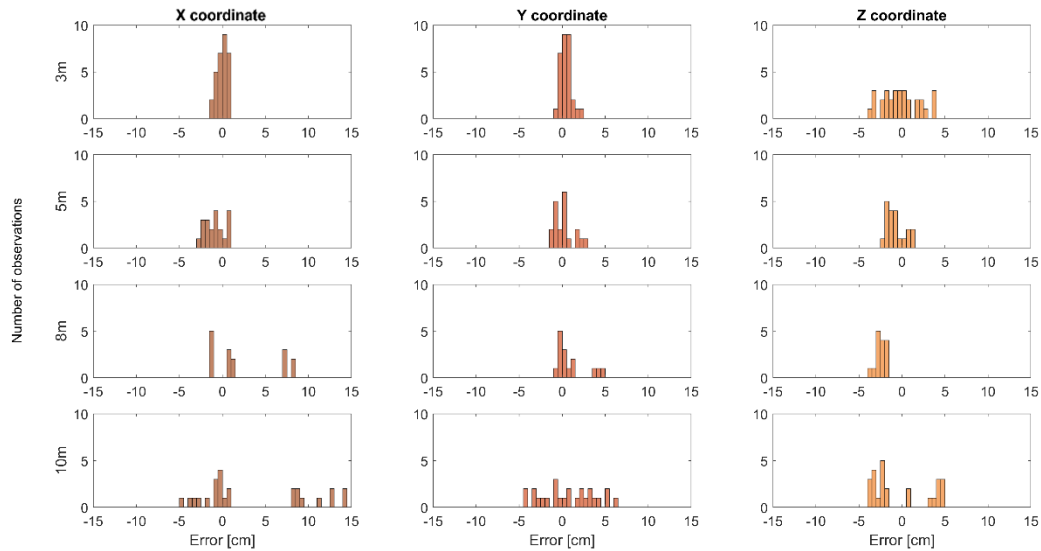


Figure 72: Distribution of the errors of the measurements taken along the “U-trajectory”

10.2.1 Error of the X Coordinate

The position error of the X coordinate of measured targets is visualized in Figure 73. The mean error of each measurement class is visualized together with the minimum and maximum errors of each measurement class. As described in Section 8.2.1, the error of the X coordinate is expected to be equal for the targets measured in the images taken along the “I-trajectory” and the “U-trajectory”.

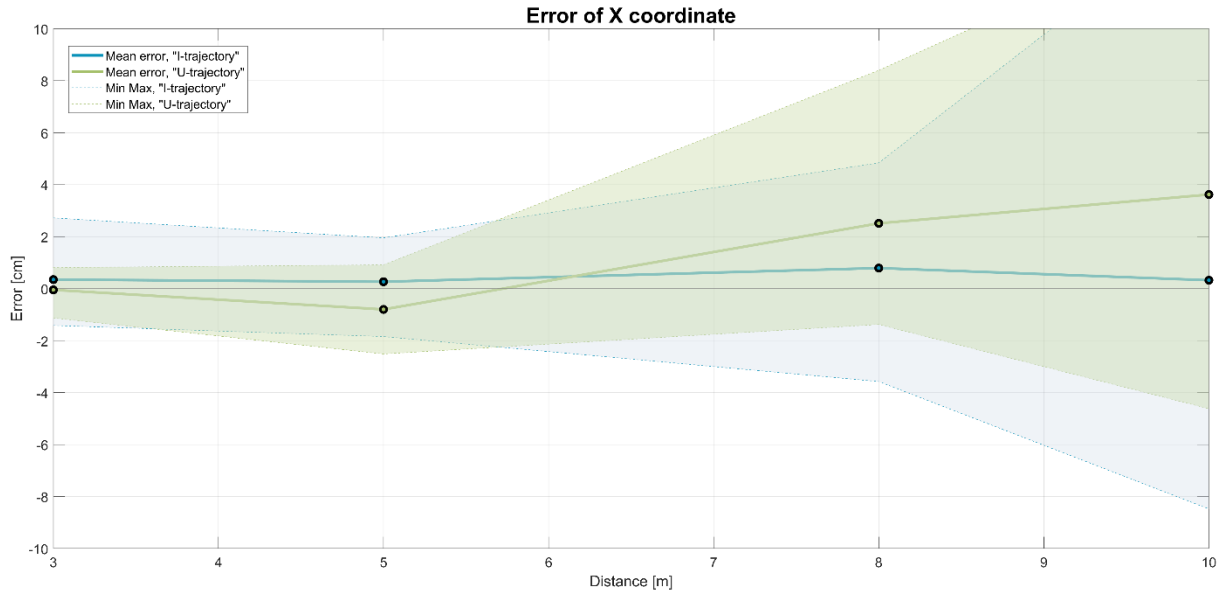


Figure 73: Errors of the X coordinate of measured targets

The minimum and maximum error visualized in Figure 73 correspond to the minimum and maximum error of the X coordinate shown in the first column of Figure 71 and Figure 72. The error of the X coordinate is dramatically increased when the measurements are performed in images that are captured from a distance bigger than 5 m. Due to higher distances, the points measured in images are heavily influenced by the uncertainty of GNSS measurements presented in camera poses (see Section 4.3.2).

The optimal geometry is provided for the measurements taken from the 3 m and 5 m distance. The X coordinate measured in the images taken from 3 m and 5 m distance can therefore always be defined with less than a 3 cm error.

10.2.2 Error of the Y Coordinate

The position errors of the Y coordinate of measured targets are visualised in Figure 74. The mean error of each measurement class is visualized together with the minimum and maximum errors of each measurement class. As described in Section 8.2.2, the mean measurement error is expected to be smaller for the measurements taken along the “U-trajectory”.

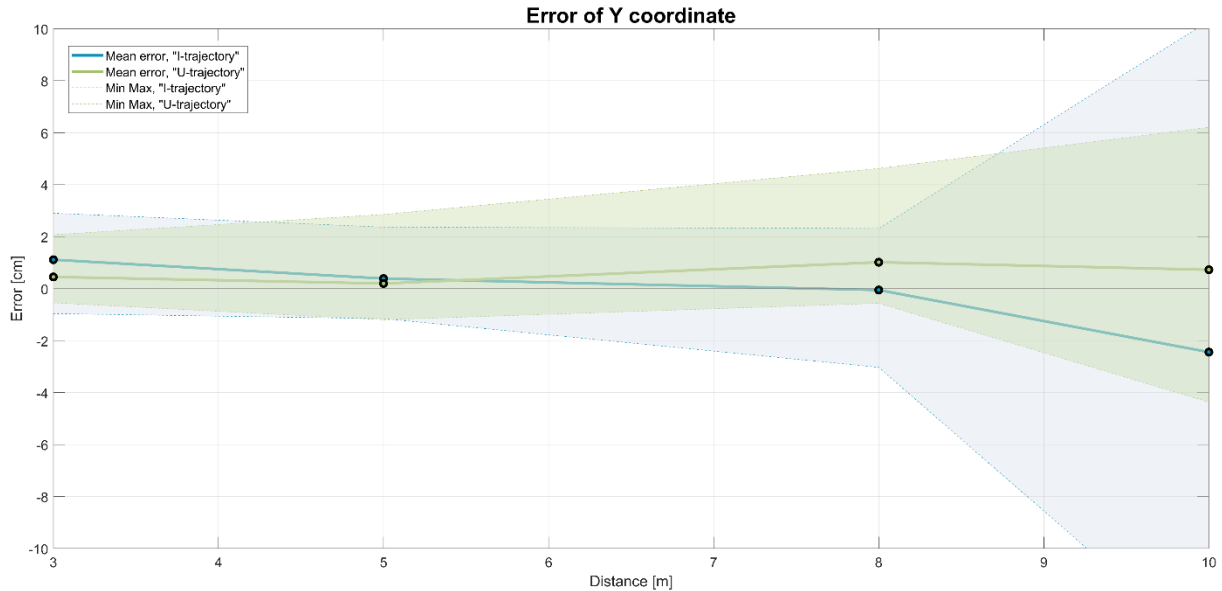


Figure 74: Errors of the Y coordinate of measured targets

The minimum and the maximum error visualized in Figure 74 correspond to the minimum and maximum error of the Y coordinate shown in the second column of Figure 71 and Figure 72. The error of the Y coordinate dramatically increases when the measurements are performed in images that are captured from the distance bigger than 5 m. Due to higher distances, the points measured in images are heavily influenced by the uncertainty of GNSS measurements presented in camera poses.

The optimal geometry is provided for the measurements taken from 3 m and 5 m distance to the wall of the object. The comparison of the mean error of the Y coordinate can therefore be made for the measurements taken along both trajectories placed at the distance of 3 m and 5 m. As expected, the mean error of the Y coordinate is smaller when the images are captured along the “U-trajectory”. As visualized in Figure 74, the biggest difference can be seen in measurements taken from the distance of 3 m. At that distance, the Y coordinate of measured targets can be determined with a much bigger confidence.

10.2.3 Error of the Z Coordinate

The position errors of the Z coordinate of measured targets are visualised in Figure 75. The mean error of each measurement class is visualized together with the minimum and maximum errors of each measurement class. As described in Section 8.2.3, the error is expected to be smaller for the targets measured in images which were taken along the “U-trajectory”.

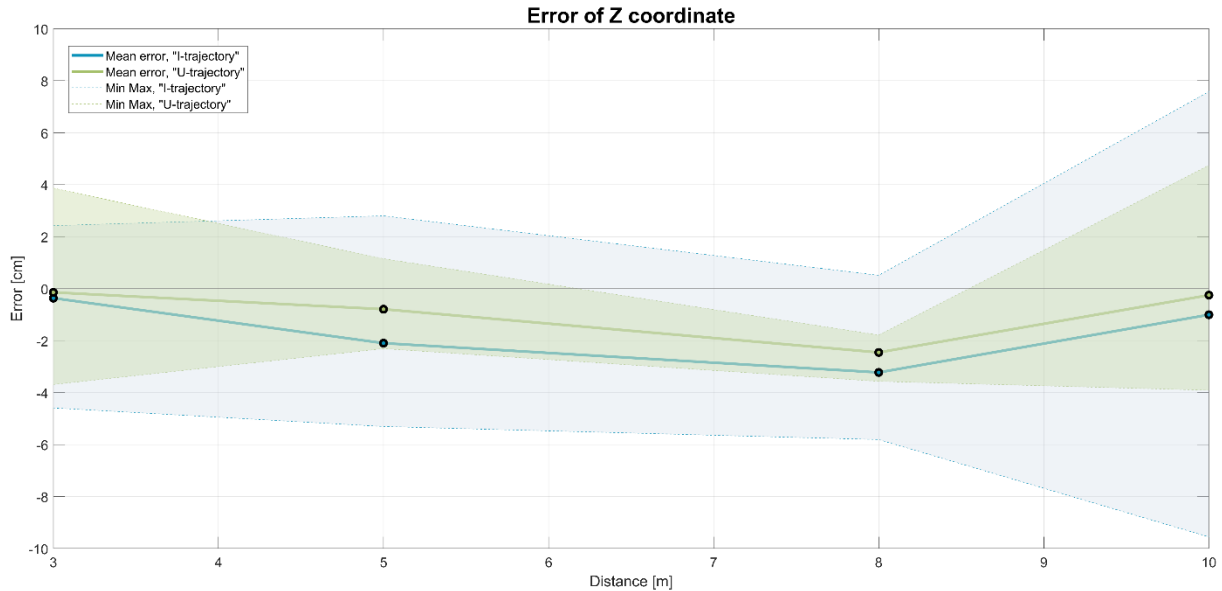


Figure 75: Errors of the Z coordinate of measured targets

The minimum and the maximum error visualized in Figure 75 correspond to the minimum and maximum error of Z coordinate shown in the third column of Figure 71 and Figure 72.

As seen in Figure 75, the position error of the Z coordinate is much smaller when the targets are measured in images taken along the “U-trajectory”. Due to a better geometry of the images taken along the “U-trajectory”, a better adjustment of the camera poses is provided.

It is visible that the systematic error is presented in the Z coordinate of measured targets. The error increases together with the increasing distance. As all the measurements were performed with the same sensor, the systematic error could be caused by an inaccurate calibration of the external orientation of the camera (see Section 6.1.2).

10.3 Accuracy

In order to investigate the capability of photogrammetric measurements taken with the FuMo, the measurements with the sensor were performed in the test field, which is described in Section 7.

The accuracy was investigated for the measurements taken along different trajectories. As described in Section 4.3.2, it was expected to achieve more accurate measurements when the images are taken from shorter camera-to-object distances. Namely, with bigger camera-to-object distance the accuracy of the determined target coordinates gets lower.

Furthermore, the accuracy was determined for the target coordinates measured in images that were taken along two different types of trajectories. It was investigated how the type of trajectory influences the accuracy of the measurements. It was expected that higher accuracy can be achieved when the target coordinates are measured in images captured along the “U-trajectory”. Better accuracy can be achieved due to optimal geometry of the images that are captured along the “U-trajectory”.

The accuracy of each measurement class was calculated as described in Section 9.2.3. It was computed using the absolute measurement error of all targets measured within one distance class.

Firstly, the distribution of the 3D error was visualized for each measurement class. The distribution of the 3D error of the targets is visualized in Figure 76 for the measurements taken along the “I-trajectory”. The distribution of the 3D error of the targets measured in images taken along the “U-trajectory” is visualized in Figure 77.

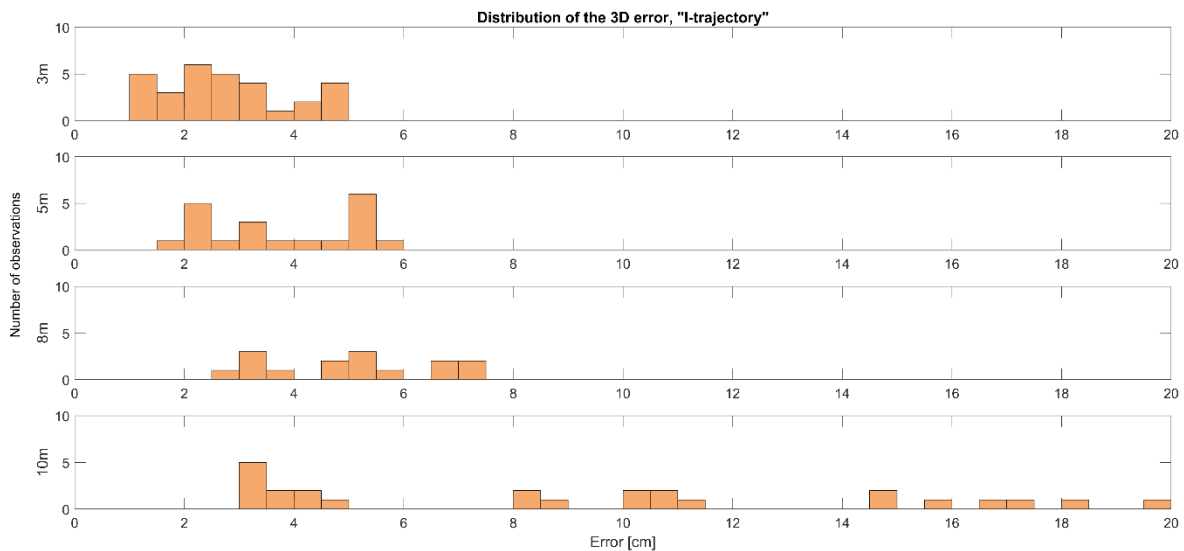


Figure 76: Distribution of the 3D error of the measurements taken along the “I-trajectory”

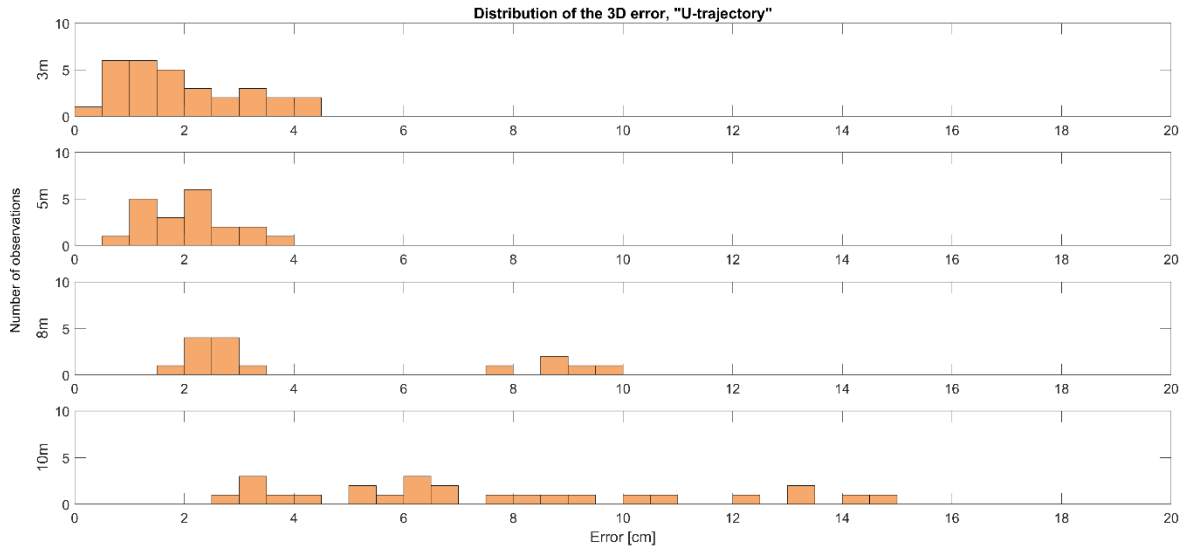


Figure 77: Distribution of the 3D error of the measurements taken along the “U-trajectory”

The uncertainty of the GNSS measurements has the biggest influence on the uncertainty of determined position of camera poses. As described in Section 4.3, the uncertainty that is presented in the camera poses is translated along the image rays to the measured point coordinates. The uncertainty presented in measured target coordinates increases together with the increasing camera-to-object distance (see Section 4.3.2). Therefore, a much bigger 3D error is presented in target coordinates measured in images that were captured from the distance of 8 m and 10 m.

The accuracy of the measurements was calculated using the 3D error of all target coordinates measured within one measurement class. It was calculated as a mean value of all 3D errors. As shown in Figure 78, the accuracy was visualized together with the minimum and the maximum values of each measurement class.

The minimum and maximum errors visualized in Figure 78 correspond to the minimum and maximum errors shown in Figure 76 and Figure 77.

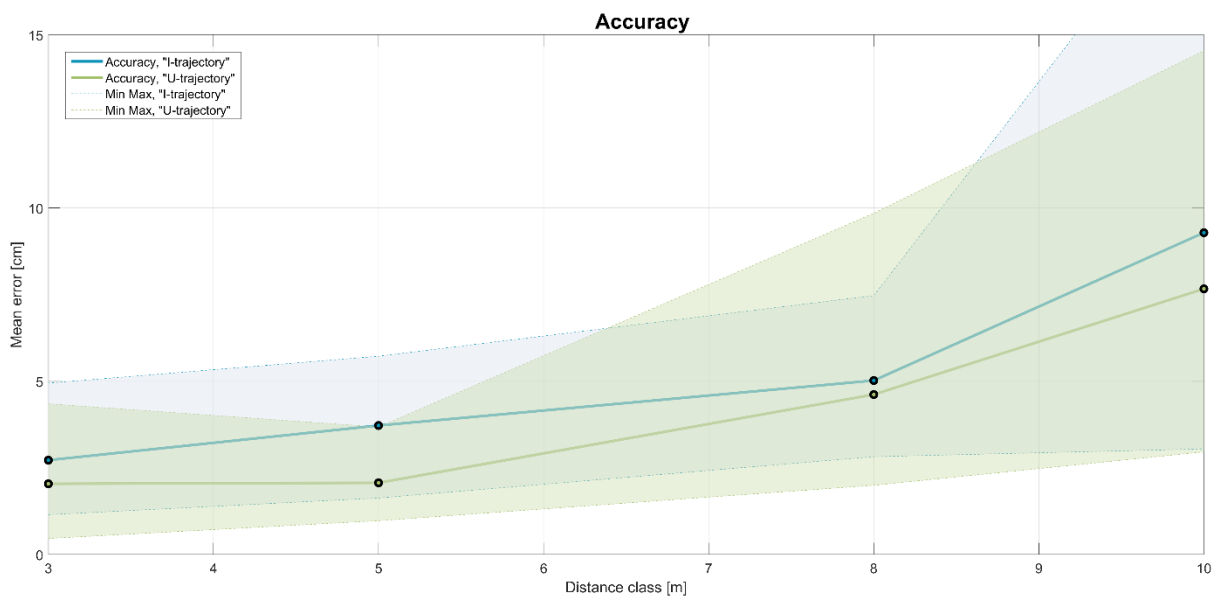


Figure 78: Accuracy of the target coordinates measured in images taken with the FuMo

As expected, the accuracy of the measurements taken from the 3 m distance is approximately 3 cm. The accuracy of the measurements decreases together with the increasing camera-to-object distance.

As described in Section 7.5.2, the optimal geometry is provided for the measurements taken up to 5 m distance from the wall of the object in the test field. The targets measured from the distance up to 5 m therefore have less than a 6 cm error presented in their coordinates.

The target measured in images taken from the distance of 8 m can be determined with the error that is even bigger than 10 cm. Namely, the photogrammetrically measured target coordinates are determined by means of triangulation. The uncertainty of measurements therefore linearly increases together with the increasing camera-to-object distance (see Section 4.3.2). In addition, optimal geometry of the images used for the measurements was not provided for the images captured from the distance of 8 m (see Section 7.5.2).

The determined accuracy of the measurements in the images which are taken from distances bigger than 8 m is between 5 cm to 9 cm. Due to the big distance and due to the non-optimal geometry of the images, the 3D error can reach up to 20 cm. Such measurements could be used for the measurements of the object dimensions, where it is crucial that the points are accurately determined relative to one another.

The accuracy of the measurement taken from the distances shorter than 3 m cannot get higher than 3 cm. Namely, the accuracy of 3 cm is also the accuracy of the GNSS measurements, which are used for defining the camera poses from which the images were taken.

The accuracy of the measurements can be improved by taking the measurements along the “U-trajectory”. As better geometry of the images is provided, smaller errors are presented in the measured points. The error presented in the measurements taken along the “U-trajectory” can be approximately 1 cm smaller than the measurements taken along the “I-trajectory”.

11 Limitations of the FuMo

In order to achieve optimal results while measuring points photogrammetrically with the FuMo, the limitations of the system have to be understood. The limitations of the system are based on the measurements performed in the test field, which is described in Section 7. In the following sections it is described what should be considered before performing the measurements with the FuMo.

11.1 GNSS Reception

The reception of the GNSS signal is of significant importance while performing measurements with the FuMo. The camera pose from which the images are captured is determined with the GNSS measurements. If the GNSS signal is not available, the camera poses from which the images were taken cannot be determined. The measurements in images are therefore not possible.

In order to provide optimal accuracy of the GNSS measurements, the access to the open sky should be available. If possible, the areas where the multipath of the signal is present should be avoided.

11.2 Lighting Conditions

As the photogrammetric measurements are performed using images, there should be enough light available while capturing the images. The illuminance should be at least 98.5 lux while capturing the images. At that amount of light it is still possible to recognise the details in captured images. Figure 79 shows the image that was captured while the illuminance was 98.5 lux.



Figure 79: The image captured with the illuminance of 98.5 lux

If there is too much light present while capturing the images, the images cannot be usable to determine the coordinates of image points. When the sun illuminates the object directly, the details in the images may not be recognisable. As seen in Figure 80, the black-and-white targets cannot be recognised in the image. In worst case there might not be enough features recognisable in the images for the algorithm to generate the features. In such case the camera poses cannot be adjusted and the images cannot be used for the photogrammetric measurements.



Figure 80: The sun illuminating the object directly

It is also recommended not to capture the images with the FuMo, when the sun is behind the captured object. As seen in Figure 81, due to the high amount of illuminance presented in one part of captured image, some objects of interest might not be recognisable in images.



Figure 81: Sun behind the captured object

11.3 Camera-to-object Distance

Camera-to-object distance has a big influence on the accuracy of the photogrammetric measurements taken with the FuMo. As described in Section 10.3, the measurements taken from the shorter distances can be defined with the accuracy of 3 cm. As listed in Table 14, the measurement accuracy gets lower with the increasing camera-to-object distance.

The measurements from the camera-to-object distance up to 5 m could be used for surveying applications where the accuracy of a few centimetres is satisfying. The measurements from distances bigger than 5 m are less accurate. They could be used for the measurements of object dimensions. They could also be used for measurements where the relative position of measured objects of interest is more important than the accuracy of the coordinates in the terrestrial coordinate system.

The camera-to-object distance should be considered also when the objects of interest are located much higher than the sensor capturing the images. The measurement height presents the height of the object, up to where the object is still captured in the images. As visualized in Figure 82, the measurement height increases together with the increasing camera-to-object distance. The range of measurement height in dependence of camera-to-object distance is listed in Table 14.

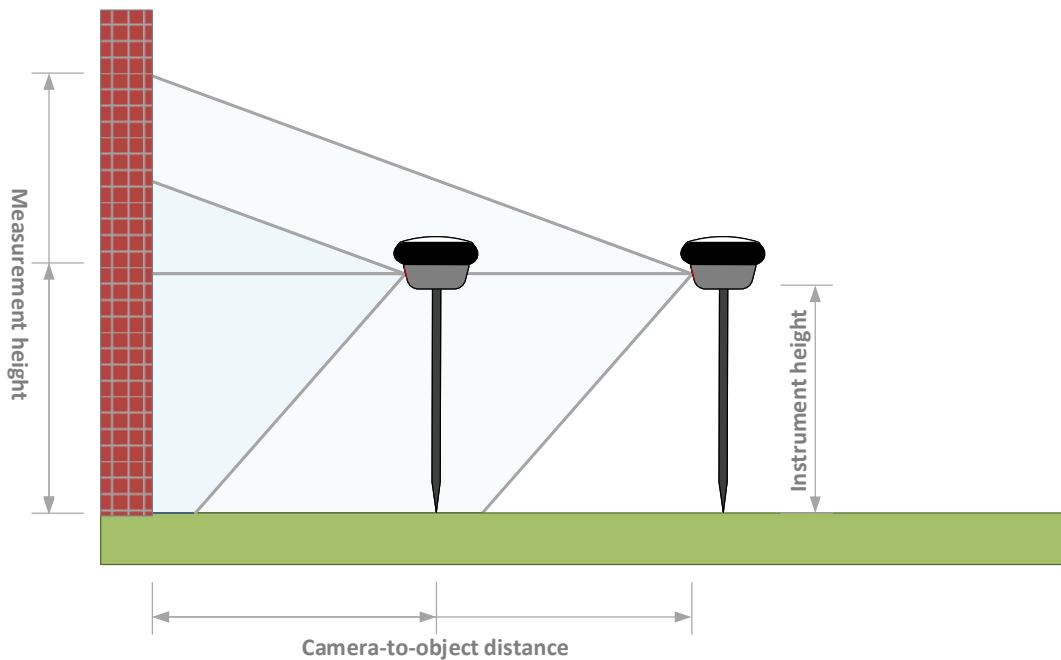


Figure 82: The measurement height increases with a bigger camera-to-object distance

Table 14: The accuracy and the range of the measurement height in dependency of camera-to-object distance

Camera-to-object distance	Accuracy [cm]	Measurement height range [m]
3	3 cm	3.5
5	3 cm	4.2
8	5 cm	5.3
10	8 cm	6.1

11.4 Trajectory

In order to perform more accurate measurements with the FuMo, it is suggested to capture images along the “U-trajectory”. When there is not enough place to take measurements along the horizontal “U-trajectory”, the vertical “U-trajectory” depicted in Figure 56 can be used.

11.5 Structure of an Object

To adjust camera poses from which the images were taken, the features have to be generated in images (see Section 5.2.1). If there are not enough features recognisable in the images, camera poses cannot be adjusted. The measurements can therefore not be performed in the images.

In order to ensure that the camera poses can be adjusted, enough details should be recognisable in the images.

11.6 Fast Rotations and Bumps

The initial camera poses from which the images were taken are determined using the GNSS and IMU measurements. The IMU provides the information about the lateral and angular movements of the sensor.

However, the IMU integrated in the FuMo can measure the accelerations of the sensor up to 2 g^[2]. When the acceleration of the sensor is bigger than 2 g, the initial camera poses cannot be defined. Such acceleration of the FuMo can be caused e.g. by a bump in a moment of measurements. A bump is an unintended movement of the sensor caused by the user. During the bump, the sensor’s acceleration is more than 2 g. The initial camera poses from which such images were captured are defined with big errors. The images can therefore not be used for photogrammetric measurements.

In addition, the IMU can measure the rotations up to ± 300 degrees per second (dps). When the sensor rotates more than ± 300 dps while capturing the images, the measured rotation of the sensor is still ± 300 dps. The initial camera poses are therefore defined with big errors. Such images cannot be used for photogrammetric measurements.

^[2] g denotes the local acceleration due to the gravity near Earth's surface. $g = 9.8 \frac{m}{s^2}$

11.7 Changing Surrounding of Image Point

As described in Section 5.3, the image coordinates of an object of interest are defined in one image by the user. The same target is in other images found automatically by the algorithm. The reference matrix that is determined around the image point in the image is searched for along the epipolar line in other images. If a suitable matrix is not found in other images, the coordinates of the measured object of interest cannot be determined automatically.

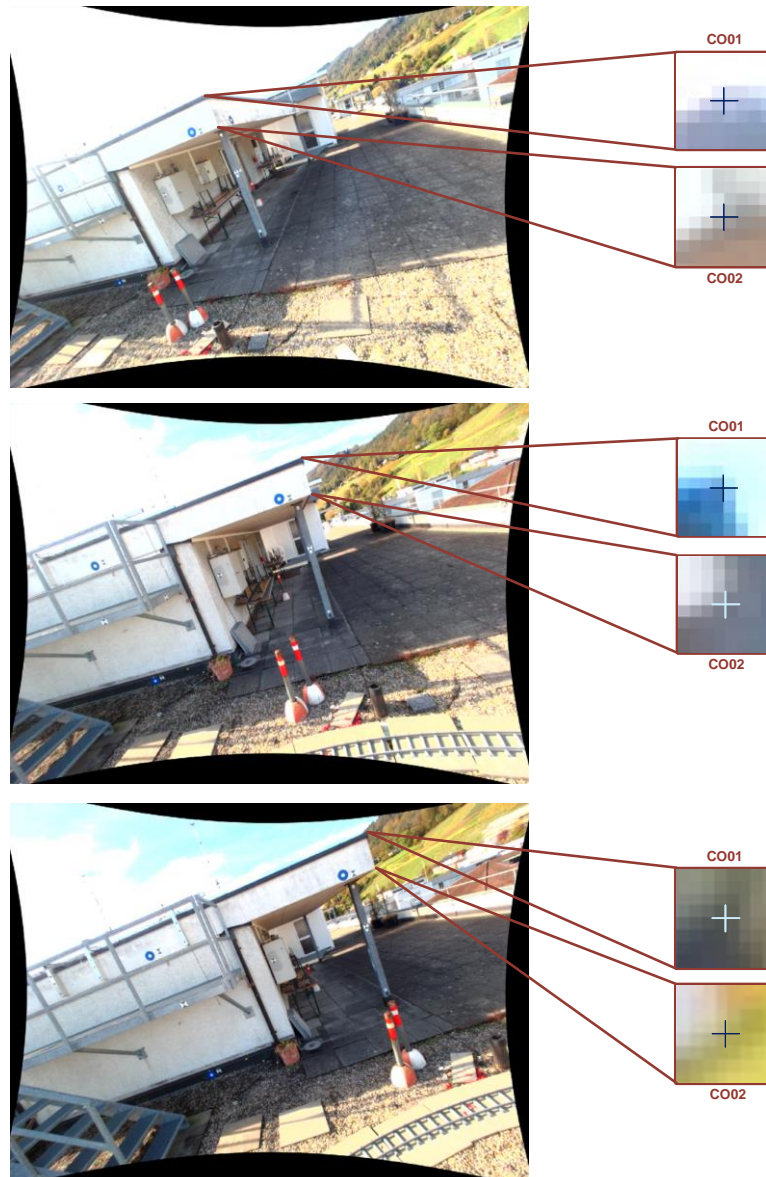


Figure 83: Changing surrounding matrix of the image point

The matrices of objects of interest CO01 and CO02 are depicted in the captured images as shown in Figure 83. The matrices of the CO01 captured in images cannot be correlated due to the changing surrounding of the image point. The matrices of the CO02 captured in images can also not be correlated. The measurements of such objects of interest can therefore not be automatically performed in images.

12 Conclusion and Outlook

When the measurements of multiple points have to be performed in a terrestrial coordinate system in a very short time interval, terrestrial photogrammetry can be applied. To simplify the photogrammetric measurements, the camera can be combined with a GNSS sensor and an IMU. A Functional Model (FuMo) was designed by Leica Geosystems AG, while combining all three components. While performing the measurements with the system, the attitude of the FuMo can be determined at every moment when the images are taken. The feature generation algorithm can be used to detect the features in single images. That way the relative geometry of the images is provided. In the next step, the features can be used together with the attitude of the sensor in the Structure from Motion algorithm. The algorithm determines the approximate camera poses from which the images were taken. Afterwards, the Bundle Adjustment algorithm iteratively adjusts the camera poses in the space. That way the best approximation of the camera poses from which the images were taken is determined in near real-time. The user can therefore perform the measurements of the object points in captured images right away.

The big advantage of the system is that additional points can be measured in the images at any time. There is no need to make plans before performing the measurements in the field. In addition, the data does not need to be processed by the user. Therefore, no additional knowledge is required for users in order to obtain the point coordinates.

In order to investigate the capability and the limitations of the system, measurements with the FuMo were performed in the test field. The test field was established on the roof of the Leica Geosystems building B26, where a good reception of the GNSS signal was ensured. The disadvantage of the test field was the lack of the space on the roof, where the measurements took place. Namely, when the images were captured in the test field at the distances bigger than 5 m from the wall of the object, the optimal geometry of the images could not be achieved. When performing additional test measurements in the future, a new test field should be established where more space is available. This would make it possible to perform qualification measurements, where the optimal geometry can be achieved also for the images captured from distances bigger than 5 m.

According to the processed test measurements, the geometry of the captured images significantly influences the accuracy of the measurements. The images that are captured along the “U-trajectory” can provide a better accuracy of the object point measurements compared to images captured along the “I-trajectory”. Furthermore, the object points measured in the images that are taken from shorter camera-to-object distances can be determined with higher accuracy. The object points measured in the images captured from the camera-to-object distance up to 5 m can be determined with an error smaller than 6 cm. The measurements of object points in the images taken from the distances between 5 m and 10 m can be determined with an error up to 15 cm.

In addition, the limitations of the system were determined during the measurements. As the measurements are based on the photogrammetry, optimal illumination has to be available while capturing the images. The FuMo has to constantly move around in order to capture the images of the object from different perspectives. Due to the IMU implemented in the system, the FuMo has to constantly move around in order to correct the bias of the sensor. The GNSS sensor needs access to the open sky during the whole time of capturing the images. When the GNSS signal is not available or

when the GNSS signal is affected by the multipath, the camera poses cannot accurately be adjusted in the space.

Considering the achieved accuracy and limitations of the system, such kind of measurements can be used for numerous surveying applications. As the relative accuracy of object points measured in captured images reaches centimetre level, such measurements are also suitable in the field of architecture, archaeology and in many other fields.

The accuracy of the system could be improved in order to be able to use the FuMo in the fields where more accurate measurements are required. The accuracy of GNSS measurements has the biggest influence on the accuracy of the object points measured by the FuMo. By improving the accuracy of the position information, more accurate positions of the camera poses could be determined. Using even more precise IMU could improve the accuracy of the orientation information of the camera poses. To minimize the systematic error of the measurements, a more accurate calibration of the main components and a more accurate synchronisation of the measurements should be provided. Furthermore, by providing better quality of the images, the limitations of the system could be improved. Consequently, the Structure from Motion and the Bundle Adjustment algorithms could adjust the camera poses more accurately, which would lead to a better accuracy of measured object point coordinates.

In the future, the process of test measurements should be upgraded. The measurements should be taken along the trajectory which is placed around the test object. The start point and the endpoint of the trajectory should coincide. The coordinates of an object point that is captured in the first and in the last image could be measured, in order to investigate the reliability of the system.

Furthermore, additional development of the system could take place in the future. By integrating an additional algorithm in the system, the point cloud of captured object could automatically be generated from the images. Such system could be used e.g. for simple calculation of the volume of the captured object.

13 References

- Fussell, A. (1982). Terrestrial photogrammetry in archaeology. *World Archaeology*.
- Hagan, T. O. (1980). A Case for Terrestrial Photogrammetry in Deep-Mine Rock Structure Studies. *International Journal of Rock Mechanics and Mining Sciences & Geomechanics Abstracts*.
- Hilton Marvin. H., B. F. B. (1985). Application of Close-Range Terrestrial Photogrammetry to Bridge Structures. *Virginia Highway & Transportation Research Council*.
- Kraus, K. (2007). *Photogrammetry: Geometry from Images and Laser Scans*. (S. K. Ian Harley, Ed.). De Gruyter.
- Leick, A. (1995). *GPS Satellite Surveying*. John Wiley & Sons, Inc.
- Li Zhilin Zhu Qing, G. C. (2005). *Digital Terrain Modeling, Principles and Methodology*. (G. C. Li Zhilin Zhu Qing, Ed.). CRC PRESS.
- Szeliski, R. (2010). *Computer Vision: Algorithms and Applications*. (S. Richard, Ed.). Springer.
- Thomas Luhmann, Stuart Robson, Stephen Kyle, J. B. (2014). *Close-Range Photogrammetry and 3D Imaging*. (S. K. J. B. Thomas Luhmann Stuart Robson, Ed.). De Gruyter.
- Ullman, S. (1979). *The interpretation of structure from motion*. (U. S., Ed.). Proceeding of the Royal Society of London.

Appendix A Calculation of the Area Captured in One Pixel

In order to calculate the size of the area that is captured in one pixel from specified camera-to-object distance, the specifications of the camera were used. The values are listed in Table 15.

Table 15: The FuMo camera specifications

FoV_{Hz}	Horizontal Field of View	86.6665°
FoV_V	Vertical Field of View	65°
	Horizontal resolution	1280 pixels
	Vertical resolution	960 pixels
	Resolution	$1.22MP$

The principle of calculating the size of an area that is captured in one pixel from different camera-to-object distances is described separately for horizontal and vertical direction in following two sections.

A.1 Horizontal Length

In order to calculate how big the horizontal length of the area captured in one pixel is, the horizontal length of the whole area that is captured in the sensor should be calculated. The problem is solved trigonometrically using the Pythagorean Theorem, as visualized in Figure 84.

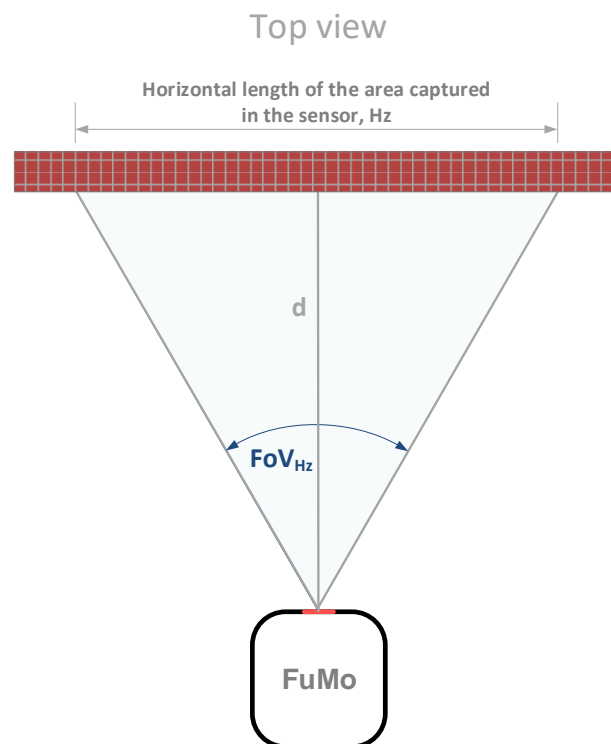


Figure 84: Horizontal Field of View, camera-to-object distance and the area captured in sensor

The size of the whole horizontal area that is captured in the sensor is calculated as follows:

$$Hz = 2 \cdot \left(d \cdot \tan \frac{65^\circ}{2} \right) \quad (13.1)$$

To calculate the average length of horizontal area that is captured in one pixel px_{Hz} , the Hz value has to be divided by the number of pixels that are placed horizontally in one line of the sensor:

$$px_{Hz} = \frac{Hz}{1280} \quad (13.2)$$

A.2 Vertical Length

To calculate the vertical length of the area captured in one pixel, the vertical length of the whole area that is captured in the sensor has to be calculated. The problem is solved trigonometrically using the Pythagorean Theorem, as visualized in Figure 85. But the calculation is not the same as when calculating the horizontal length of the area that is captured in one pixel.

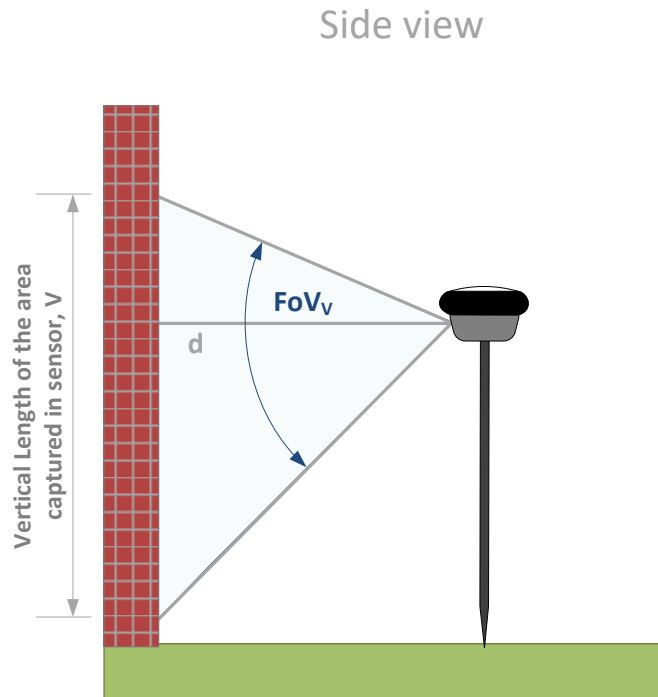


Figure 85: Vertical Field of View and the vertical length of the area captured in sensor

The camera inside the FuMo is not oriented horizontally inside the sensor, but it is tilted 12° downwards (see Figure 86). The vertical size of the area captured in the sensor is therefore calculated in two steps. Firstly, the sizes of both areas V_1 and V_2 are calculated as follows:

$$V_1 = d \cdot \tan(V_p) \quad \text{and} \quad V_2 = d \cdot \tan(V_m) \quad (13.3)$$

By adding V_1 to V_2 , the vertical size of the area captured in the sensor can be calculated as follows:

$$V = V_1 + V_2 \quad (13.4)$$

The distance can now be divided by the number of pixels that can be found in one column of the sensor:

$$px_v = \frac{V}{960} \tag{13.5}$$

The calculated value px_v represents average size of vertical area that is captured in one pixel.

Side view

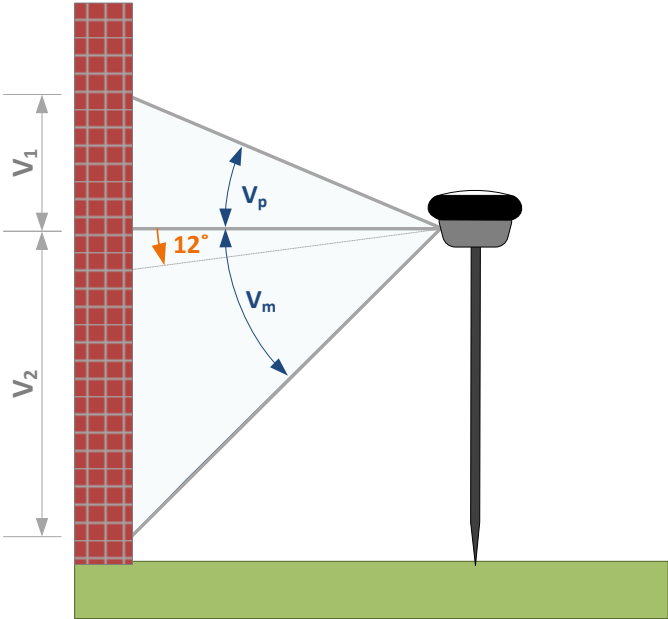


Figure 86: Camera of the FuMo is tilted 12° downwards